Charge Photogeneration in Organic Solar Cells

Tracey M. Clarke and James R. Durrant*

Centre for Plastic Electronics, Department of Chemistry, Imperial College London, London, SW7 2AZ, United Kingdom

Received August 5, 2009

Contents

1. Introduction

1.1. Organic Solar Cells

In recent years, organic solar cells utilizing π-conjugated polymers have attracted widespread interest in both the academic and, increasingly, the commercial communities. These polymers are promising in terms of their electronic properties, low cost, versatility of functionalization, thin film flexibility, and ease of processing. These factors indicate that organic solar cells, although currently producing relatively low power conversion efficiencies ($\sim$5−7%),[1–3] compared to inorganic solar cells, have the potential to compete effectively with alternative solar cell technologies. However, in order for this to be feasible, the efficiencies of organic solar cells need further improvement. This is the focus of extensive studies worldwide.

The backbone of a π-conjugated polymer is comprised of a linear series of overlapping p_z orbitals that have formed via sp^2 hybridization, thereby creating a conjugated chain of delocalized electron density. It is the interaction of these π electrons that dictates the electronic characteristics of the polymer. The energy levels become closely spaced as the delocalization length increases, resulting in a 'band' structure somewhat similar to that observed in inorganic solid-state semiconductors. In contrast to the latter, however, the primary photoexcitations in conjugated polymers are bound electron−hole pairs (excitons) rather than free charge carriers; this is largely due to their low dielectric constant and the presence of significant electron−lattice interactions and electron correlation effects.[4] In the absence of a mechanism to dissociate the excitons into free charge carriers, the exciton will undergo radiative and nonradiative decay, with a typical exciton lifetime in the range from 100 ps to 1 ns.

Achieving efficient charge photogeneration has long been recognized as a vital challenge for molecular-based solar cells. For example, the first organic solar cells were simple single-layer devices based on the pristine polymer and two electrodes of different work function. These devices, based on a Schottky diode structure, resulted in poor photocurrent efficiency.[5–7] Relatively efficient photocurrent generation in an organic device was first reported by Tang in 1986,[8] employing a vacuum-deposited CuPc/perylene derivative donor/acceptor bilayer device. The differing electron affinities (and/or ionization potentials) between these two materials created an energy offset at their interface, thereby driving exciton dissociation. However, the efficiency of such bilayer devices is limited by the requirement of exciton diffusion to the donor/acceptor interface, typically requiring film thicknesses less than the optical absorption depth. Organic materials usually exhibit exciton diffusion lengths of $\sim$10 nm and optical absorption depths of 100 nm, although we note significant progress is now being made with organic materials with exciton diffusion lengths comparable to or exceeding their optical absorption depth.[9–12]

The observation of ultrafast photoinduced electron transfer[13,14] from a conjugated polymer to C_{60} and the

* To whom correspondence should be addressed. E-mail: j.durrant@imperial.ac.uk.

10.1021/cr900271s
Published on Web 01/11/2010

Tracey M. Clarke obtained her Ph.D. degree in 2007 at the University of Otago (New Zealand), studying computational chemistry and Raman spectroscopy of oligothiophenes. After this, she accepted a postdoctoral research associate position at Imperial College London, working with James Durrant on the spectroscopic characterization and analysis of polymer-based solar cells and their constituent materials, using techniques such as transient absorption spectroscopy.

James R. Durrant is Professor of Photochemistry in the Department of Chemistry, Imperial College London, and Deputy Director of Imperial College's Energy Futures Lab. Following undergraduate studies in Physics, his Ph.D. and postdoctoral studies focused on the primary processes of plant photosynthesis. He joined the Chemistry Department in 1999, where he established an interdisciplinary research group focusing upon chemical approaches to solar energy conversion. His research is based around employing photochemical studies to elucidate design principles which enable technological development. His group is currently researching organic and dye-sensitized nanostructured solar cells as well as photoelectodes for solar fuel generation. He has published over 170 research papers and 5 patents and has recently been awarded the 2009 Environment Prize by the Royal Society of Chemistry.

consequent enhancement in charge photogeneration yield opened up the potential to employ solution-processable polymers in the next generation of solar cells. A key breakthrough in the utilization of such materials was the introduction of the bulk heterojunction[15] to overcome the primary issue in bilayer devices: the short exciton diffusion length limiting the active layer thickness (this is generally a more severe limitation for polymers than small molecule materials). Bulk heterojunctions involve a bicontinuous interpenetrating network of the electron donor (polymer) and acceptor materials (fullerene). This enhances the donor/acceptor interfacial area available for exciton dissociation and thus reduces the distance the exciton needs to travel before reaching an interface. Charge photogeneration is therefore increased in this case. The overall function of such

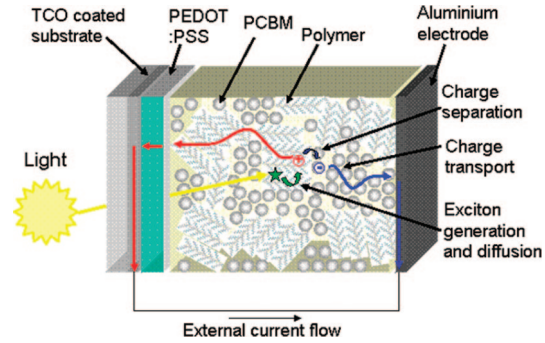

Figure 1. Schematic of the charge photogeneration and transport processes in a polymer:fullerene photovoltaic device. Reprinted with permission from ref 17. Copyright 2008 Material Research Society.

bulk heterojunction solar cells is illustrated in Figure 1 and reviewed elsewhere in this issue.[16]

The process of charge photogeneration in a polymer:fullerene blend can be summarized in a series of sequential steps as follows. Absorption of a photon, usually by the donor, generates the exciton. The exciton subsequently diffuses until it reaches the polymer:fullerene interface, where it may be quenched by electron transfer from the polymer to the fullerene (see section 3.1 for a more detailed description). However, this electron transfer does not necessarily directly generate free (dissociated) charge carriers. Despite being located on different materials, the electron and hole pair are still expected to exhibit significant Coulomb attraction (of the range 0.1−0.5 eV), potentially resulting in the formation of Coulombically bound interfacial electron−hole pairs. The overall process of charge photogeneration requires dissociation of these initially generated bound electron−hole pairs into free charge carriers, which can then be transported to and collected by the device electrodes. The term 'charge photogeneration' used herein refers to the yield of fully dissociated (free) charges.

A key challenge for the development of organic photovoltaic devices is to develop a predictive understanding of the relationship between molecular structure and photovoltaic device performance. The molecular structures of the main polymers and acceptors discussed in this review are displayed in Figure 2. These molecular structures can influence device performance in many ways; for example, the HOMO/LUMO energy gap governs the optical band gap of the device (although the exciton binding energy also needs to be taken into account), while the charge carrier mobilities influence the charge collection efficiency. In this review, we focus on one specific aspect of the materials structure/device function relationship: the efficiency of charge photogeneration at the donor/acceptor interface. In particular, we concentrate on the behavior of the interfacial bound electron−hole pair states referred to above, which appear to be of great significance in organic photovoltaic devices.

These Coulombically bound electron−hole pair states are comprised of partially charge-separated states, where the hole is primarily localized on the donor HOMO orbital and the electron on the acceptor LUMO orbital but where the Coulomb attraction between the electron and hole remains significantly greater than k_BT. A widely ranging nomenclature is currently employed in the literature to refer to such states, including geminate pairs, bound

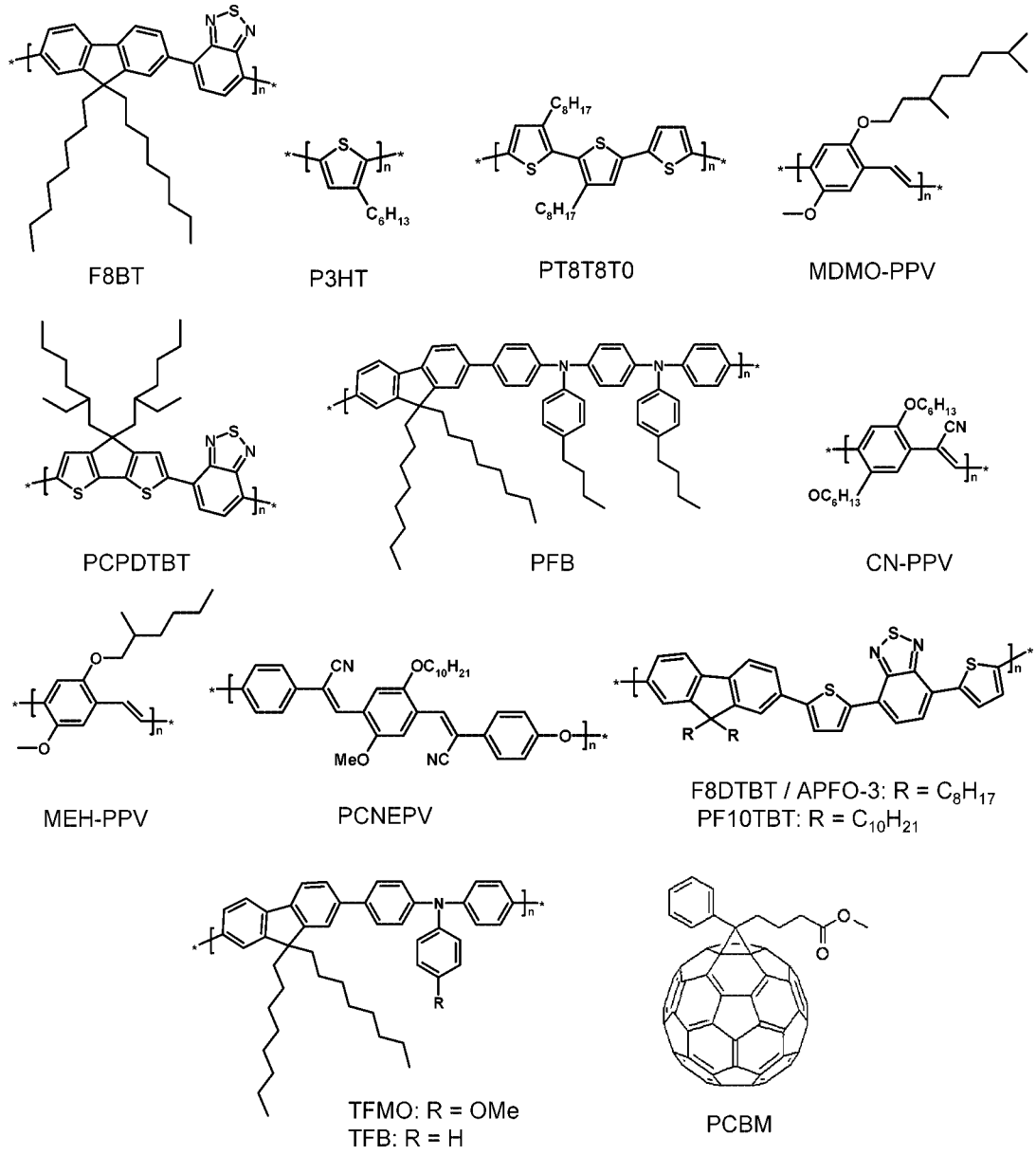

Figure 2. Structures of the polymers (and PCBM) discussed in this review.

polaron (or electron−hole or radical) pairs, charge-transfer excitons, and exciplexes.[18–28] In some cases the nomenclature differs to reflect particular characteristics of these states. For example, the term 'charge-transfer state' has been used to refer to such interfacial states that exhibit an observable transition dipole to the molecular ground state, as evidenced by the observation of weak charge-transfer optical absorption and (electro)luminescence bands.[18,29–32] In some cases, this luminescence can be relatively intense, appearing as a red-shifted and broadened photoluminescence (PL)[19,25] analogous to that observed for bound excited-state complexes (exciplexes) in solution. In other cases, different terminology is used to differentiate between thermally hot and thermally relaxed charge-transfer states.[21] For simplicity, throughout this review we will follow the most commonly used terminology and refer to all such states as 'charge-transfer' (CT) states. This terminology indicates that such states are intermediate in terms of charge separation between excitons and fully dissociated charges. We note however that this 'charge-transfer' terminology does not necessarily imply the observation of radiative coupling to the electronic ground state.

Several factors influence the overall process of photocurrent generation in organic solar cells, as has been the subject of several recent reviews.[7,33–40] The photocurrent generation efficiency is directly related to the fraction of light absorbed by the blend film,[7] which is a function of the absorption spectra (e.g., optical band gap), the absorption strength (extinction coefficient), and the absorbing layer thickness. Conjugated polymers typically have high extinction coefficients, but their optical band gaps are often not well matched to the solar emission spectrum, thus limiting the fraction of solar radiation absorbed. In addition, the nanomorphology created upon blending the two materials together is crucial in determining the efficiency of exciton diffusion to the donor/acceptor interface as well as, potentially, the efficiency by which the interfacial charge-transfer states can dissociate into free charges. The energy levels of the donor and acceptor are also critical to ensure efficient exciton quenching at the interface and to determine whether this

quenching is associated with electron or energy transfer processes.[41] Following donor/acceptor electron transfer, two recombination pathways may compete with photocurrent generation. Geminate recombination of the initially generated bound charges (or charge-transfer states) back to the ground state may compete with dissociation of these charges into free charge carriers. Alternatively, bimolecular recombination, the recombination of the dissociated free charge carriers, competes with charge transport to the electrodes and therefore may influence photocurrent generation.

1.2. Charge Photogeneration

The primary process in almost all electronic (as opposed to thermal) solar energy conversion systems is the utilization of incident solar energy to generate separated electronic charges. These energetic charges can subsequently be used for electrical power generation (photovoltaics) or employed to drive redox chemistry (photosynthesis). Efficient energy transduction requires separation of this photogenerated electron−hole pair into long-lived dissociated charges with a high quantum yield and minimal loss of free energy. A potential concern in this charge-separation process is that the electron and hole must overcome their mutual Coulomb attraction, V

$$V = \frac{e^2}{4\pi\varepsilon_r\varepsilon_0 r} \quad (1)$$

where e is the charge of an electron, ε_r is the dielectric constant of the surrounding medium, ε_0 is the permittivity of vacuum, and r is the electron−hole separation distance. Gregg et al.[42] presented a comparison of inorganic and organic semiconductors on the basis of their respective Coulomb potentials. In conventional inorganic photovoltaic devices, such as those based on silicon p−n junctions, overcoming the Coulomb attraction is facile due to the high dielectric constant of silicon ($\varepsilon_r \approx 12$) and because the electronic states involved are already highly delocalized (corresponding to a larger average 'r' in eq 1). Similarly, dye-sensitized photoelectrochemical solar cells exhibit a high dielectric constant for the electron acceptor nanoparticles (TiO_2, $\varepsilon_r \approx 80$) in addition to a high ionic strength electrolyte. As a result, after the initial electron injection step from the molecular excited state, the Coulomb attraction of electrons and holes in dye-sensitized photoelectrochemical cells is effectively screened.[43] However, for solar cells based upon on molecular materials, overcoming this Coulomb attraction is significantly more demanding due to both their smaller dielectric constant ($\varepsilon_r \approx 2-4$) and the more localized nature of the electronic states involved. As such, achieving efficient charge photogeneration is a key challenge for solar energy conversion technologies based upon molecular materials.

The most sophisticated examples of molecular-based solar energy conversion systems are undoubtedly the natural photosynthetic reaction centers. Despite the wide range of photosynthetic organisms, the primary functional components of their reaction centers are remarkably invariant. Charge photogeneration in such reaction centers is achieved by the use of a redox relay or cascade, as illustrated in Figure 3. Light absorption by the reaction center results, after various energy transfer steps, in the formation of a short-lived (nanoseconds) molecular singlet excited state localized on a primary donor species. Charge separation is achieved by an energetically downhill electron transfer from the donor excited-state LUMO orbital to a neighboring molecular acceptor, achieving an initial separation of the electron and hole. Subsequent secondary electron (and hole) transfers produce further charge separation, resulting in the almost unity quantum yield generation of a long-lived (milliseconds to seconds) charge-separated state. These long-lived charge pairs are subsequently coupled to multielectron redox chemistry that ultimately results in the storage of the incident solar energy in chemical bonds (sugars). However, as is apparent from Figure 3b, the photoinduced charge separation achieved in the natural photosynthetic reaction centers comes at a significant energy cost. The long-lived charge-separated state generated in these reaction centers typically retains only one-half the free energy of the initial molecular excited state. This loss of free energy is required both to drive the sequence of electron transfer steps at sufficient rates to compete with the unwanted charge recombination pathways back to the ground state and to prevent thermally driven electron transfer back to the initial short-lived excited state. It is thus apparent that even for these highly evolved photosystems, charge photogeneration comes at a significant energy cost, which of course has an impact upon the overall energy conversion efficiency of biological photosynthesis.

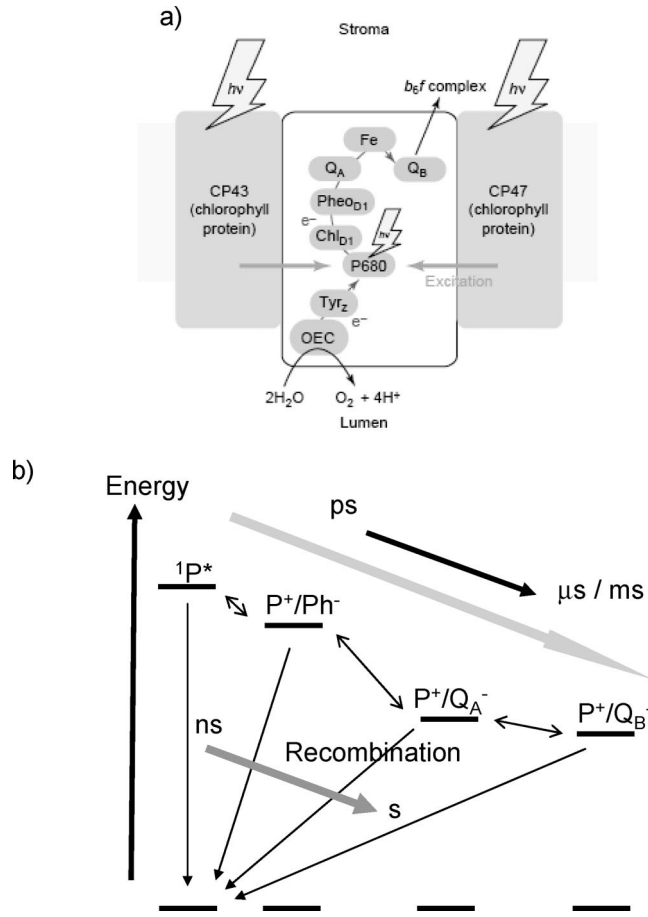

Figure 3. (a) Schematic of the photosystem II reaction center of higher plants. Reprinted with permission from ref 44. Copyright 2004 Elsevier. (b) State diagram schematic of the energetics and kinetics of charge separation in this reaction center.

There have been numerous studies of photoinduced charge separation in molecular mimics of the natural photosystems based on molecular donor/acceptor redox relays. Extensive studies of these donor/acceptor systems in dilute solution have led to a detailed understanding of their structure/function relationship in terms of nonadiabatic electron transfer theory[45–48] (see section 2.2 for summary). This has

in turn led to impressive advances in the molecular control of electron transfer dynamics in such systems. It has been shown, for example, that charge photogeneration in these systems is dependent upon the use of redox relays to increase the spatial separation of the charges and on control of the state energetics to minimize activation barriers to forward charge separation while ensuring large activation barriers for the undesired recombination pathways, leading to reports of remarkably efficient, long-lived charge separation.[45,46,48,49]

The use of solid films allows, in principle, the formation of percolation pathways to achieve the electrical 'wiring' of charge photogeneration at the donor/acceptor interface to external device electrodes, as illustrated in Figure 1. Typical examples of organic donor/acceptor heterojunction photovoltaic devices are polymer:fullerene blend and small molecule bilayer solar cells. The mechanism of charge photogeneration in such devices is of particular interest. These organic materials typically do not exhibit the highly delocalized electronic states, weak electron−lattice interactions, and high dielectric constant present in silicon solar cells. Moreover, the interfaces are typically fabricated from one donor and one acceptor material and therefore do not exhibit the redox relay of distinct molecular donor and acceptors utilized in photosynthetic reaction centers to achieve efficient charge photogeneration. The mechanism by which such devices can overcome the Coulomb attraction of the photogenerated electron−hole pair, and in particular achieve this with a high quantum and energy efficiency, is central to the development of such devices.

The significance of this charge photogeneration challenge for organic solar cells can be readily appreciated by simple consideration of the energetics of the donor/acceptor interface. It is generally agreed that the initial charge-separation step, electron transfer from the donor exciton state into the acceptor conduction band (or the reverse hole transfer from acceptor excited states), can be achieved by utilizing a suitable energy offset between the donor and acceptor LUMO levels, as illustrated in Figure 4a. This requires that the energy offset is greater than the Coulomb binding energy of the exciton, E_B^{exc} (we discuss the details of these energetics in section 3.3 below), enabling the initial electron transfer step to be energetically downhill.[50] However, as the donor and acceptor molecules are physically adjacent at the charge-separation interface, this initial electron transfer step results in only a modest spatial separation of the electron and hole, typically of the same order of magnitude as the size of the molecules (or molecular orbitals) concerned: 0.5−1 nm. At this spatial separation, the electron and hole still exhibit a significant Coulomb attraction. Employing a simple point charge approximation (eq 1), the magnitude of this Coulomb attraction can be estimated to be in the range 0.1−0.5 eV, as illustrated in Figure 4b (we will refer herein to this attraction as the charge-transfer-state binding energy E_B^{CT}). The magnitude of this Coulomb attraction is clearly sizable compared to the thermal energy (0.025 eV) and, in principle, represents a large energetic barrier to charge photogeneration at donor/acceptor organic interfaces.

There now exists several donor/acceptor organic heterojunctions that can yield photovoltaic devices with near unity quantum yields of photocurrent generation and increasingly efficient overall device efficiencies. Thus, it is clear that it is possible to achieve efficient charge photogeneration at organic donor/acceptor interfaces, even when employing low dielectric constant materials and without the use of redox

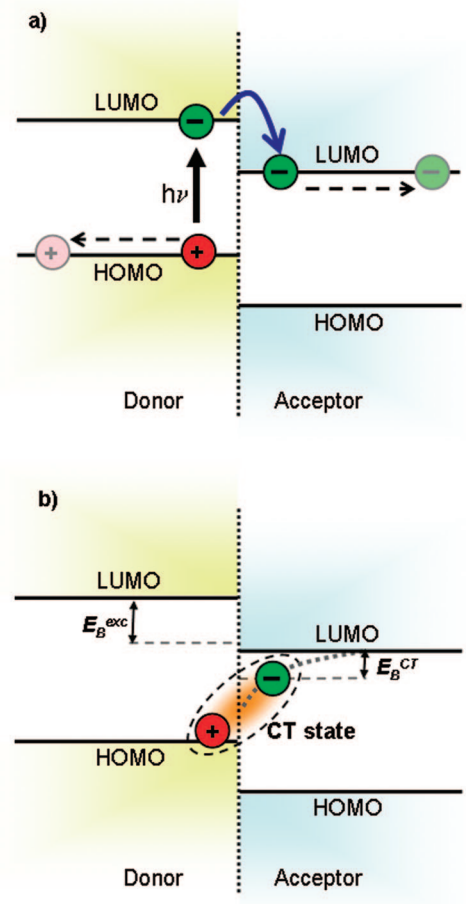

Figure 4. (a) Energy level diagram of a donor/acceptor interface showing a simplified viewpoint of photoexcitation of an electron into the donor LUMO followed by electron transfer into the acceptor LUMO and migration of the separated charges away from the interface. (b) Illustration of the formation of interfacial electron−hole pairs or charge-transfer (CT) states. The energy of this state depends upon the Coulomb attraction of the electron and hole and therefore their spatial separation, as illustrated by the dotted curve. (b) Typical binding energies for the exciton and CT states (E_B^{exc} and E_B^{CT}, respectively). E_B^{exc} corresponds to the difference between the optical and electrochemical band gaps. Note that for simplicity, the energy of the exciton and CT states are shown relative to the polaron HOMO level. Figure 4b adapted with permission from ref 51. Copyright 2008 American Physical Society.

relays. There are, however, many more examples of organic donor/acceptor heterojunctions that achieve efficient exciton quenching at the donor/acceptor interface but do not achieve efficient photocurrent generation. This can often be attributed to inefficient charge percolation or transport, i.e., poor 'wiring' of the interface to the device electrodes. However, in many other systems the charge collection process appears to be relatively efficient; in such cases it appears likely that poor photocurrent generation is related to the efficiency of charge photogeneration at the donor/acceptor interface. Indeed, many reports have related subunity photocurrent quantum yields to charge photogeneration limitations.[21,25,38,52,53] Moreover, the voltage dependence of charge photogeneration has been widely proposed as a key factor limiting the voltage output of such devices.[27,32,54] It is thus apparent that understanding the mechanism of charge photogeneration at donor/acceptor interfaces is not only of academic interest but also of technological importance for the development of efficient organic photovoltaic devices.

Our understanding of the mechanism of charge photogeneration in organic solar cells remains incomplete. However, significant progress has been made over the past few years, both experimentally and theoretically, on this topic. In particular, progress has been made in understanding the roles of macroscopic electric fields, interfacial energetics, and nanomorphology in determining the efficiency of this process. In this review, we discuss this progress, focusing in particular upon the role of interfacial charge-transfer states in influencing the efficiency of photocurrent generation in organic solar cells. The following section will summarize two significant theories relevant to charge separation at such donor/acceptor interfaces: nonadiabatic electron transfer theory and the Onsager theory of charge dissociation. The third section will concentrate on the current understanding of charge photogeneration in polymer:fullerene solar cells from the viewpoint of the charge-transfer state: its formation, recombination, and dissociation. The final section will discuss the implications for materials and photovoltaic device design.

2. Theoretical Background

2.1. Properties of Excitons

Photoexcitation of a conjugated polymer generates a singlet excited state in which the electron and hole are still influenced by a strong Coulomb attraction; this state is termed a singlet exciton. The Coulomb interaction causes a large binding energy for the exciton (E_B^{exc}) that is significantly greater than the thermal energy k_BT. Other contributors to the appreciable binding energy are electron−lattice and electron−electron interactions.[4] The exciton is required to overcome this binding energy in order to dissociate within its lifetime and achieve charge photogeneration; this typically occurs at the interface with an electron acceptor but can also occur through interactions with impurities and defect sites or under the influence of an applied electric field. The properties of excitons in polymer materials have been studied extensively using both experimental and theoretical methods.[4,55−61] Some of these properties, such as the exciton binding energy and diffusion length, are important parameters for organic solar cells as they strongly influence the probability of exciton dissociation and thus the efficiency of charge photogeneration.

The exciton of a conjugated polymer is spatially more localized compared to excitations in inorganic semiconductors. The creation of this localized electronic excited state in a conjugated polymer is accompanied by a localized relaxation of the surrounding molecular structure.[4] This occurs because of the strong electron−phonon coupling in these materials, and the term 'exciton' in this context therefore refers to both the electronic excitation and the local structural deformation it induces. In nondegenerate polymers such as polythiophene, this structural relaxation is characterized by a reversal of the C−C bond length alternation to create a domain of semiquinoidal bond sequences localized over several monomer units. The magnitude of this bond length reversal is greatest at the center of the exciton and progressively diminishes along the chain until an aromatic bond structure is restored. This bond rearrangement can result in a relatively more rigid, planar geometry in the excited state compared to the ground state, as is evident from photoluminescence spectra as an enhancement in the vibrational fine structure compared to the inhomogeneously broadened ground-state absorption spectra.[62,63] Note that both polymer polarons and triplet excitons also possess these localized structural deformations.[64−67] The spatial extent of the structural changes depends upon the nature of the excitation and the chemical structure. In PPVs, for example, photoluminescence data suggest that the singlet exciton extends over six monomer units,[68] whereas the triplet exciton of PPV has been reported to have a much more pronounced structural deformation localized over a shorter length: only one or two monomer units.[58] These structural relaxation effects (electron−lattice interactions) are part of the reason for the relatively high exciton binding energies in conjugated polymers compared to conventional inorganic semiconductors.[4] One of the other reasons is the low dielectric constant, which prevents effective screening of charge and results in a large Coulombic interaction between the excited electron and hole, as discussed above.

Efficient device performance relies upon the photogenerated exciton moving to a donor/acceptor interface so that exciton dissociation can occur.[69] Due to their electrical neutrality, the motion of excitons is not affected by electric fields, and thus, they diffuse through the blend randomly. This diffusion is typically described as a Förster-type incoherent energy transfer process, which can be either intramolecular or intermolecular and usually acts to lower the energy of the exciton. This downhill energy transfer can result in trapping of the exciton in the tail of the inhomogeneously broadened density of states; the trap sites are also often associated with defects and aggregates. At this point, any further exciton migration will rely on thermal fluctuations. At the same time, if the initially generated exciton is vibrationally excited, the diffusion process allows time for intramolecular vibrational relaxation to take place (within 100 fs).[55] Exciton dissociation can therefore occur from either the vibrationally excited 'hot' exciton (i.e., the Franck−Condon state)[70−72] or the thermally equilibrated, geometrically relaxed, 'cold' exciton.[55,73]

Another important parameter of polymer excitons is the diffusion length, the distance an exciton can migrate before relaxing back to the ground state. Dissociation of the exciton into charges must therefore occur within this distance. Clearly, this will limit the extent of phase segregation possible in a bulk heterojunction blend for efficient device performance. In general, phase segregation on the order of the exciton diffusion length is desired. A typical method of estimating this parameter is to assess the photoluminescence quenching of polymer/acceptor bilayers as a function of layer thickness. Measurements of this type,[56,59,74] and also using photocurrent experiments,[60] have yielded exciton diffusion lengths of 5−14 nm for PPV derivatives and 3−9 nm for P3HT.[75,76]

2.2. Nonadiabatic Electron Transfer Theory

Once the photogenerated exciton has diffused to a donor/acceptor interface, it can be dissociated by an interfacial electron transfer reaction. In cases where the donor and acceptor phases are intimately mixed, such that excitons are generated directly at the donor/acceptor interface and thus avoiding the need for exciton diffusion, this electron transfer reaction can occur extremely rapidly, on the femtosecond time scale.[14,77,78] Marcus's theory of semiclassical nonadiabatic electron transfer, first developed in 1956,[79] has been successfully applied to a number of chemical systems[47,80] and also been extended to photoinduced charge transfer in conjugated polymer blends.[81−84] Marcus theory considers the

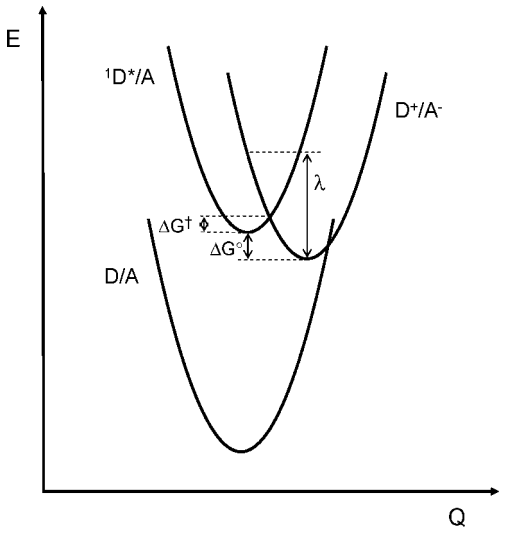

Figure 5. Potential energy surfaces for a D/A system (where D refers to the electron donor and A the electron acceptor), where photoexcitation generates ^{1}D*/A and subsequent electron transfer generates D^+/A^-. $\Delta G°$ is the energy difference between the two surfaces' minima; the energy barrier for the reaction, $\Delta G^\dagger$, is the energy difference between the reactant's minimum and the point of intersection between the two surfaces, and λ is the reorganization energy.

reactant and product potential energy surfaces as two intersecting harmonic oscillators (parabolas) with the horizontal axis as the reaction coordinate, representing the motion of all nuclei in the system, as illustrated in Figure 5. Electron transfer must occur at the intersection point in order to satisfy both energy conservation requirements and the Franck−Condon principle, which states that electron transfer occurs so rapidly compared to nuclear motion that effectively no change in nuclear configuration occurs during the transfer. The intersection point therefore represents the energy level and nuclear configuration that the reactant state must achieve (through vibrational motion) in order for isoenergetic electron transfer to occur. It therefore follows that electron transfer is an activated process with an energy activation barrier $\Delta G^\dagger$, which Marcus theory states is a function of the Gibbs free energy, $\Delta G°$, and the reorganization energy, λ:

$$\Delta G^\dagger = \frac{(\lambda + \Delta G°)^2}{4\lambda} \tag{2}$$

The reorganization energy refers to the energy required to bring the reactant and its surrounding medium to the equilibrium geometry of the product state. It can be considered as comprising of an 'inner' (vibrational) contribution, reflecting the changes in nuclear geometry occurring upon electron transfer, and an 'outer' (solvent) contribution, concerning the changes in polarization of the surrounding medium to stabilize the product state after electron transfer. The vibrational contribution can be determined from the force constants for all vibrations in the reactant and product, while the solvent contribution can be calculated by applying the dielectric continuum model of the solvent.[47]

The rate constant for electron transfer, k_{ET}, can therefore be determined in terms of a Fermi's Golden rule type analysis as:

$$k_{ET} = \frac{2\pi}{\hbar} V^2 FC = \frac{2\pi}{\hbar\sqrt{4\pi\lambda kT}} V^2 \exp\left(-\frac{(\lambda + \Delta G°)^2}{4\lambda kT}\right) \tag{3}$$

The matrix element term V refers to the electronic coupling between the reactant and product states and thus depends upon the overlap of the electronic wave functions of the electron donor and acceptor. Strong coupling denotes the adiabatic limit, where the two potential energy surfaces effectively 'split' into a lower surface and an upper one, electron transfer proceeding along the lower surface. If, however, the electronic coupling is relatively weak, as we consider herein, then such splitting is small relative to k_BT and electron transfer occurs nonadiabatically, as described by eq 3. We note eq 3 corresponds to a semiclassical analysis, treating the electronic coupling quantum mechanically but the nuclear motion classically. In addition, it is possible to treat the nuclear motion quantum mechanically, where the Franck−Condon (FC) factor is analyzed in terms of nuclear tunnelling.[47]

The exponential term in eq 3, corresponding to the Franck−Condon factor, predicts that as $-\Delta G°$ increases, so does the electron transfer rate, until the maximum rate is reached when $\lambda = -\Delta G°$. At this point the reaction has no activation barrier. Further increases in $-\Delta G°$ will *decrease* the reaction rate; this is called the Marcus inverted region and has been observed experimentally.[85,86] Indeed, this concept is a key feature of the efficient function of natural photosynthetic reaction centers. In these reaction centers, the energetics (both λ and $\Delta G°$) are such that all the desired, forward electron transfer steps are activationless ($\lambda = -\Delta G°$) while all the undesired reverse recombination reactions to the ground state are highly activated in the Marcus inverted region ($-\Delta G° > \lambda$). A similar design concept has been widely utilized for achieving efficient charge photogeneration in molecular donor/acceptor relays in solution.[47,85]

Studies of electron transfer in oligomer−fullerene dyads[83] and donor−acceptor dendrimers[82] have used Marcus theory to explain their results as a function of solvent polarity. Charge transfer occurs in the Marcus normal region: as the solvent polarity is increased, the charge-separated state is increasingly stabilized and the barrier to electron transfer is reduced, enhancing the rate. In contrast, charge recombination is in the Marcus inverted region; thus, the barrier to charge recombination decreases in polar solvents, consistent with the greater recombination rate observed experimentally.[83]

For solid films, the nonadiabatic theory detailed above may need to be modified to reflect the presence of a band of acceptor states (i.e., a conduction band) rather than a discrete molecular level. This requires integration of eq 3 over the density of available states, as described previously.[87] Electron transfer in the solid state has, for example, been investigated by van Hal et al.,[83] where different results for the forward and reverse electron transfer rates were observed and compared to that in solution. In this case, the forward electron transfer rate was substantially increased in the solid state relative to the most polar solvent, while the reverse (recombination) rate was much slower. This was rationalized by assuming an intermolecular electron transfer in the solid state, unlikely to occur in solution. The slower recombination lifetime in the solid state was assigned to dissociation of the initially generated charges into separated charges, resulting from a transition from intramolecular geminate recombination

dominating in solution to bimolecular recombination in the solid film. Similar transitions in charge carrier dynamics between solution and films have been reported for other molecular systems.[88,89]

2.3. Onsager Theory

The electron transfer reaction from the photoexcited donor to the acceptor fullerene, by virtue of the low dielectric constant intrinsic to conjugated polymers, initially generates a Coulombically bound electron−hole pair. This 'charge-transfer' (CT) state must overcome its Coulomb interaction in order to generate the free, fully dissociated, charge carriers. However, this dissociation process can be difficult due to the polymers' low charge carrier mobilities and poor screening of charge. As such, if dissociation does not take place within the lifetime of the CT state, then geminate recombination (known to be a significant loss mechanism in organic solar cells) will occur.

Geminate recombination was first described quantitatively by Onsager.[90] The model he proposed calculates the probability that a Coulombically bound electron−hole pair in a weak electrolyte undergoing Brownian random motion will escape its Coulomb attraction and generate free charges (the process of autoionization). More specifically, the model proposed that photon absorption generates a localized hole and a hot electron; the latter, by virtue of its excess thermal energy, then undergoes rapid motion until it thermalizs at distance a (the thermalization length) from the localized hole, as illustrated in Figure 6. The resultant electron−hole pair is referred to herein as a charge-transfer (CT) state. The competition between dissociation of this CT state and its recombination back to the ground state depends upon the magnitude of the Coulombic attraction felt by this CT state. In particular, Onsager proposed a definition for a Coulomb capture radius (alternatively called the Onsager radius), r_c, defined as the distance at which the Coulomb attraction energy equals the thermal energy k_BT

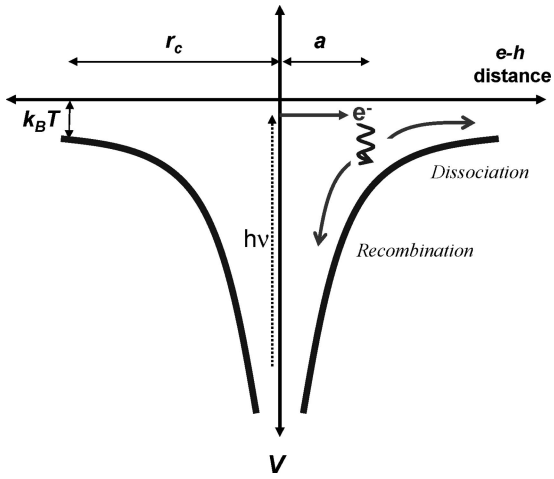

Figure 6. Potential energy diagram summarizing Onsager theory for autoionization. The red curve illustrates the potential energy resulting from Coulomb attraction as a function of electron−hole ($e-h$) separation. Photoexcitation results in generation of a hot, mobile electron. This electron subsequently thermalizes at a particular distance from the hole (the thermalization length, a). If a is less than the Coulomb capture radius, r_c (as is typical for single-component organic systems), then the electron−hole pair (which we refer to herein as a charge-transfer state) can either undergo geminate recombination or dissociate into free charges.

$$r_c = \frac{e^2}{4\pi\varepsilon_r\varepsilon_0 k_B T} \tag{4}$$

where e is the charge of an electron, ε_r is the dielectric constant of the surrounding medium, ε_0 is the permittivity of vacuum, k_B is Boltzmann's constant, and T is temperature. If the thermalization length a is greater than the Coulomb capture radius, the charge carriers are considered to be fully dissociated. If, however, the thermalization length is smaller than r_c, then the dissociation of the CT state into free charges occurs with an escape probability of $P(E)$ while geminate recombination to reform the ground state occurs with a probability of $1 - P(E)$. Equation 4 therefore emphasizes the importance of the dielectric constant of the material. Inorganic semiconductors typically have very high dielectric constants ($\varepsilon_r > 10$); thus, the Coulomb capture radius is small and free charge carriers are produced with high efficiency. In organic semiconductors, however, the low dielectric constants ($\varepsilon_r < 4$) induce large Coulomb capture radii and the probability (in the absence of a donor/acceptor interface) that the charges will escape the Coulomb attraction and migrate beyond this distance is significantly reduced.

The escape probability $P(E)$ depends on the strength of any applied electric field, E, the distance at which the two thermalized charges are generated, a, and the temperature, T. In the absence of electric fields (or any influences other than the Coulomb potential), the probability of escape from geminate recombination (defined as the infinite separation of the two ions) is proportional to the negative reciprocal of the CT-state electron−hole separation distance, a. The presence of an electric field lowers the Coulomb potential barrier in the downfield direction,[91] thereby enhancing the fraction of escaping ions. For *low* field strengths, the escape probability is given by[92]

$$P(E) = \exp\left(\frac{-r_c}{a}\right)\left(1 + \frac{e r_c}{2k_B T}E\right) \tag{5}$$

where a is the initial separation of the two thermalized ions (i.e., the thermalization length), r_c is the Coulomb capture radius, e is the electron charge, k_B is the Boltzmann constant, T is the temperature, and E is the electric-field strength. As such, at low field strengths the escape probability scales linearly with field intensity. A plot of $P(E)$ versus E under such low field conditions gives a slope to intercept ratio of $e^3/2\varepsilon_r k_B^2 T^2$ and is thus independent of a. Since this ratio contains only easily observable parameters such as temperature and dielectric constant, it has proven a useful indicator for the applicability of Onsager theory and successfully been applied to a number of systems.[54,92–96]

Onsager's original work was modified in 1984 by Braun, who highlighted the importance of a finite lifetime for the CT state, especially in solids.[97] This modification stemmed from the observation that, using the conventional Onsager model, the electric-field dependence of the free charge carrier yield indicated larger thermalization lengths (2.5−3.5 nm) than considered typical for a nearest-neighbor charge-transfer exciton (less than 1 nm). Onsager theory contains the boundary condition that if the separation between the two ions reaches zero, then recombination occurs and the pair irreversibly disappears. Braun stated that this condition is inappropriate due to the finite lifetime of the CT state. On the basis of the two decay processes for the CT state, Braun's revised model defines the electric-field-dependent dissocia-

tion into free charges by the rate constant $k_d(E)$ and the rate constant for geminate recombination back to the ground state as k_f

$$P(E) = \frac{k_d(E)}{k_f + k_d(E)} = k_d(E)\tau(E) \quad (6)$$

where $P(E)$ is the escape probability and $\tau(E)$ is the lifetime of the CT state. A key factor in Braun's model that significantly differentiates it from Onsager's model is that dissociation of the CT state into free charge carriers is a reversible process: during the lifetime of the CT state, many attempts to dissociate may occur and the CT state can be regenerated from these partially dissociated charges with a rate constant of k_r. Using Onsager's original equation for the relative effect of an applied electric field on the dissociation of a weak electrolyte,[98] the dissociation rate is defined as

$$k_d(E) = \frac{3\langle\mu\rangle e}{4\pi\langle\varepsilon_r\rangle\varepsilon_0 a^3} \exp\left(\frac{-\Delta E}{k_B T}\right)\left[1 + b + \frac{b^2}{3} + \frac{b^3}{18} + ...\right] \quad (7)$$

where $\langle\mu\rangle$ is the spatially averaged sum of the electron and hole mobilities, $\langle\varepsilon_r\rangle$ is the spatially averaged dielectric constant, ΔE is the Coulomb attraction of the initial generated ion pair after thermalization, $\Delta E = e^2/4\pi\langle\varepsilon_r\rangle\varepsilon_0 a$, and $b = e^3E/8\pi\langle\varepsilon\rangle\varepsilon_0 k_B{}^2T^2$, where the final summation is the approximation of a first-order Bessel function. A typical illustration of $P(E)$ as a function of electric field, determined for different thermalization lengths a, is shown in Figure 7. It is apparent that with the fit parameters employed the charge dissociation yield at low field increases with thermalization length a. However, these yields are all low, and efficient charge photogeneration is only predicted in the presence of significant electric fields ($\sim 10^7$ V cm^{-1}).

In addition, it has been reported that in disordered materials (such as a polymer:fullerene blend) a distribution of CT-state separation distances is very likely and should be included in the model.[96,97] As such, eq 6 can been integrated over this distribution

$$P(T, E) = N_F \int_0^\infty P(r, T, E)F(r)dx \quad (8)$$

where $P(r,T,E)$ is the probability that a CT state generated at distance x apart, with temperature T and field E, will escape recombination; $F(r)$ is a distribution function of ion pair separations, and N_F is a normalization function. Note that Braun's modified model maintains the same slope to intercept ratio as the conventional Onsager theory but can now describe charge generation more accurately, with thermalization radii consistent with nearest-neighbor interactions.

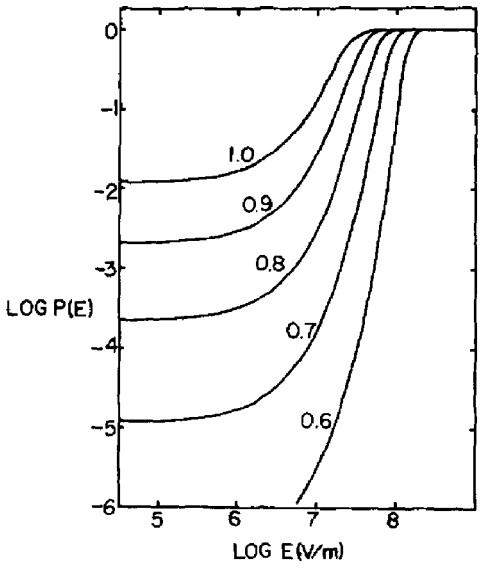

Figure 7. Electric-field dependence of CT-state dissociation probability as a function of thermalization length, a (nm), showing in increase in escape probability with increasing a. The fit parameters are as follows: $\langle\mu\rangle = 1 \times 10^{-4}$ m^2/(V s), $\langle\varepsilon\rangle = 3.0$, $T = 300$ K, and $\tau = 10^{-8}$ s. Reprinted with permission from ref 97. Copyright 1984 American Institute of Physics.

Further modifications to Onsager's original model have also been suggested as additional limitations have been identified. For example, Tachiya[92] noted that Onsager's theory was no longer applicable when materials with very high electron mobilities are used. The photoionization of tetramethyl-*p*-phenylenediamine in tetramethylsilane,[99] for instance, produced an observed slope to intercept ratio 25% lower than that predicted, while other solvents hexane and 2,2,4-trimethylpentane produced the expected result. The Smoluchowski equation (used by Onsager) describes the Brownian motion of a particle only when its mean free path is negligibly short compared to the length scales used in the equation. A high electron mobility implies a large mean free path; thus, Onsager's theory fails under this condition. Tachiya's new model incorporated the effect of electron mobility by calculating the electron's trajectory under the influence of the Coulomb potential and was able to explain other experimental results from the literature.

Another modification to Onsager's theory suggested by Wojcik and Tachiya[100] includes a finite distance-dependent intrinsic reaction rate, extending the work done by Hong and Noolandi.[94] This revision enables Onsager theory to be more readily applied to charge photogeneration in conjugated polymers. In some previous instances,[101,102] a very large initial electron−hole separation was required in order to fit to Onsager's model; Wojcik's revised model allowed more reasonable separations to be utilized. Furthermore, Barth and Bässler[103] showed that the efficiency of CT-state separation was increased by the presence of energetic disorder above that predicted from conventional Onsager−Braun theory (at low temperatures only). This occurs because the CT state is injected with a nonequilibrium energy that facilitates dissociation.

Modeling studies of charge photogeneration at donor/acceptor interfaces, most incorporating Onsager theory, have been relatively limited to date. Blom et al. provided most of these, as discussed in section 3.7.[54,74,96,104–106] The importance of the donor/acceptor interface was highlighted in the dipolar layer model suggested by Arkhipov et al.[107] This model suggests a reason for the efficient exciton dissociation into free charge carriers at a donor/acceptor interface despite the strong Coulomb interaction, based upon the idea that initial formation of the charge transfer state induces the formation of interfacial partial dipoles. These partial dipoles effectively generate a repulsive potential barrier separating the electron and the hole, decreasing the likelihood of geminate recombination. The model requires that the polymer chains are aligned parallel to an interface with an array of ordered acceptor molecules; this implies that both molecular order at the donor/acceptor interface and a sufficient concentration of acceptor is crucial for prevention of geminate recombination. Peumans and Forrest[24] provided one of the first reports

to investigate donor/acceptor interfaces in organic systems, where they used kinetic Monte Carlo modeling based on Onsager theory to assess the effect of donor/acceptor interfaces on dissociation of the CT state and stated that Arkhipov's model[107] had too many restrictions. They suggested instead that the presence of the interface facilitated CT-state dissociation because of a number of other factors, including the confinement of the available volume for geminate recombination to the interface, and the orientation of the $e-h$ pair at the interface such that dissociation occurs perpendicular to the interface surface. It was also observed from their model that if the electron mobility exceeded the hole mobility by a factor of 100, this also improved the dissociation probability. This was attributed to the electron in the CT state sampling a larger volume of space prior to returning to the interface (where geminate recombination may occur), thus enhancing the probability of its escape. This effect of mobility has also been observed in another study, where the presence of traps (effectively immobilizing one of the charges in the CT state) was associated with an enhancement of the dissociation probability.[108]

While Onsager theory has proven very effective in predicting experimentally observed variations in charge photogeneration in certain systems (e.g., homogeneous systems without a donor/acceptor interface) and in particular their dependence upon macroscopic electric fields, there remain significant challenges in the application of this theory to predict absolute yields of charge photogeneration at organic donor/acceptor heterojunctions. For example, current implementations of Onsager theory do not include explicit consideration of dynamic lattice distortions/relaxations addressed in the nonadiabatic theory detailed above (i.e., the concept of a reorganization energy). Furthermore, it is difficult to obtain reliable estimates for the thermalization and Coulomb capture lengths (a and r_c, respectively) in organic films. Applying eq 4 and employing $\varepsilon_r = 3.5$, typical for organic semiconductors, one obtains a Coulomb capture length r_c of ~16 nm at room temperature (298 K). However, typical organic semiconductors exhibit high levels of energetic disorder (of the order of 100 meV or more, although note that Barth et al.[103] concluded that disorder does not affect charge photogeneration efficiency at room temperature),[109,110] as well as large polarization (reorganization) energies of the dissociated charges (100s of meV).[111] As such, a more reasonable estimate of the *effective* Coulomb capture radius is likely to result from an estimation of the distance at which the Coulomb attraction equals the random energetic disorder (~100 meV). This estimate gives a significantly smaller Coulomb capture radius of ~4 nm. Similarly, empirical data on the thermalization length a is currently very limited, in particular in regard to how the presence of a donor/acceptor interface may influence this thermalization length compared to homogeneous systems.[24] A further complication is determination of the electric fields present at the donor/acceptor interface. These may be influenced by not only macroscopic electric fields generated by charge on the device electrodes but also by screening of this electrode charge by charge in the photoactive layer, the presence of interface dipoles,[107,112] and the fact that for bulk heterojunctions the interface will be randomly orientated relative to the macroscopic field. Finally, we note that Onsager theory assumes that the initial generation of the CT state is not electric-field dependent. However, a number of studies have shown that, in the case of conjugated polymers, this assumption may not be correct.[113,114] In particular, exciton dissociation in pristine polymers (as measured by photoluminescence quenching) has been shown to be enhanced by the application of an electric field.[73]

3. Charge Photogeneration in Organic Bulk Heterojunction Solar Cells

3.1. Charge Separation Interface

Building upon the Onsager picture of charge photogeneration in homogeneous systems described above, Figure 8 illustrates the process of charge photogeneration at an organic donor/acceptor interface. The corresponding state energy level diagram is shown in Figure 9, adapted from a recent review by Brédas et al.,[38] which also provides a summary of some of the limits to our understanding of the processes illustrated in this diagram. Photoexcitation promotes an electron from the donor's HOMO into the LUMO, generating the S_1 singlet exciton state (for simplicity, we neglect the potential formation of acceptor excitons). This donor S_1 state (the exciton) can be quenched by electron transfer from the donor to the acceptor. This initial electron transfer step may generate an interfacial charge-transfer (CT) state. This CT state will, in general, initially form with excess thermal energy but subsequently thermally relax with an electron−hole separation distance a (the thermalization length). In cases where the exciton is generated directly at the donor/acceptor interface, the exciton may also be thermally hot. Due to its relatively weak electronic coupling, the CT state can undergo reasonably rapid spin mixing between its singlet and triplet states. These CT states can undergo geminate recombination to form either the ground state, S_0, or a triplet exciton, T_1, depending on their spin state. Alternatively, this CT state can undergo full charge separation to form dissociated charge carriers. Following Onsager theory, the efficiency of this dissociation process will depend critically upon the magnitude of the thermal-

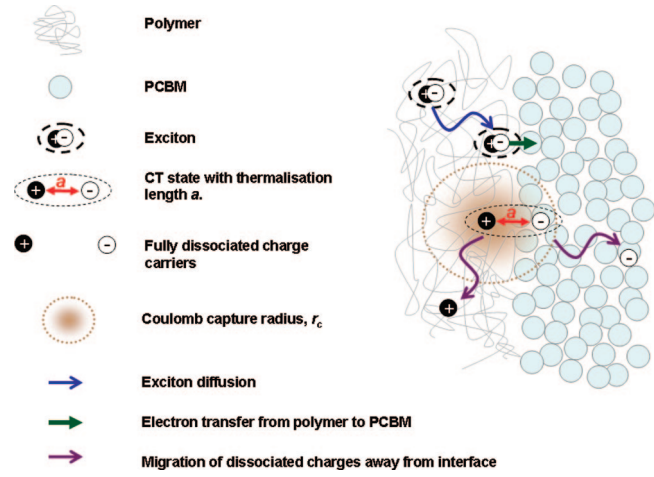

Figure 8. Schematic of charge dissociation at the polymer:PCBM interface. The polymer singlet exciton diffuses to the interface, where electron transfer to the PCBM occurs to generate the charge-transfer (CT) state. The CT state (laterally offset from the site of exciton dissociation for clarity) has an initial electron−hole separation distance of a (the thermalization length). Onsager theory would predict that the probability of full dissociation into the free charge carriers (the CS state in Figure 9) depends upon the ratio between a and the Coulomb capture radius, r_c. For simplicity, the Coulomb capture radius is drawn as spherical (i.e., isotropic), although in practice it is expected to be anisotropic due to the presence of the donor/acceptor interface.

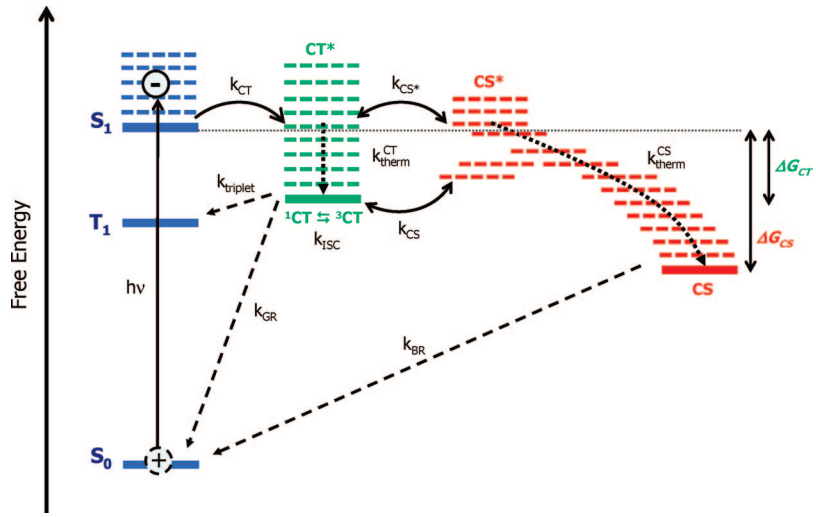

Figure 9. Energy level diagram summarizing the main processes involved in charge photogeneration. *hv*: Photoexcitation to singlet exciton (S_1). k_{CT}: Exciton dissociation to form the hot charge-transfer (CT) state. k^{CT}_{therm}: Thermal relaxation of the CT state. k_{ISC}: Spin mixing of the ^{1}CT and ^{3}CT states. $k_{triplet}$: Geminate recombination of the ^{3}CT to the triplet exciton, T_1. k_{GR}: Geminate recombination of the ^{1}CT state back to the ground state, S_0. k_{CS*}: Dissociation of the hot CT state into a fully charge-separated (CS) state. k_{CS}: Dissociation of the thermally relaxed CT state into the CS state. k^{CS}_{therm}: Thermal relaxation of the CS state and migration away from the donor/acceptor interface, resulting in an increase in state degeneracy (entropy) and charge localization on lower energy sites (traps etc.). k_{BR}: Bimolecular recombination of the CS state. This diffusion-limited bimolecular process may result from either direct recombination or, more probably, reformation of interfacial charge-transfer states (shown as reversible arrows in processes k_{CS*} and k_{CS} and subsequent geminate recombination (k_{GR})).[28] Adapted with permission from ref 38. Copyright 2009 American Chemical Society.

ization length a versus the Coulomb capture radius r_c. These carriers can then diffuse away from one another and, if successful in avoiding bimolecular recombination, will be collected at the electrodes.

Figure 9 emphasizes the potential importance of charge-transfer (CT) states in the charge photogeneration mechanism. In particular, within this viewpoint the yield of fully dissociated charges is likely to depend on the kinetic competition between the relevant processes. For the case where charge photogeneration occurs primarily from the hot CT state, the key kinetic competition will be between thermalization and dissociation (processes k^{CT}_{therm} and k_{CS*} in Figure 9). However, when charge photogeneration occurs primarily from the relaxed CT state, the primary kinetic competition will be between geminate recombination and dissociation (processes $k_{triplet}/k_{GR}$ and k_{CS} in Figure 9). As electron transfer proceeds to generate the CT state, the separation distance between the electron and hole increases and the charges therefore experience less Coulombic attraction. If the $e-h$ separation distance does increase further and the charges avoid geminate recombination by escaping beyond the Coulomb capture radius, then the free fully dissociated charge carriers have formed. Due to the energy offset of the donor and acceptor energy levels, the electron injected into the acceptor will initially be thermally hot (corresponding to the 'crossing point' in Marcus electron transfer theory). Following the Onsager picture, the efficiency of the overall dissociation process is likely to depend upon the distance from the donor/acceptor interface at which the electron loses its excess thermal energy (the thermalization length a).

We note that most considerations of charge photogeneration do not include consideration of the change in entropy associated with changing from a single species (the exciton) to two separated charges with random positions relative to each other. Such analyses can therefore often be ambiguous as to whether they are considering potential or free energies. Figure 10 illustrates the potential importance of entropy

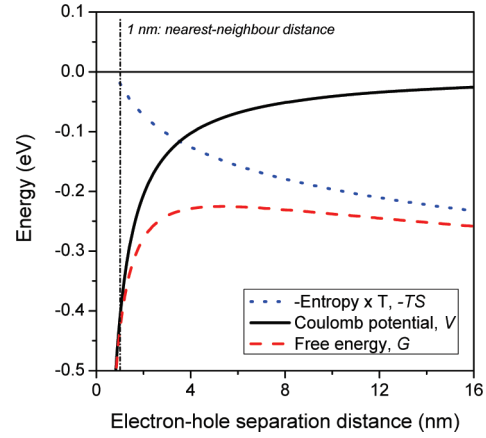

Figure 10. Illustration of the energetics of electron−hole pairs at a typical donor/acceptor interface, showing calculations of the Coulomb potential energy (from eq 1), the entropy contribution to the free energy ($-TS = -k_BT \ln W$), where W is the electronic degeneracy, and the free energy ($G = H - TS$) as a function of electron−hole separation distance. For simplicity we assume the hole to remain localized at the interface and only consider the electron movement. The parameters used in the calculations are $\varepsilon_r = 3.5$ and $T = 298$ K. W was approximated as the number of C_{60} species in the volume of a hemisphere extending from the interface, assuming each C_{60} molecule occupies 1 nm^3.

contributions to the overall interfacial energetics. It is not intended to be rigorous calculation but only an approximate illustration of these energetics. A simple point dipole calculation is employed to determine the Coulomb attraction of the CT state relative to the dissociated charges at a typical donor/acceptor heterojunction, following eq 1. The calculation assumes $\varepsilon_r = 3.5$ and neglects macroscopic electric fields. It assumes that the initial electron transfer from the donor to the acceptor yields a charge separation of 1 nm, corresponding to the typical dimensions of donor and acceptor orbitals. The resultant potential energy of the thermalized CT state as a function of spatial separation of the electron and hole is shown as the solid line in this figure.

It is apparent that the potential well depth, corresponding to the Coulomb attraction of a nearest neighbor electron−hole pair localized at the donor/acceptor interface, is ∼0.4 eV. This Coulomb attraction energy reduces to 0.1 eV (corresponding to typical estimates for energetic disorder in organic materials) at ∼4 nm. We consider this as a reasonable estimate for the effective Coulomb capture radius r_c. The dashed line corresponds to the associated free energy, which differs from the potential energy (the solid line) by the inclusion of the increase in entropy (dotted line, corresponding to $-TS$) as the charge separation distance is increased (see caption for details). This entropy increase derives from the greater number of acceptor molecules available for the electron as the separation increases (we assume the hole remains relatively immobile). It is apparent that this entropy contribution serves to stabilize the CS states relative to the CT state. It is also evident that this entropy contribution to the total reaction free energy is of a similar order of magnitude to the Coulomb binding energy. The effects of Coulomb attraction and entropy are counterpoised, resulting in a maximum in the free energy surface at ∼5 nm. Charge dissociation will, in general, lead to formation of a quasi-static thermal equilibrium of CT and CS states. This equilibrium will subsequently decay either by charge collection at the device electrodes (photocurrent generation) or by recombination to the ground state. This illustration is not intended to be real analysis of the interfacial energetics; for example, it neglects both the formation of interfacial dipoles and energetic disorder. However, it does emphasize that the increase in degeneracy (entropy) is a key factor stabilizing charge separation at the donor/acceptor heterojunction.

The overall free energy loss associated with charge photogeneration is illustrated in Figure 9 as ΔG_{CS}. We define ΔG_{CS} as the difference in energy between the singlet exciton and the dissociated charge-separated state,[23,27] where the latter can be estimated as the energy difference between the electron affinity of the acceptor and the ionization potential of the donor ($IP_D - EA_A$). The ΔG_{CS} is correlated with the LUMO level offset between the donor and acceptor, but it also includes the effect of the Coulomb binding energy of the exciton, E_B^{exc}. We note that this ΔG_{CS} differs from the free energy driving the initial separation of the exciton to form the charge-transfer state (which we refer to later as ΔG_{CT}) due to the difference in free energies of the charge-transfer and charge-separated states. In terms of the overall efficiency of solar energy conversion, a key challenge is to minimize the free energy loss associated with charge photogeneration (ΔG_{CS}).

A related concern is to maximize the lifetime of the charge-separated states to enable efficient charge collection by the device electrodes. As such, a compromise is required between the need to optimize charge separation by a high interface surface area and large donor/acceptor electronic coupling and the need to maximize the lifetime of the charge-separated states by minimizing interface surface area and reducing donor/acceptor electronic coupling. Balancing these two opposing requirements is important for achieving high overall device efficiencies.[115]

Of particular importance is the role of interfacial charge-transfer states in the charge photogeneration process. Unfortunately, there are relatively few experimental reports in the literature that directly investigate the formation and dissociation of CT states in organic donor/acceptor blends due to the difficulties in measuring such a short-lived species. In addition, most reports agree that the transient absorption spectrum of the CT state is indistinguishable from that of the dissociated charges,[116–119] although there are exceptions to this conclusion.[120–123] The following sections will discuss in detail the presence and significance of the CT state, focusing on the varied attempts to measure and model its generation, dissociation, and recombination.

3.2. Evidence for the Presence of Interfacial Charge Transfer States in Organic Donor/Acceptor Films

Interfacial charge-transfer (CT) states in donor/acceptor heterojunctions are most easily observed if they are coupled radiatively to the ground state; steady-state and time-resolved photoluminescence (PL) measurements can therefore be applied.[18,19,21,22,25,26,124–126] Emissive CT states have been shown to be characterized by a broad, red-shifted PL band (usually with a long radiative lifetime) that occurs only in the blend and cannot be assigned to PL from either of the individual components. For example, it has been reported by Friend et al. that emission from such CT states (often referred to as 'exciplex' emission) is generally observed for polyfluorene donor/acceptor blends,[125] with this phenomenon being observed in poly(dioctylfluorene):PFB,[125] PFB:F8BT,[21,127,128] and TFB:F8BT blends[21] (polymer structures are displayed in Figure 4). CT emission has been observed in other polymer:polymer blends as well,[129] such as MDMO-PPV:PCNEPV[22] and other PPV-based polymers.[26] This red-shifted, long-lived emission has proved to be an effective probe of the function of CT states in influencing charge photogeneration, as we discuss below.

Although most examples of CT emission come from polymer:polymer blends, there have been reports of such emission from polymer:fullerene blends. One such example is a paper by Loi et al.,[19] which compared the emission behavior of F8DTBT:PCBM blends (F8DTBT has also been called APFO-3 in the literature) with F8BT:PCBM. In the case of F8BT:PCBM, no evidence of CT emission was observed. This is consistent with the high ionization potential (IP) of F8BT (5.9 eV) raising the energy of the charge-separated state such that it is thermodynamically unfavorable. In contrast, F8DTBT has a much lower IP (∼5.5 eV) and the charge-separated state is thus expected to be the lowest energy excited state. Indeed, in addition to strong PL quenching in the blend, the CT state of F8DTBT:PCBM was observed as the typical red-shifted emission (Figure 11a). Emissive polymer:small molecule CT states have also been noted in several other reports.[18,25,130,131]

We note that, in certain polymers, CT emission has also been observed in pristine polymer films. For example, photoluminescence measurements on CN-PPV solutions compared to films revealed evidence for emissive CT states in the form of a weaker, significantly red-shifted emission peak in the solid state that decayed several times slower than the corresponding emission peak in the solution.[126] This was attributed to the formation of interchain excitons ('excimers'), equivalent to CT states under our definition. The lack of such an emission for MEH-PPV, however, was attributed to the larger interchain distance for this polymer, thereby reducing the wave function overlap and the efficiency of radiative decay. It was concluded that the MEH-PPV CT state, if generated, is more likely to relax nonradiatively back to the ground state.

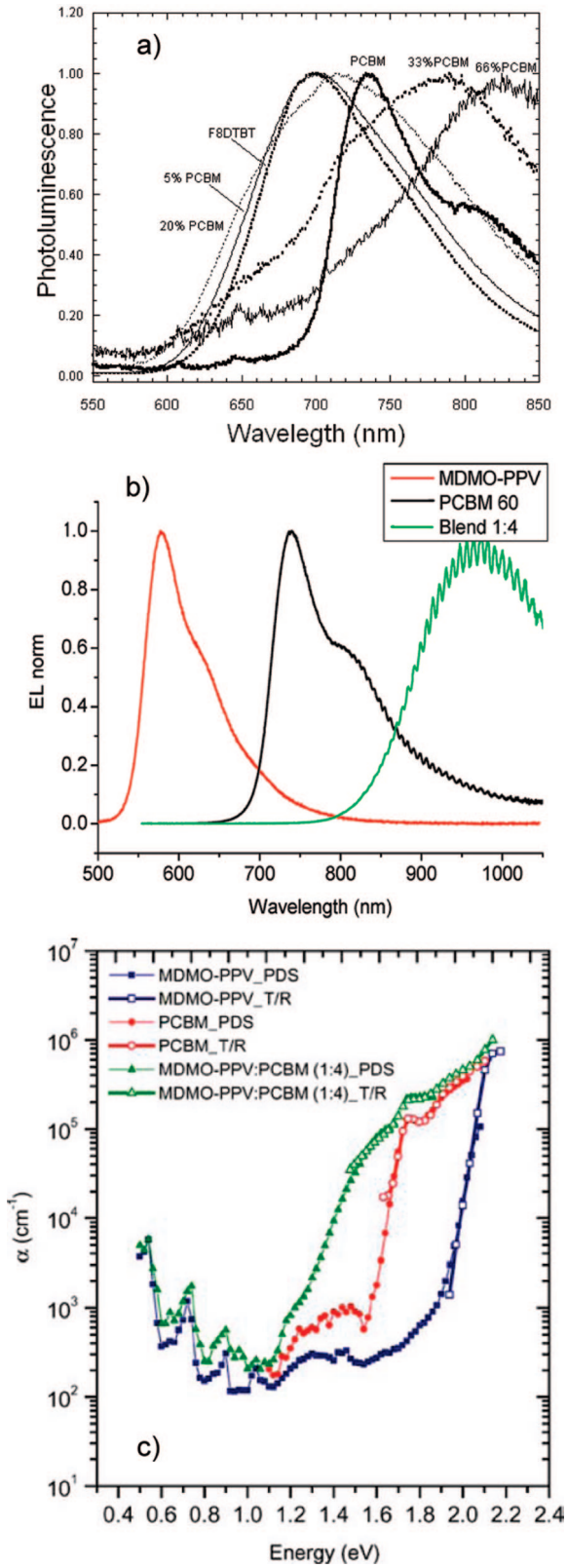

Figure 11. (a) Normalized photoluminescence spectra of F8DTBT and PCBM blends with varying composition ratio, showing formation of the red-shifted CT state at high PCBM concentrations. Reprinted with permission from ref 19. Copyright 2007 Wiley. (b) Normalized electroluminescence spectra of pristine MDMO-PPV, PCBM, and the blend. Reprinted with permission from ref 28. Copyright 2009 American Chemical Society. (c) Absorption spectra of MDMO-PPV, PCBM, and the blend film utilizing both PDS and standard absorption spectroscopy, showing the additional ground-state absorption in the blend film assigned to the CT state. Reprinted with permission from ref 30. Copyright 2005 Springer.

Electroluminescence (EL) also provides a useful method for examining CT-state emission. In this case, CT states are created by charge carrier injection into a device. This is followed by recombination to form the lowest energy excited state of the blend system: the CT state. As such, CT emission can be observed without interference from coinciding photoluminescence bands of the individual components in the blend and can thus be observed in systems where the CT emission is too weak to be observed by photoluminescence studies. In this context, EL studies have recently been employed to observe CT-state emission in a series of polymer:PCBM blend films, including P3HT:PCBM, MDMO-PPV:PCBM, and APFO-based polymers.[28,132] In each of these examples, red-shifted electroluminescence in the blend film was observed compared to the EL of the pristine materials. The CT emission of MDMO-PPV:PCBM, for instance, was observed at 970 nm, whereas the pristine polymer EL was measured at ~580 nm and PCBM at ~740 nm, as shown in Figure 11b.

Although the CT state can most easily be observed if it is emissive, recent results in the literature suggest that this species can also exhibit ground-state optical absorption. Because of the very low absorption extinction coefficients of the CT state,[32] standard steady-state absorption spectroscopy is not an appropriate technique; this has often led to the conclusion that no ground-state interaction exists at the donor/acceptor interface, in part justifying the use of the term 'exciplex' in the literature. Goris et al. provided the first reports on this topic, using photothermal deflection spectroscopy (PDS) as a more sensitive probe of the sub-band-gap transitions in MDMO-PPV:PCBM[30] and P3HT:PCBM[133] blend films that are not present in spectra of the individual materials. This is shown for MDMO-PPV:PCBM in Figure 11c. The origin of the sub-band-gap absorptions in both systems was, however, initially attributed to defects. Subsequently, it has been proposed that such sub-band-gap absorption transitions arise due to direct optical excitation from the electronic ground state to an interfacial charge-transfer state.[18] This study of TFMO:PCBM blend films revealed, in addition to the red-shifted emission attributable to the CT state, a clearly visible sub-band-gap absorption in the PDS spectrum. This species was suggested to be critical to the charge photogeneration process as it was only observed in those systems where a reasonable photocurrent was produced. The observation of direct optical excitation of the CT state implies significant wave function overlap across the donor/acceptor interface for the ground and/or CT states. Indeed, using Raman spectroscopy (an excellent probe of the changing electron density in conjugated systems upon electron transfer), Paraschuk et al.[29] concluded a partial electron transfer of 0.1 *e* in the ground state for MEH-PPV/trinitrofluorenone.

The presence of this ground-state interaction suggests that the excited CT state can be directly generated using sub-band-gap photoexcitation, and this has indeed been observed.[32,134] In particular, Sheng et al.[134] observed that excitation coincident with the CT-state absorption directly produced evidence of polymer polarons, as measured using photomodulation spectroscopy of MEH-PPV:PCBM. Conversely, excitation of the same blend using higher energies (coincident with the polymer absorption) produced spectral signatures of both polymer singlet excitons and polarons. Furthermore, the polarons generated using sub-band-gap excitation of the ground-state CT state occurred only in the

blend film and not in the pristine polymer. However, it should be noted that polarons generated via this mechanism may still be Coulombically bound and, in addition, are unlikely to make a large contribution to the photocurrent due to the low absorption extinction coefficient of the CT state.[32]

Indirect evidence of charge-transfer-state formation and recombination has come from observation of enhanced triplet exciton yields in donor/acceptor blend films, assigned to geminate charge recombination from triplet CT states. In general, we expect rapid spin mixing, via hyperfine interaction spin dephasing[135] or spin−orbit coupling,[136] of the CT state that is facilitated by the weak spin−spin interaction (compared to the singlet exciton) and results in near degeneracy of the singlet and triplet CT states. Geminate recombination of the CT state can therefore proceed not only to the singlet ground state but also to the triplet exciton. We note that the efficient generation of polymer triplets rather than charge carriers requires that the energy level of the polymer triplet lies below that of the charge-separated state. This is particularly likely to be the case for high-IP polymers, as the high IP raises the energy of the charge-separated state above that of the polymer triplet, as observed in both polythiophene and polyfluorene systems (vide infra).[18,137,138] This charge-separation/recombination mechanism for triplet formation has been widely reported in photosynthetic reaction centers and donor/acceptor systems in solution[47,48] and oligothiophene:fullerene blends in thin films.[139]

There have been several reports of triplet formation in organic donor/acceptor blend films assigned to geminate recombination from interfacial charge-transfer states. For example, Ohkita et al.[140] utilized transient absorption spectroscopy (TAS) to investigate triplet formation in a series of polythiophene:PCBM blend films. For all blend films studied, the polymer singlet exciton photoluminescence was strongly quenched relative to the pristine polymers, even for only 5 wt % added PCBM, indicating that the yield of direct intersystem crossing (ISC) from the polymer singlet exciton to the triplet exciton would be very low. However, for the amorphous polythiophenes studied, significant triplet yields were observed in the blend films, based on oxygen-quenching studies and a monoexponential decay of the transient signal. The authors concluded that the polymer triplets were generated by geminate recombination from the triplet CT state, as discussed above. This phenomenon has also been observed in other systems, including polymer:polymer blend films.[118,141,142] Furthermore, the efficient generation of polymer triplets in these blend films rather than charge carriers indicates that the energy level of the polymer triplet lies below that of the charge-separated state. This was attributed to the high ionization potentials of these polymers, such as $PT_8T_8T_0$ with an IP of 5.6 eV. This IP is appreciably higher than P3HT, for example, which has an IP of approximately 4.9 eV. The high IP raises the energy of the charge-separated state above that of the polymer triplet, thereby suppressing this pathway. As such, the formation of triplets represents a significant loss mechanism in this system. Greenham et al. reported a detailed kinetic model of these processes for PFB:F8BT blend films.[141,142] They also demonstrated that formation of these triplet exciton occurs with the same time constant as decay of the CT-state emission (∼100 ns), thereby providing confirmation that the observed triplet excitons were indeed formed by charge recombination from the interfacial CT state.[142]

A more recent study also concluded that geminate recombination forms triplet excitons in this PFB:F8BT blend system.[118] Ultrafast transient absorption measurements indicated a delayed increase in the intensity of the F8BT triplet-state absorption band as the CT-state absorption band decayed. This ISC/recombination process occurred with high efficiency, with ∼75% of CT states following this pathway prior to 40 ns. In addition, simultaneous anisotropy measurements showed that the polaron transient absorption band retained a high level of polarization anisotropy into the nanosecond time regime, suggesting a highly immobile CT state at the donor/acceptor interface.

It can be concluded from the above that there is now clear evidence for the formation of charge-transfer states in organic donor/acceptor films. We will discuss below the functional importance of such states in limiting charge photogeneration and overall photovoltaic function.

3.3. Exciton and Charge Transfer-State Binding Energies

In this section we consider estimates of the binding energies of the excitons and charge-transfer states, E_B^{exc} and E_B^{CT}, respectively. The exciton binding energy, E_B^{exc}, is typically defined as the potential energy difference between the neutral singlet exciton and the two fully dissociated, structurally relaxed charge carriers in the same material. Similarly, we define the charge-transfer-state binding energy, E_B^{CT}, as being the potential energy difference between the thermally relaxed, nearest neighbor charge-transfer state at the donor/acceptor interface and the two fully dissociated, structurally relaxed charge carriers in the donor and acceptor materials. We consider first E_B^{exc} and then E_B^{CT} and conclude with a comparison of these two binding energies.

Efficient quenching of the singlet exciton by electron transfer at the donor/acceptor interface places certain restrictions on the energetics of the system. In particular, there must be sufficient energy present to overcome the Coulomb binding energy of the exciton, E_B^{exc}. However, direct experimental measures of the magnitude of this binding energy remain controversial. The source of this dissension results in part from the disordered nature of conjugated polymers, which prevents parameters such as the exciton binding energy from being well defined. For PPVs,[143,144] estimates for the exciton binding energy range from less than 0.1 eV to over 1 eV. In polydiacetylenes, E_B^{exc} has been estimated at ∼0.5 eV by a comparison of the onset of the ground-state absorption (1.8−1.9 eV) and the onset of photoconductivity (2.3−2.5 eV);[145] this was supported by independent electroabsorption measurements.[146,147] However, this polymer is very different from other commonly studied polymers, such as PPV, in that it has a much higher level of crystallinity, which may possibly affect the exciton properties. PPV has therefore also been examined in this respect; the observation that the onsets of both optical absorption and photoconductivity occur at the same energy for PPV has led some authors to suggest a very small E_B^{exc} (<0.1 eV) for this polymer; consequently, the primary photoexcitations are claimed to be mobile charge carriers.[143,144] However, extensive optical spectroscopy studies performed at low excitation densities have indicated the presence of an intrachain singlet exciton in PPV,[57,148,149] and there is also a significant body of experimental and theoretical[4,150] work that indicates a higher E_B^{exc} for PPV, of the order of ∼0.4 eV. For instance, the energy splitting between the first excited singlet and

triplet is over 0.7 eV, suggesting a large exchange interaction,[151,152] and efficient fluorescence quenching of pristine PPV requires a strong electric field.[153,154] These authors suggest the coinciding photoconductivity/absorption onsets are due to surface photoionization or sensitization by impurities acting as electron donors. Polyalkylthiophenes have been less extensively studied in this regard, but electroabsorption results indicate an exciton binding energy of ~0.6 eV.[155]

Experimental estimates of the exciton binding energy have often been based upon estimates of the minimum LUMO level offset required to separate excitons at organic donor/acceptor interfaces. We note that such analyses do not consider the presence of interfacial charge-transfer states. It has been suggested in the literature that a LUMO level offset of 0.3 eV is sufficient for efficient charge separation,[156] and this value is used in many other studies as a justification for lowering the polymer LUMO in order to achieve a smaller band-gap material without sacrificing V_{OC} (by raising the donor HOMO instead).[35,36] We note, however, that experimental data to support the validity of this 0.3 eV LUMO level offset requirement is very limited. The most commonly cited papers to support this value are theoretical studies of PPV polymer blends which stated 0.35 eV as the energy required for a transition between intrachain and interchain excitons.[37,157] As such, this value cannot be expected to apply to every blend system and certainly not to all donor/acceptor heterojunctions.

We turn now to consideration of experimental measurements of the charge-transfer-state binding energy E_B^{CT}. For a CT state that is emissive (i.e., geminate recombination back to the ground state is a radiative process), its energy can be estimated directly from the photoluminescence spectrum. Alternatively, it is possible to utilize oxidation and reduction potentials from cyclic voltammetry in conjunction with singlet exciton energies estimated from absorption spectroscopy for this purpose.[27] The energy of the CT state, E_{CT}, is approximated as the difference in energy between the electron affinity of the acceptor and the ionization potential of the donor ($IP_D - EA_A$) plus another term to account for the binding energy of the CT state, E_B^{CT}.[31] The binding energy of a CT state is usually estimated to be lower than the singlet exciton (due to the increased electron−hole separation distance) and is typically estimated at approximately 0.1−0.5 eV.[22,74,130,158] This is, however, still significant and needs to be overcome in order for the charges to be fully dissociated. For example, in one of the most detailed studies reviewed here, Veldman et al.[27] estimated the energy of the CT state of P3HT:PCBM to be $E_{CT} = 1.0$ eV. In conjunction with the energy of the charge-separated state estimated as $E_{CS} = IP_D - EA_A = 0.7$ eV, this gives an approximate CT-state binding energy E_B^{CT} of 0.3 eV.

The energy of the CT state can be tuned by altering the composition of the blend. This was noted by Loi et al.,[19] where CT emission in F8DTBT:PCBM blends was investigated. As the concentration of PCBM in the blend was increased, the red shift of the CT emission (compared to the pristine components' emission) became larger. This was attributed to the higher dielectric constant of PCBM ($\varepsilon_r = 4$) than the polymer: as the PCBM content is increased, the effective dielectric constant of the blend is also increased, stabilizing the CT state and consequently lowering its energy.[19] This has also been observed elsewhere.[25,32] In addition, the improved screening of the charges should also reduce the effective Coulombic interaction between the hole and the electron and thus decrease the Coulomb capture radius, facilitating dissociation of the CT state into free carriers. This was suggested in a similar study by Nelson et al.[18] The energy of the CT state also appears to be sensitive to film processing; for example, thermal annealing decreases the energy of the CT state for P3HT:PCBM.[28] This was also observed by Goris et al.[133] as a small decrease in the energy of the sub-band-gap absorption after annealing of P3HT:PCBM, assigned to the tail of the density of states extending deeper into the band gap. It is also consistent with other, more recent, reports that conclude a decrease in energy of the P3HT:PCBM CT state after annealing, on the basis of Fourier-transform photocurrent spectroscopy[32] and cyclic voltammetry (inferred from a decrease in polymer ionization potential).[52]

In our discussion of binding energies above, we avoided specifying whether these binding energies are potential or free energies. As we illustrated in Figure 10, the entropy contribution to the overall free energy change associated with charge photogeneration can be of similar order of magnitude to the enthalpy (potential energy) change. Most discussions of binding energies focus only upon the Coulomb attraction energy and therefore address only potential rather than free energy, although some studies have considered free energy.[27] In general, a potential energy approach is relevant to consideration of the energy barrier impeding exciton or CT-state separation and therefore to kinetic analyses of this separation, while a free energy analysis is necessary where reverse processes (e.g., recombination of separated polarons to form interfacial CT states) are considered. A full analysis of this issue is however beyond the scope of this review.

We further note that analyses of the LUMO level offset required to overcome the Coulomb attraction of the exciton do not consider the Coulomb attraction of the initial generated charge-transfer states. In this respect, the HOMO−LUMO diagrams frequently portrayed in the literature can be misleading as they do not take this phenomenon into account. As we discuss above, estimates of E_B^{CT} are typically non-negligible relative to the E_B^{exc}. In the extreme limit where $E_B^{exc} = E_B^{CT}$, the initial exciton quenching to yield charge-transfer states would only require a LUMO level offset greater than k_BT (neglecting kinetic considerations). In terms of exciton quenching, it may therefore be most relevant to consider the energy difference between the exciton and thermally relaxed charge-transfer state, indicated as ΔG_{CT} in Figure 9. This point has been considered by Janssen et al.,[27] who examined ΔG_{CT} for a series of polymer:PCBM blends. It was concluded that only a minimal driving force is required to generate the CT state, $\Delta G_{CT} < 0.1$ eV; as such, the principal energy loss required for charge separation occurs after the initial creation of the CT state and is associated with overcoming the Coulomb binding energy of the CT state. This conclusion is consistent with the report by Ohkita et al.[23] (vide infra) and suggests that the majority of free energy required for driving the generation of free charge carriers is associated with the dissociation of the CT states into free charges, as we discuss further in section 3.6.

3.4. Photophysics of Charge Photogeneration in Organic Films

In this section we consider the results of general photophysical studies of charge photogeneration in organic films. This section provides the background and context to our more

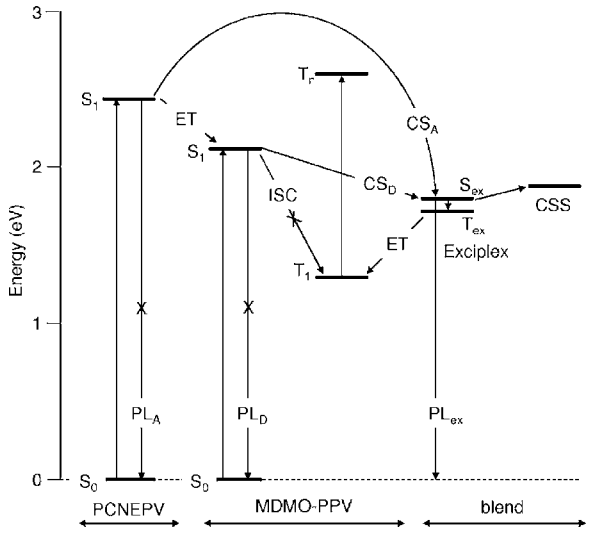

Figure 12. Illustration of the energetics of the states involved in charge-separation in a polymer:polymer blend and the associated energy, electron, and intersystem crossing processes. Reprinted with permission from ref 22. Copyright 2005 American Physical Society.

in-depth consideration of the role of interfacial donor/acceptor charge-transfer states in charge photogeneration which we address in sections 3.5−3.10.

3.4.1. Interfacial Energetics: Singlet and Triplet Exciton Energies versus CT-State Energies

A fundamental requirement for the energy levels presented in Figure 9 is a downhill energetic driving force such that the donor is capable of transferring an electron to the acceptor. This was observed in studies by Sensfuss et al.[159] and Janssen et al.,[27] both of which examined photogeneration (or lack thereof) in polymer:acceptor blends where the constituents' energy levels were varied. Conversely, if the driving force for charge separation is too large, then Marcus inverted region kinetics will result, lowering the rate constant for electron transfer.[160] A second fundamental thermodynamic requirement for efficient charge photogeneration is that the charge-separated state must be the lowest energy excited state in the system.[41] As discussed above, it is possible that the donor ionization potential may be large enough to raise the energy of the charge-separated state such that it is higher than the other possible states, namely, the singlet and triplet states of the acceptor and/or the polymer triplet state. This would effectively deactivate the charge-separation pathway and therefore suggests that the relative energies of all the states presented in Figure 9 are of crucial importance in achieving efficient charge photogeneration. For example, energy transfer can occur from the donor singlet exciton to the acceptor, and this process can compete with the more desirable process of electron transfer.[161] Efficient energy transfer generally requires a good overlap between the donor emission and acceptor absorption spectra and also strong dipole−dipole coupling, although the latter may not be necessary for polymer:fullerene blends and/or dyads.[162] A typical state diagram, illustrating the energetics of singlet and triplet excitons, the energy of the interfacial charge-transfer state (referred to in the diagram as the exciplex state) and the dissociated polarons is shown in Figure 12.

The concept of energy versus electron transfer was examined by Halls et al.[157] One blend system, MEH-PPV:CN-PPV, demonstrated electron transfer and produced reasonably efficient devices. DMOS-PPV:CN-PPV, on the other hand, exhibited energy transfer, where excitation of the DMOS-PPV in the blend led to emission exclusively from the CN-PPV. Theoretical calculations on both systems indicated that the energy of the charge-separated state is lower than the S_1 state of CN-PPV only for MEH-PPV:CN-PPV. In DMOS-PPV:CN-PPV the energies of these two states are reversed; therefore, energy transfer is the preferred pathway instead of electron transfer. This example shows how a change in substitution, and thus in the frontier molecular orbitals, can affect the outcome of an exciton at a donor/acceptor interface.

Benson-Smith et al.[18,137] studied a series of polyfluorene polymers in blends with PCBM and found that those with a high ionization potential (above 5.5 eV) produced evidence of PCBM triplets instead of the desired charge carriers. The photoluminescence spectrum of the polyfluorene blends (with 5 wt % PCBM) revealed total quenching of the polymer emission and a PCBM singlet peak at 710 nm, thereby indicating an efficient energy transfer process from the polymer exciton to the PCBM. The presence of PCBM triplets was subsequently observed in the transient absorption spectra with a characteristic ^{3}PCBM* peak at 720 nm[163] that decayed monoexponentially with a lifetime of $\sim$10 μs. The absence of charge separation in these blends and resulting lack of long-lived polarons was indeed attributed to the high ionization potentials raising the energy of the charge-separated state above that of the PCBM singlet. A similar, earlier study of F8BT:PCBM blend films[138] also observed PCBM triplet states assigned to singlet energy transfer from the F8BT to PCBM followed by intersystem crossing. This triplet formation is consistent with its poor device performance.[19] For polymers with lower IPs, however, evidence of polymer polarons was observed in the transient spectra,[18,137] further supporting the argument for the importance of the energy of the charge-separated state. In addition, one polymer (RedF, a fluorene/benzodithiazole-based polymer) with an intermediate IP of 5.3 eV produced both polarons and PCBM triplets, depending upon the blend composition. Triplets were present at low PCBM concentrations (5 wt %), while polarons were measured at high concentrations (50 wt %). It was noted in a study by Janssen et al.[25] that increasing the concentration of PCBM in a polyfluorene blend lowered the energy of the CT state: it is therefore possible that such an effect is also applicable to RedF, where increasing the PCBM content lowers the energy of the CT state below that of the PCBM singlet. The above results thus show that the energy of the charge-separated state is of great importance in achieving efficient charge photogeneration. Lowering the polymer HOMO to achieve a higher V_{OC} should therefore be treated with caution as this may raise the energy of the charge-separated state to the point where it is no longer thermodynamically accessible and alternative pathways to lower energy triplet states may be activated instead. This could be highly detrimental to the charge photogeneration yield.

Donor/acceptor energy transfer does not necessarily constitute a loss mechanism, as in the above examples, although it should be noted that in general it does reduce the energy of the exciton. After energy transfer from the donor to acceptor, charge separation could then occur via hole transfer from the acceptor HOMO to the donor HOMO. This indirect electron transfer process, which produces the same end result as direct electron transfer, has been observed for oligophenylene−fullerene

dyads.[162,164] In these studies, it was observed that the second step (the electron transfer) only occurred in polar solvent due to the stabilization of the charge-separated state. However, the above examples do highlight the need for energy levels to be tuned in order to ensure the charge-separation pathway is energetically favorable.

3.4.2. Geminate versus Bimolecular Recombination Kinetics

Bimolecular recombination involves the recombination of fully dissociated charge carriers that did not previously belong to the same charge-transfer state. Geminate (monomolecular) recombination, in contrast, involves recombination of charge carriers that were generated from the same exciton. There are two possibilities for this type of recombination. First, geminate recombination could occur between the two charges while Coulombically bound in the CT state. Second, if after escaping their Coulombic attraction both charges remain confined by the physical sizes of their respective domains, such that each electron can only recombine with its original hole, then recombination remains a monomolecular, geminate process.

Bimolecular recombination differs from monomolecular (or geminate) recombination in that the charges must diffuse to within their Coulomb capture radius of each other before recombination. Except for the case of very high charge densities, this diffusion process significantly retards the overall kinetics. Thus, in general, geminate recombination dynamics are expected to be faster than bimolecular recombination. Typical time scales reported for geminate recombination in organic donor/acceptor films range from hundreds of picoseconds up to $\sim$100 ns.[77,116,120,165–167] Bimolecular recombination dynamics have been observed extending out to the millisecond time scale, although these can accelerate into the nanosecond time scale as the charge density is increased. Apart from distinguishing these recombination processes on the basis of their time scale,[77] it is also possible to distinguish them in terms of their kinetic and excitation density behavior. In general, the dynamics of geminate recombination should be independent of excitation density (except at very high excitation densities such that different CT states interact with each other) and exhibit monoexponential decay dynamics. In contrast, bimolecular recombination involves the recombination of two fully dissociated charge carriers and thus follows (for equal charge densities and in the absence of disorder) second-order kinetics. This results in the recombination dynamics exhibiting power law type decay dynamics that accelerate as the excitation density is increased. In practice, the bimolecular recombination dynamics of organic donor/acceptor films have been shown to be strongly influenced by the presence of charge trapping.[23,168–174]

It should be emphasized that the bimolecular recombination accelerates strongly with increasing excitation density and can, at high excitation densities, give similar decay dynamics to geminate recombination processes. In order to ensure charge carrier densities comparable to those in typical organic solar cells under normal operation (approximately $10^{16}-10^{17}$ cm^{-3}), excitation densities should be $\ll$100 μJ cm^{-2}, resulting, for example, in optical density (ΔOD) transients of typically less than 10^{-3}.

3.4.3. Ultrafast Spectroscopy of Charge Transfer States in Organic Films

Several studies have reported ultrafast transient optical studies of charge photogeneration in organic donor/acceptor blend films, including the first study by Brabec et al., who reported charge generation in MDMO-PPV:PCBM blend films occurring within <100 fs.[14,78,120,175] Several of these studies have addressed the formation and decay of CT states in particular. In general, ultrafast spectroscopy of charge-transfer states in organic films is complicated by the similarity of their photoinduced absorption spectra to that expected for dissociated polarons. One strategy to address this is two-pulse femtosecond measurements of photocurrent generation, which has been employed to monitor CT states in pristine MeLPPP.[176] This technique is considered to be capable of distinguishing between CT states and fully dissociated polarons. The first femtosecond pulse generates the intrachain exciton, while the second pulse (with a variable time delay and a sub-band-gap photon energy that is unlikely to directly excite the polymer) re-excites the CT state into a higher lying state with a greater dissociation probability. For pristine MeLPPP, it was observed that the second pulse probed a neutral excitation and produced an increase in the photocurrent. This 'neutral' species was assigned to the CT state, which dissociated into free charge carriers upon excitation by the second pulse, thereby enhancing the photocurrent. Pre-existing fully dissociated polarons would not have increased the photocurrent after the second pulse. In the case of pristine MeLPPP, only approximately 10% of photons generate CT states and the singlet exciton is therefore the primary photoexcitation. Since not all CT states will go on to dissociate into the free charge carriers, it is evident that charge photogeneration is highly inefficient in the pristine polymer.

The same technique was applied to blend films of MeLPPP (a ladder-type PPV derivative) and MDMO-PPV with PCBM.[117] Despite a larger hole mobility for MeLPPP, device performance was more than an order of magnitude greater for MDMO-PPV:PCBM. For MeLPPP:PCBM, the polaron absorption measured at 1.9 eV prior to 100 ps was assigned to CT states on the basis that, as observed for the pristine polymer, the sub-band-gap second pulse enhanced the photocurrent (Figure 13a). The rise time of the photocurrent corresponded to the formation time of the CT state and decreased with increasing PCBM concentration, consistent with a shorter migration time of the polymer exciton before reaching a donor/acceptor interface. For 20 wt % PCBM, for instance, CT-state formation is complete within 15 ps. The results for MDMO-PPV:PCBM were very different: the measured polaron absorption at 1.78 eV prior to 100 ps was assigned to fully dissociated charges because application of the second pulse did not increase the photocurrent, as shown in Figure 13b. This comparison suggests that dissociation of CT states into free charge carriers occurs on a much faster time scale for MDMO-PPV:PCBM compared to MeLPPP:PCBM and therefore is significantly more efficient. This would increase the relative charge photogeneration yield for MDMO-PPV, consistent with its greater device performance.

An ultrafast spectroscopic study by Moses et al.[120] investigated the connection between thermal annealing and geminate recombination of P3HT:PCBM blend films and concluded that thermal annealing resulted in a shorter lifetime of the CT state due to enhanced dissociation into the free charge carriers. Thermal annealing is well known, particularly

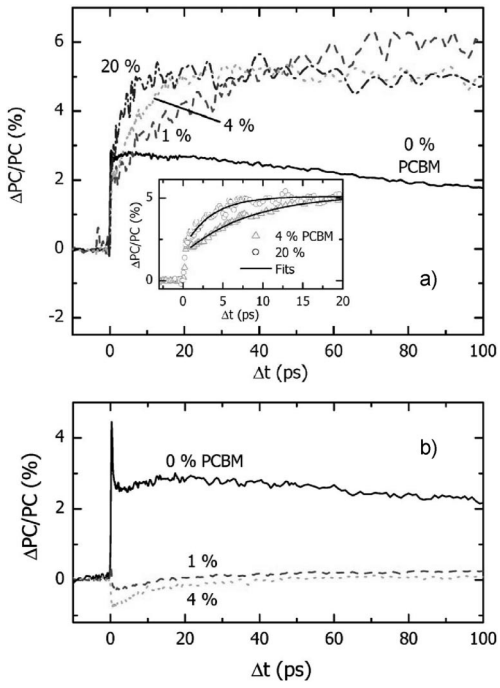

Figure 13. Time-resolved two-pulse photocurrent data for (a) MeLPPP:PCBM and (b) MDMO-PPV:PCBM with varying blend composition after application of two laser pulses (see text for details), where the second laser pulse has an energy coincident with the polaron absorption at 1.9 (a) and 1.78 eV (b), respectively. Reprinted with permission from ref 117. Copyright 2005 American Physical Society.

for P3HT:PCBM, for its ability to significantly enhance device efficiencies,[177–180] primarily through an increase in photocurrent (see section 3.9 below). Moses' conclusions[120] are based on a re-evaluation of the transient absorption spectrum of P3HT:PCBM reported by Österbacka et al.,[181,182] where two 'localized' polaron transitions and two 'delocalized' polaron transitions are measured. Moses et al. suggest that the 'delocalized' polaron bands are due to dissociated polarons and the 'localized' bands are due to the P3HT polaron within the CT state. Note that this group appears to be one of the few that have concluded that fully dissociated polarons and CT states have different absorption spectra; most reports state that the transient absorption bands of the CT state will be identical to those of the dissociated charges.[116–118] Clearly, this is a topic that requires further investigation.

3.5. Functional Importance of Charge Transfer States for Charge Photogeneration

The efficiency of dissociation of the CT state into free charge carriers is a crucial factor determining the charge photogeneration yield. In this and the following sections we consider the evidence that such charge-transfer states do indeed influence the efficiency of charge photogeneration and photocurrent generation in organic donor/acceptor solar cells.

One study which yielded relatively clear evidence that exciton quenching may not be a sufficient indicator of charge photogeneration in organic donor/acceptor films is that of Okhita et al.[23] Photoluminescence quenching for a series of polythiophenes with varying ionization potentials blended with PCBM was measured relative to pristine polymer films. This PL quenching was complemented by transient absorption measurements of the yield of dissociated charges,

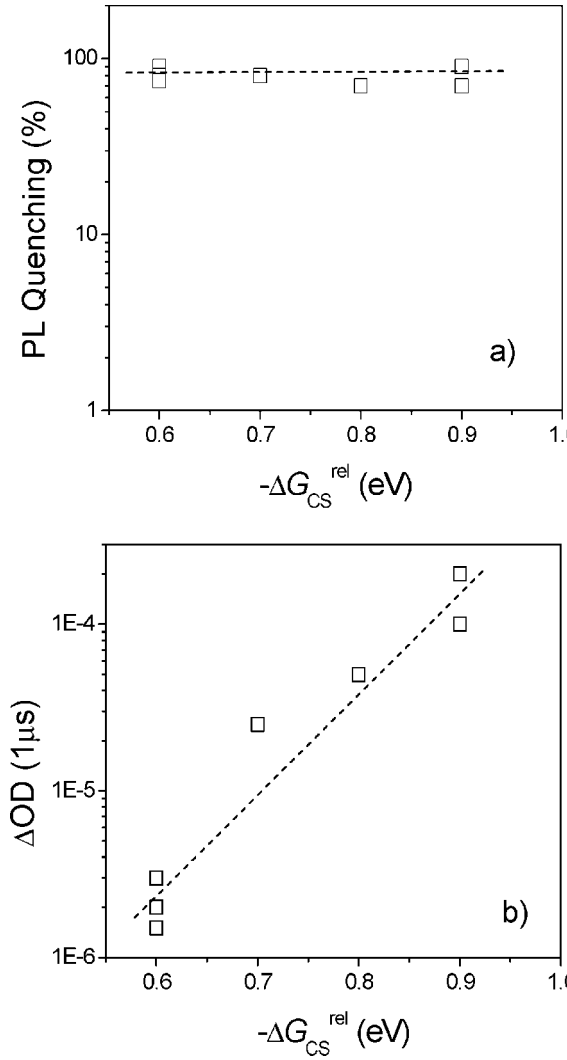

Figure 14. Comparison of the (a) PL quenching and (b) polaron yield, ΔOD, as a function of the free energy of charge separation, ΔG_{CS}, for a series of polythiophenes with varying ionization potential blended with 5 wt % PCBM, showing that PL quenching is an inadequate measure of charge photogeneration. Adapted with permission from ref 23. Copyright 2009 American Chemical Society.

measured by the magnitude of the power law decay phase monitored at 1000 nm (corresponding approximately to the absorption maxima of the photogenerated polarons) and at 1 μs (corresponding to the typical time scale for charge collection in bulk heterojunction devices). The power law decay dynamics (and time scale) allowed this signal to be assigned specifically to dissociated charges. Ohkita et al.[23] observed that despite over 70% PL quenching for all blend films studied (with only 5 wt % PCBM), the dissociated polaron yield, as measured using transient absorption spectroscopy (TAS), varied by over 2 orders of magnitude across the series, as illustrated in Figure 14. This result strongly suggests that for this materials series exciton quenching is not the limiting factor for charge photogeneration: the efficiency of the CT-state dissociation into free charges is instead. These studies of PL quenching and dissociated polaron yields have subsequently been extended to a range of other materials and processing conditions.[52,183,184] In all cases, it was observed that PL quenching was not a reliable indicator of charge photogeneration. This conclusion has been reached by other groups as well.[28] Moreover, a direct correlation has been observed between the polaron yield

estimated from the transient signal amplitude and the device photocurrent,[185] suggesting that TAS can be used a reliable indicator for device performance.

The other relatively direct measurements of the role of CT states in limiting charge photogeneration have come from measurements of exciplex-like CT emission in polymer:polymer blend films. For example, an inverse correlation has been observed between the CT emission intensity and the external quantum efficiency (EQE) in studies as a function of thermal annealing.[26] This inverse correlation, implying an improved dissociation of CT states upon annealing, was interpreted as an indication of the key role of CT states in influencing charge photogeneration. Similarly, Offermans et al.[22] also observed an inverse correlation between CT-state PL intensity and polaron yield, which was also correlated with the enhanced device efficiency. Enhanced CT-state dissociation with a subsequent increase in device performance has been concluded in numerous other studies as a result of thermal annealing[52,53,120] or increasing the PCBM concentration.[25,54] Analogous evidence for the role of CT states in limiting charge photogeneration in a pristine polymer film has been reported by Hertel et al.,[113] who employed electric-field-induced photoluminescence quenching and photocurrent densities of the pristine polymer MeLPPP. The expected optical charge generation/fluorescence quenching ratio of one was not observed; ratios of below one were measured at all applied fields and for all excitation energies, implying that exciton quenching in this polymer does not directly generate free charge carriers; this was attributed to the formation of CT states.

The above papers provide general evidence indicating the importance of CT states in determining the yield of charge photogeneration. The majority of these studies that have considered the functional role of charge-transfer states in determining device efficiencies have focused upon comparative studies as a function of interfacial energetics, electric field, nanomorphology, and molecular structure. We therefore turn now to considering each of these issues in turn.

3.6. Role of Excess Thermal Energy in Driving Charge Dissociation

As described in section 2.3, Onsager theory utilizes the idea that photoexcitation initially generates a hot electron (and/or hole). This electron then thermalizes at a particular distance from the hole (the thermalization length). The efficiency of charge photogeneration is then dependent upon this thermalization length compared to the Coulomb capture radius. This concept can be translated directly to charge photogeneration at donor/acceptor interfaces. In general, the exciton will thermally relax prior to charge separation (except for direct photoexcitation at the interface). However, in general, the electron injected into the acceptor will be thermally hot relative to the acceptor LUMO level (corresponding to the crossing point in Marcus theory). As such, it is plausible that the same consideration of thermalization length of the electron versus Coulomb attraction distance can be applied to determine the yield of charge photogeneration at donor/acceptor interfaces. In this context, it is possible that the amount of excess thermal energy of the injected electron may significantly determine the efficiency of charge photogeneration. This section considers the evidence that this is indeed the case.

Two reports in 2004 provided evidence that excess thermal energy is indeed necessary to overcome the Coulombic

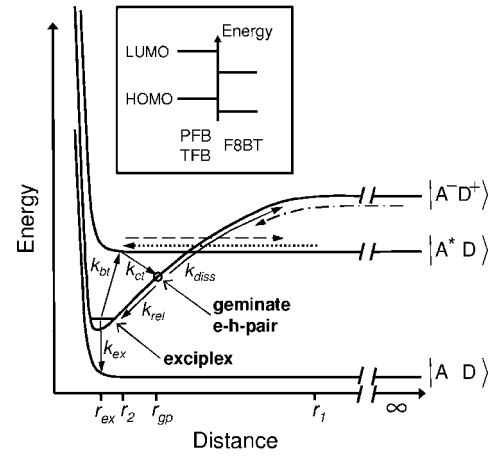

Figure 15. Potential energy diagram for the species involved in charge photogeneration at polymer/polymer interfaces proposed by Friend et al., where k_{ct} is the rate of thermally hot CT-state formation, k_{rel} is the rate of thermal relaxation to the 'exciplex' state, k_{diss} is the rate of dissociation of the thermally hot CT state, k_{ex} is the rate of radiative decay of the 'exciplex', and k_{bt} is the rate of re-excitation of the 'exciplex' to regenerate the exciton. Reprinted with permission from ref 21. Copyright 2004 American Physical Society.

binding energy of the CT state at organic donor/acceptor interfaces in order to generate the fully dissociated charge carriers.[21,24] One paper, by Friend et al.,[21] focused upon electric-field-dependent photoluminescence measurements of emissive CT states in PFB:F8BT and TFB:F8BT blend films (see also discussion in section 3.7). It was concluded that thermal relaxation of the CT state leads to an emissive state with a shorter spatial separation compared to the initially generated, vibrationally hot CT state; this relaxed, emissive CT state was termed an exciplex. The Coulomb binding energy of this exciplex, by virtue of its shorter electron−hole separation distance, was proposed to be too great to allow dissociation into the free charge carriers. Instead, this state decayed by radiative and nonradiative geminate recombination (or by thermal excitation to reform the exciton). Dissociation into free charge carriers therefore must take place from the thermally excited CT state prior to thermal relaxation to the exciplex. This model is summarized in Figure 15. Relating this model to Figure 9, the model suggests that the key kinetic competition limiting charge dissociation is the thermalization process k^{CT}_{therm} versus the dissociation process k_{CS*}. In this case, the observation of exciplex-like emission from the thermally relaxed CT state is indicative of failed dissociation, and the charge photogeneration yield will (in the simplest case where dissociation of the relaxed CT state is negligible) be independent of the kinetics of geminate recombination of this relaxed state. A second paper by Peumans and Forrest[24] employed Monte Carlo calculations to simulate the dissociation of charges at a donor/acceptor interface based upon Onsager theory. The model assumed that the electron was injected with an excess thermal energy corresponding to the free energy difference between the exciton and the dissociated charges, ΔG_{CS} (see Figure 9). These calculations were observed to be in agreement with photocurrent generation efficiencies for small molecule bilayer organic solar cells.

Both of these papers[21,24] addressed the role of excess thermal energy in overcoming the Coulomb attraction of interfacial CT states. This concept was further examined by Ohkita et al.[23] In their work, they employed transient

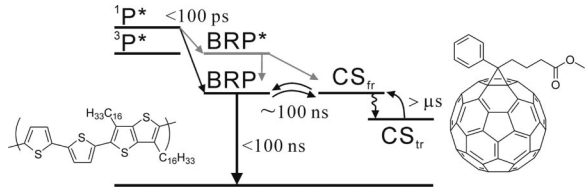

Figure 16. Model of charge photogeneration in polythiophene:PCBM blend films. In this figure 'BRP' refers to 'bound radical pair' states, corresponding to the CT-state nomenclature used in this review. This reference suggested that the primary charge photogeneration route proceeds via dissociation of the thermally hot BRP* state. Reprinted with permission from ref 23. Copyright 2008 American Chemical Society.

absorption spectroscopy to monitor the yields of dissociated polarons for a series of polythiophenes blended with 5 wt % PCBM. A clear correlation was observed between the yield of dissociated polarons and the free energy of charge separation, ΔG_{CS}, with the yield varying by over 2 orders of magnitude for a 0.3 eV change in ΔG_{CS} (see Figure 14b). This change in polaron yield was assigned to variations in the efficiency of dissociation of interfacial CT states (PL data indicated it could not be assigned to differences in exciton quenching, vide supra). The correlation between polaron yield and ΔG_{CS} is particularly striking as it implies that the efficiency of dissociation is dependent upon the energy of the starting exciton (ΔG_{CS}). Subsequent studies of alternative polythiophene:PCBM blends have also shown a correlation between polaron yield and ΔG_{CS}, in agreement with the initial observation of Ohkita et al.[52,185,186] The authors rationalized their results in terms of a 'hot' CT-state model in which a high ΔG_{CS} provides the initially formed CT state with sufficient excess thermal energy to overcome the Coulombic binding energy and thus efficiently dissociate into separated charges, as illustrated in Figure 16.

The role of hot CT states in mediating charge dissociation has been most recently studied by Muntwiler et al.,[51] who employed two-photon photoemission spectroscopy to probe charge-transfer states at a pentacene/vacuum interface. They concluded that the large binding energy of the lowest energy 1s CT state would prevent it from contributing to charge photogeneration but that efficient charge separation would be likely to involve hot CT states with lower effective binding energies. Moreover, Sheng et al.[134] employed a range of optoelectronic techniques to demonstrate that while sub-band-gap excitation of MEH-PPV:C_{60} can generate localized CT states, these states do not result in efficient photocurrent generation.

All of these studies provide evidence indicating that hot CT states may be critical to achieving efficient charge photogeneration at donor/acceptor interfaces. Recent theoretical calculations by Kanai and Grossman[187] support this conclusion. Moreover, as pointed out by Brédas et al.,[38] it is plausible that thermal relaxation of CT states may be slow relative to intermolecular electron transfer steps, which have been shown to be achievable on the 100 fs or faster time scale.[14,78,120,165,173,175,188] The role of excess thermal energy in driving charge dissociation is closely analogous to the Onsager theory for charge photogeneration, with the thermalization length increasing with the amount of initial excess thermal energy. The requirement for excess thermal energy to drive separation has important implications for photovoltaic device efficiency as the requirement for a large ΔG_{CS} (corresponding to a large initial thermal energy of the CT state) limits the energy available to be output as electrical power. We discuss this point further in section 4. We also note that studies demonstrating a clear correlation between charge photogeneration and ΔG_{CS} are very limited to date. Most studies of charge and photocurrent generation in organic solar cells have focused upon the effect of electric fields and nanomorphology instead, as we discuss in the following sections.

3.7. Role of Electric Fields in Driving Charge Dissociation

The processes of CT-state dissociation and geminate recombination can be difficult to quantify. One potentially useful method of examining the CT state is to exploit its electric-field-dependent behavior. According to Onsager theory, separation of the CT state to produce the fully dissociated charge carriers can be driven by the presence of an electric field, which reduces the Coulomb potential barrier in the downfield direction and thus enhances the dissociation probability. As the field strength increases, so does the dissociation probability of the CT state. This effect can be assessed by measuring CT-state emission intensity and lifetime or using photocurrent measurements.[22]

Electric-field-dependent photoluminescence measurements of PFB:F8BT and TFB:F8BT blends[21] have indicated that applied electric fields can preferentially quench CT-state emission, as shown in Figure 17a. However, time-dependent PL as a function of electric field revealed that while the CT-state generation (which occurs within 1 ns) efficiency was field dependent, its decay rate was not. This is in contrast to PF10TBT:PCBM blends (vide infra)[25] and suggests that, in this case, a CT-state precursor is quenched by the electric field. It was also observed that the exciton decay dynamics were field independent as well; therefore, a nonradiative intermediate state must exist that can be dissociated by an electric field. It was concluded that this state is the vibrationally excited CT state created by the initial electron transfer from the exciton. By applying Onsager theory to the electric-field-dependent results (Figure 17b), the electron−hole separation distance of the initially formed CT state (i.e., the thermalization length) was estimated to be 2.2 nm for TFB:F8BT and 3.1 nm for PFB:F8BT. The greater electron−hole separation for PFB:F8BT is consistent with a higher dissociation efficiency of the CT state and its consequently higher measured photocurrent yield.

Offermans et al.[22] investigated the behavior of MDMO-PPV:PCNEPV CT states under an applied electric field. It was observed that the PL intensity of the CT state decreased under the influence of an electric field, suggesting its dissociation into free charge carriers. The lifetime of the CT-state emission decreased with increasing applied bias, as expected (Figure 17c). In addition, the PL intensity of the CT emission also increased when low temperatures (80 K) were tested, thus indicating that the probability for dissociation of the CT state depends upon the available thermal energy.

Electric-field-dependent photogeneration was further studied by the Janssen group[25] in an analysis of PF10TBT:PCBM films. The key observation in these experiments was the presence of an emissive CT state, which was therefore used as a probe to examine the field dependence of its dissociation into free charge carriers. The primary observation in this respect was that the electric field selectively quenched the CT-state emission and *not* the singlet exciton emission, as concluded from a comparison of the differential PL spectrum

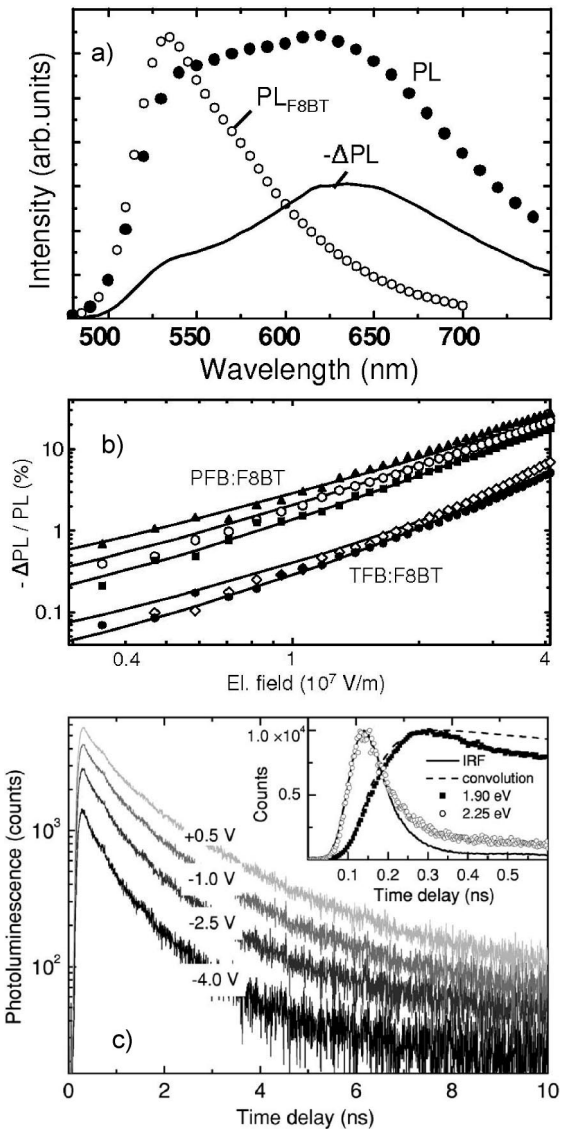

Figure 17. (a) Photoluminescence spectra of pristine F8BT (PL_{F8BT}) and the PFB:F8BT blend (PL), and reduction of photoluminescence intensity due to an applied reverse bias of 10 V ($-\Delta PL$) for a PFB:F8BT blend device at 340 K. (b) Effect of the electric-field strength on the CT-state PL quenching with fits (solid lines) using Onsager theory. (a and b) Reprinted with permission from ref 21. Copyright 2004 American Physical Society. (c) Effect of applied bias on the photoluminescence lifetime for MDMO-PPC: PCNEPV, with the inset showing the data at the early time domain. Reprinted with permission from ref 22. Copyright 2005 American Physical Society.

and the electroluminescence spectrum (where the CT state is formed directly by charge carrier injection). In conjunction with the decrease in lifetime of the CT state with increasing electric field, this was taken as evidence that the electric field acts to dissociate the CT state into free charge carriers.

It is important to note that the above studies addressing the influence of electric fields on CT (or exciplex) emission only observed significant effects of the applied electric field under strong reverse bias conditions (typically up to -10 V, corresponding to electric fields of $\sim 10^8$ V m^{-1}). Only relatively modest effects (ca. <10%[21,25]) were observed over the operating range of organic photovoltaic devices (from 0 to +1 V). This is in agreement with a recent study by Shuttle et al.,[189] which employed transient absorption spectroscopy to determine that the yield of dissociated polarons in P3HT: PCBM devices was almost independent of electric field from 0 to +0.6 V (<10% change), thus discounting a significant change in geminate recombination losses over this bias range. Thus, on the basis of these photophysical studies, it may be concluded that, at least for these material systems, macroscopic electric fields may not strongly influence charge photogeneration over the bias range corresponding to device operation.

The competition between CT-state dissociation and recombination has also been extensively explored using modeling studies of device current/voltage behavior. Blom et al. estimated the CT-state dissociation efficiency for MDMO-PPV:PCBM devices utilizing a numerical simulation based on Onsager theory (eqs 7 and 8) to explain their photocurrent results as a function of electric field.[96] Close to the flat band potential (corresponding to $\sim V_{OC}$), the photocurrent scaled linearly with voltage, as expected for a low electric field strength. As $V_0 - V$ increased further, a saturation regime was observed. At very high reverse voltages, the photocurrent became independent of electric field and temperature, suggesting that every CT state is dissociated into free charge carriers under the influence of the large electric field. Blom's model included the rate for geminate recombination and the electron−hole separation distance as the only adjustable parameters, and these were estimated from the dissociation probability by fitting the temperature dependence of the photocurrent. Under short circuit conditions, it was calculated that only 60% of MDMO-PPV:PCBM CT states fully dissociate at room temperature, thereby constituting a significant loss mechanism for the cell. The same model was also applied to thermally annealed P3HT:PCBM cells,[105] where a dissociation probability of 90% was estimated, significantly higher than that calculated for MDMO-PPV and consistent with the better device performance.

Blom et al. also applied their model to a study of MDMO-PPV devices as a function of PCBM concentration.[54] It was observed that the dissociation efficiency of the CT state progressively increased with PCBM concentration, reaching a maximum at 67%, coinciding not with the optimal cell performance (achieved at 80% PCBM) but with the onset of phase segregation instead. This implies that a minimum domain size is required for efficient CT-state dissociation. The increasing dissociation efficiency with PCBM concentration was also attributed to the enhanced effective dielectric constant and charge carrier mobility.

This model, employing an electric-field-dependent charge photogeneration term and other similar device models, has now been extensively used by many groups to successfully analyze the current/voltage behavior of organic solar cells.[190–197] However, it should be noted that Blom et al.'s model appears to be in some conflict with photophysical analyses, as noted previously.[25] The uncertainty lies not in whether charge photogeneration is electric-field dependent (this seems clearly established, consistent with the Onsager model described in section 2.3) but in whether the magnitude of the dependence is sufficient to have a significant impact upon charge photogeneration over the operating range of organic photovoltaic device operation. The electric fields likely to be present in such devices are relatively modest. They are expected to increase linearly from flat band conditions, which can be approximated to V_{OC} (this is likely to be a slight underestimation). For example, for a typical P3HT:PCBM solar cell, with $V_{OC} \approx 0.6$ V and a film thickness of 200 nm (and neglecting any charge screening), the electric-field

strength, E, is approximately 3×10^6 V m^{-1}. In order to obtain a strong enough dependence of $P(E)$ upon device voltage to fit the empirical current/voltage behavior, Blom et al. assumed a geminate recombination rate (k_f in eq 6) of 2×10^4 s^{-1}.[105] Similarly, for MDMO-PPV:PCBM devices, geminate recombination rates of 10^5 s^{-1} were concluded.[74,96] This contrasts with photophysical data, which indicate geminate recombination rates of $>10^7$ s^{-1} for such donor/acceptor systems.[77,108,116,164] Note, however, that Blom et al. has more recently found that a rate of geminate recombination of 1.7×10^7 s^{-1} was consistent with simulations of the current/voltage curves for PCPDTBT:PCBM.[104] The model also assumes that charge photogeneration should be negligible in the absence of macroscopic electric fields, in contrast to experimental observations of high polaron yields for donor/acceptor films in the absence of any electrodes (and therefore negligible macroscopic electric fields).[189] Liu et al.[198] emphasized that the built-in electric fields present in donor/acceptor systems are typically less than that required to efficiently separate the CT state into free charge carriers. However, they also noted that for small molecule bilayer systems unintentional doping caused by lack of complete purification may increase the effective built-in electric field present at the interface, thereby enhancing dissociation of the CT state. We note that there are other alternative models to explain the device current/voltage behavior which do not require an electric-field-dependent charge photogeneration. In particular, Shuttle et al.[189] proposed that the reduction in device photocurrent toward device open circuit results from bimolecular recombination losses with these losses increasing between short and open circuit due to the increase in charge density in the device.

In summary, there is conflicting evidence over whether the macroscopic electric fields present in organic photovoltaic devices are sufficiently large enough to have a significant effect on the charge photogeneration under the conditions of device operation. This is clearly a controversial and important topic which deserves further experimental and theoretical analysis and is indeed likely to vary between different materials systems and device structures.

3.8. Role of Nanomorphology in Charge Dissociation

Many studies have addressed the influence of blend nanomorphology on the properties of the CT state and, therefore, charge photogeneration in donor/acceptor blends. In particular, the donor/acceptor interfacial area and domain sizes (collectively referred to as phase segregation) are key parameters that have a substantial effect on charge photogeneration.[199] Optimal phase segregation must exist to minimize geminate recombination and thus maximize charge photogeneration; moreover, both exciton dissociation and charge transport requirements need to be balanced. For example, if the domain sizes are too large, the limited diffusion length of the photoinduced excitons means that some excitons will not reach an interface within their lifetime. Conversely, if the phase separation is too fine (and thus the interfacial area is too large), this may enhance geminate and/or bimolecular recombination. Indeed, it has been noted that if the domain size is smaller than the Coulomb capture radius then the charges will not be able to escape one another efficiently and geminate recombination may result.[200] We note that in this case the charges may not be confined by the Coulomb attraction but rather by the physical size of the domains. An ideal blend morphology will involve a bicontinuous interpenetrating network of donor and acceptor components with an optimized interfacial area for efficient exciton dissociation and with the scale of phase separation on the order of the exciton diffusion length and greater than the Coulomb capture radius. Achievement of this condition may not be facile, with estimates of the Coulomb capture radius typically being of similar magnitude or exceeding estimates of the exciton diffusion length. The free charge carriers then require continuous percolated pathways through the active layer to reach their respective electrodes, so avoiding recombination losses. The achievement of such an appropriate morphology has therefore been the focus of numerous studies including not only blend films but also molecular strategies to control nanomorphology (e.g., block copolymers,[201–203] donor/acceptor dyads,[43,80,83,88] double cable motifs,[204] etc). The two blend systems that have been studied most extensively in this context are MDMO-PPV:PCBM and P3HT:PCBM blends.[52,179,180,205–212]

Altering the solvent provides a relatively simple method of investigating morphology. For example, charge photogeneration as a function of morphology has been investigated experimentally using ultrafast transient absorption spectroscopy (TAS). A study by Inganäs et al.[175] used this technique to investigate blends of APFO-3 and PCBM as a function of solvent mixing, where small domains and a smooth surface were observed in the chloroform/chlorobenzene cast films and significantly larger domains on the order of several hundred nanometers for the chloroform/toluene cast sample. The TAS of the blend films (Figure 18a and 18b), probing both the polymer singlet exciton and charge-separated species at 1000 nm, revealed an initial ultrafast decay prior to ~0.5 ps, assigned to decay of the exciton and consequent formation of the CT state. The subsequent increase in signal from approximately 1 to 100 ps was assigned to dissociation of these CT states. Following this was another decay after ~100 ps; excitation-dependent studies suggested this to be bimolecular recombination decay of the dissociated charge carriers. However, the yield of fully dissociated charges and rate at which they were formed varied depending upon the solvent mixture used to spin coat the film. These results could be correlated with the different morphologies of each film (see Figure 18c). The TAS results indicated a higher charge photogeneration yield in addition to a faster rate of CT-state dissociation in the chlorobenzene cast film, where smaller domains are present. In contrast, the domains in the chloroform/toluene sample are too large to achieve efficient exciton dissociation and the charge photogeneration yield is therefore lower. Indeed, the relative charge generation yields for each sample correlated with the corresponding relative photocurrents, with the chlorobenzene sample possessing the highest photocurrent.

The effect of nanomorphology was also reported in a study by Müller et al.,[117] investigating the presence of CT states in two polymer:PCBM blends (MDMO-PPV and MeLPPP). Two-pulse femtosecond measurements of photocurrent revealed evidence of CT states in MeLPPP:PCBM but not MDMO-PPV:PCBM. It was concluded that dissociation of CT states in MDMO-PPV:PCBM is ultrafast and efficient, occurring prior to the time resolution and consistent with the greater device efficiency. This was attributed to the different blend film morphologies formed for each polymer, with MDMO-PPV showing a tendency toward aggregation into domains whereas MeLPPP does not. Furthermore, ultrafast anisotropy measurements revealed a high anisotropy

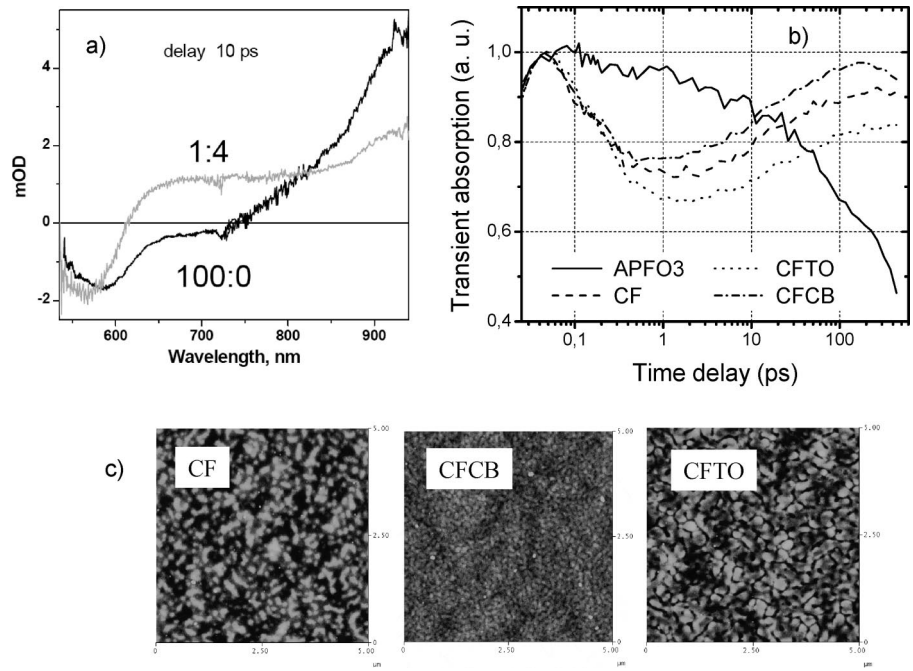

Figure 18. (a) Transient absorption spectrum for pristine APFO-3 and APFO-3:PCBM. Reprinted with permission from ref 213. Copyright 2008 Elsevier. (b) Transient absorption kinetics of pristine APFO-3 and APFO-3:PCBM spun from different solvent mixtures (CF = chloroform, CFTO = chloroform/toluene, and CFCB = chloroform/chlorobenzene) with an excitation density of 1.4×10^{13} photons cm^{-2} and a probe wavelength of 1000 nm with (c) the corresponding AFM images, where the length scale is 5 μm across the full square. Reprinted with permission from ref 175. Copyright 2006 Wiley.

for the MDMO-PPV exciton, indicating the presence of ordered domains. Conversely, the anisotropy of the polymer polaron was low, suggesting that the polaron's transition dipole moment alters within 1 ps after formation. This could be explained by a rapid intermolecular delocalization of the polaron. As such, a more delocalized polaron might result in a larger electron−hole separation distance in the CT state, thereby facilitating its dissociation. MeLPPP, on the other hand, forms finely dispersed blends with PCBM and geminate recombination is thus a significant loss mechanism. It is important to note, however, that the films used in this study were spun from toluene solutions; MDMO-PPV is known to form very large domains under these conditions that are detrimental to the photocurrent.[214] This could be an alternative explanation for the negligible presence of CT states in this polymer.[74]

A comprehensive study exploring the influence of morphology was reported by Janssen et al.,[25] where the composition dependence of the CT emission in PF10TBT:PCBM films was examined. Photoexcitation of the PF10TBT blends revealed not only the expected efficient PL quenching with addition of PCBM but also a broad red-shifted emission band attributed to the CT state (Figure 19a). This state was also observed as a very weak absorption band in the differential absorption spectra, indicative of ground-state interactions. As the PCBM concentration was increased, the CT-state emission red shifted (thus lowering the V_{OC}) and weakened in intensity. Time-resolved PL (TR-PL) measurements of the blend films revealed that the decay time of the CT emission also became progressively shorter with increasing PCBM concentration. This observation, in conjunction with the reduced PL intensity, was assigned to an enhanced dissociation efficiency of the CT state into free charge carriers with increasing PCBM concentration. The dissociation products were investigated by photoinduced absorption spectroscopy, and the presence of polymer polarons was established. The concentration of these dissociated polarons increased with increasing PCBM concentration (Figure 19b), thereby supporting the theory that higher PCBM concentrations enhance the dissociation of the CT state. The charge photogeneration yield improves as a result, consistent with the higher short-circuit currents measured for higher PCBM concentrations.

Onsager−Braun theory[25] was applied to the PF10TBT:PCBM system in order to estimate the spatially averaged mobilities $\langle\mu\rangle$ of the charge carriers and the electron−hole separation distances. For instance, the pronounced CT-state emission quenching at high weightings of PCBM was fitted using large mobilities and electron−hole separations (Figure 19d). Conversely, the reduced quenching at small PCBM concentrations, resulting in less charge photogeneration, required shorter electron−hole separations and lower carrier mobilities. The increase in $\langle\mu\rangle$ with PCBM concentration is consistent with the higher electron mobility in the PCBM domains progressively contributing more to $\langle\mu\rangle$. A high $\langle\mu\rangle$ aids in separation of the charge carriers by increasing the probability of electrons escaping beyond the Coulomb capture radius. These results were correlated with changes in morphology as the PF10TBT:PCBM blend composition is varied.[25] High concentrations of PCBM produced phase segregation and the formation of large PCBM domains (Figure 19c); this was not observed at lower PCBM concentrations. Only the sample with 80 wt % PCBM revealed nanocrystalline PCBM domains of 50−100 nm in diameter, and this was correlated with the highest device efficiency. The higher electron mobility in these domains, larger effective dielectric constant of the blend, and greater electron−hole separation distances were all suggested to facilitate the dissociation of the CT state at the donor/acceptor interface. Geminate recombination is thereby reduced, increasing the charge photogeneration yield and consequently enhancing the photocurrent and device efficiency.

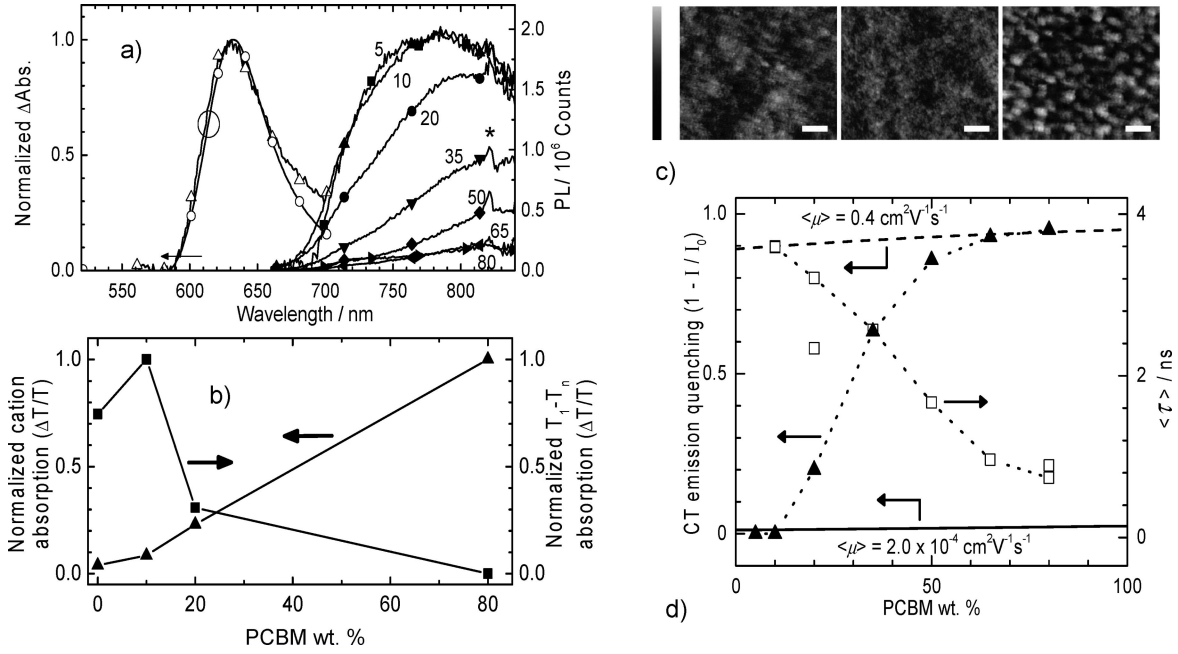

Figure 19. (a) Normalized differential absorbance (ΔAbs) spectra of PF10TBT:PCBM blends containing 10 (Δ) and 20 (○) wt % PCBM and photoluminescence spectra of blends containing 5−80 wt % PCBM corrected for the PF10TBT emission. (b) Normalized PF10TBT radical cation absorption at 0.5 eV (and the PF10TBT T_1-T_n absorption, not discussed here) as a function of the PCBM concentration. (c) AFM images of the PF10TBT:PCBM blend films containing, from left, 20, 50, and 80 wt % PCBM. (d) Normalized PL quenching at the peak wavelength and average decay time at 780 nm (the CT emission) in PF10TBT:PCBM blends as a function of the PCBM concentration. The dashed line shows the zero-field quenching of CT emission for high PCBM concentrations, calculated with Onsager theory using $E = 0$, $\langle\mu\rangle = 0.4$ cm^2 V^{-1} s^{-1}, and $a = 2.5$ nm. The solid line uses the same values except that $\langle\mu\rangle$ was set to 2.0×10^{-4} cm^2 V^{-1} s^{-1}. For both calculations $\langle\varepsilon_r\rangle$ is varied between 3.4 and 4.0 for 0−100 wt % PCBM. Reprinted with permission from ref 25. Copyright 2009 American Chemical Society.

This rationale has been invoked in a number of studies of CT-state dissociation. For example, MDMO-PPV:PCBM blends were examined by Quist et al. using time-dependent microwave photoconductivity measurements to investigate films deposited from both chlorobenzene and toluene solutions as a function of PCBM concentration.[206] This photoconductivity is expressed as the ratio $\eta\Sigma\mu/F_A$, the product of the number of charges per absorbed photon and the sum of the electron and hole mobilities. Initial TEM studies confirmed previous results[215,216] that both solvents produce evidence of phase segregation, but the onset of phase segregation occurs at a higher PCBM concentration for chlorobenzene cast films due to PCBM's greater solubility in this solvent. Increasing the PCBM concentration enhanced the transient photoconductivity signal for both solvents; furthermore, chlorobenzene-spun samples had higher photoconductivity than toluene-spun films *after* the onset of phase segregation. The authors proposed that the increases in photoconductivity could be assigned to both an increase in PCBM electron mobility and, to a lesser extent, an enhanced charge generation. In particular, it was suggested that the PCBM domains that form at higher PCBM concentrations enable the electron in a CT state to diffuse away from the interface more easily, thereby facilitating dissociation of the CT state. Electrons that escape geminate recombination in this way can contribute to the higher photoconductivity. As such, this is similar to the explanation given by Janssen et al. to explain their PCBM composition results.[25]

Other applications of Onsager−Braun theory also discuss their results in this context. For example, Monte Carlo modeling including Onsager−Braun theory has been applied to the issue of geminate recombination in the context of domain size.[217] This modeling suggested that increasing the domain size from 4 to 16 nm progressively improved the CT-state dissociation efficiency, after which the efficiency begins to saturate. This was attributed to the ease with which the geminate charges can move away from one another, which is greater in the presence of large domains.

Another example which reported a transition between geminate and bimolecular recombination correlated with a change in nanomorphology is a TAS study by Shoaee et al.,[167] where the recombination dynamics of P3HT:PCBM were compared to that of P3HT blends with other fullerene derivatives. The P3HT:PCBM film exhibited power law decay dynamics extending to the millisecond time scale, indicative of bimolecular recombination in the presence of an exponential distribution of localized states.[170] The other fullerene derivative blends, however, showed a much faster, oxygen-insensitive, monoexponential decay with an excitation density-independent lifetime of 130 ns. On the basis of these observations, this decay was assigned to geminate recombination. This transition from bimolecular to geminate recombination by altering the fullerene was correlated with morphology. Specifically, atomic force microscopy (AFM) images of the P3HT:PCBM film revealed extensive phase segregation, while the P3HT blend with the other fullerene derivative was smoother and had no discernible phase segregation at all. As such, the significantly smaller domain size in the latter blend was suggested to inhibit efficient dissociation of the CT state, resulting in the observed geminate recombination.

The above studies show clear correlations between the nanomorphology of donor−acceptor blends and charge photogeneration yields. As yet these correlations are qualitative rather than quantitative due largely to the difficulty in obtaining series of samples with a well-defined and quantifiable variation in nanomorphology. In this respect, a com-

plication arises concerning the purity of the domains. For example, it has been reported that the large micrometer-sized domains formed in xylene-spun films of PFB:F8BT contain some degree of internal intermixing on the nanometer length scale.[218] Most of the photocurrent was observed to be generated within these domains rather than at the interface of the larger domains, indicating that the extent of nanoscale intermixing was important for efficient device performance.[219,220] Similarly, McGehee et al.[221] reported intercalation of fullerene molecules into crystalline polymer domains in addition to the formation of discrete PCBM aggregates and correlated this with photocurrent generation. It thus appears likely that not only is the phase segregation length scale observed in AFM and TEM studies of polymer:PCBM blend films important but the molecular composition (purity) of the observed phases is as well. There is clear evidence that if phase segregation is on too long a length scale, charge photogeneration is reduced by exciton decay before it reaches the interface. Similarly, it is likely (and supported by experimental data) that blends that are too intimately mixed, resulting in small, isolated domains of either donor or acceptor, may suffer from higher geminate recombination and poor charge photogeneration yields as a result. The optimum nanomorphology for device function is further dependent upon achieving efficient charge collection by the device electrodes and therefore avoiding bimolecular recombination losses. It appears likely that an important factor behind the efficiency of P3HT:PCBM solar cells is the achievement of relatively optimum nanomorphology.[180,207,222] Achieving such a favorable nanomorphology using new materials possessing energy levels compatible with higher device efficiencies (e.g., lower ΔG_{CS}, lower optical band gap, etc.) is a key challenge for the development of further advances in device efficiency.

3.9. Influence of Thermal Annealing on Charge Photogeneration

A large number of experimental studies have considered the role of thermal annealing in influencing charge photogeneration in organic donor/acceptor blend films and related these observations to an increase in material crystallinity. Geminate recombination has been linked with thermal annealing in several reports, although a number of other explanations for the effect of annealing on device performance have also been suggested in the literature. The crystallinity of P3HT is increased upon thermal annealing, resulting in stronger interchain interactions[222] and thus an enhanced hole mobility. This crystallization process has been suggested to drive the formation of distinct P3HT phases and PCBM aggregates in the blend film due to the more ordered packing of the polymer chains.[180,223–226] Thus, phase segregation is enhanced upon thermal treatment. The higher photocurrents measured as a result of the altered morphology upon thermal annealing have most often been attributed to the observed increase in charge carrier mobility.[34,105,178,208,225] An alternative possibility for the increase in photocurrent is a reduction in geminate recombination losses, thereby increasing the efficiency of CT-state dissociation into the free charge carriers.[52]

The connection between geminate recombination and device performance as a function of thermal annealing was examined in a study of MDMO-PPV:PF1CVTP devices by Mandoc et al.[53] The poor device performance of this system (0.5% before annealing) was attributed to the small dielectric constant, low carrier mobilities, and a strongly bound CT state. Dissociation of the CT states into free charge carriers was thus suggested to be very inefficient. Thermal annealing doubled the device efficiency, primarily due to an increase in photocurrent. Current−voltage measurements revealed no significant improvement in charge carrier transport after annealing. However, modeling of the photocurrent (based on Onsager−Braun theory) suggested that the dissociation efficiency of CT states was considerably enhanced after annealing. This was primarily assigned to an increase in the initial electron−hole separation from 0.8 to 1.2 nm after annealing and a small increase in the rate of dissociation, k_d. The increase in electron−hole separation was attributed to changes in morphology: the enhanced phase segregation caused by annealing reduces the intermixing of polymer chains and leads to domain formation. This allows an increased delocalization of charge carriers; thus, CT states are more spatially separated. In turn, this may facilitate CT-state dissociation, leading to the increase in charge photogeneration and photocurrent.

A study of the effect of annealing on PFB:F8BT blend films by McNeill et al.[20] utilized a number of experimental techniques to conclude that geminate recombination was the limiting factor for device efficiency. Thermal annealing increased device EQE up to an optimal temperature of 140 °C, after which the EQE decreased. Photoluminescence measurements showed the PL quenching progressively decreasing with increasing annealing temperature, consistent with the growing domain sizes observed by AFM. These results indicate, therefore, that device performance is enhanced despite a decrease in exciton dissociation efficiency upon annealing. On the basis of PL, ultrafast transient absorption, and intensity-dependent photocurrent measurements it was concluded that geminate recombination limits the efficiency of PFB:F8BT solar cells; this was linked with nanoscale morphology. It was proposed that as phase segregation increased, geminate recombination is reduced and the overall yield of charge photogeneration thus improves, despite a lower efficiency of exciton quenching. Clearly, such an effect will reach an optimum: the decrease in exciton dissociation as the domain size increases will eventually prevail over the improvement in CT-state separation. For the PFB:F8BT system, this optimum was reached at a ~20 nm domain size.

McNeill et al.[227] also investigated the influence of annealing in P3HT:F8TBT films. Annealing substantially improved the device efficiency by almost an order of magnitude, and the authors concluded, on the basis of photocurrent measurements as functions of light intensity and effective applied bias, that a reduction in geminate recombination makes a significant contribution to this. However, geminate recombination was not measured directly in this case; instead, it was assigned by a process of elimination. In addition, unlike their previous study,[20] this decrease in geminate recombination was attributed not only to a more evolved phase segregation but also to an enhanced hole mobility in the P3HT domains.

The effect of annealing on P3HT:PCBM was also investigated by microsecond transient absorption spectroscopy of the yield of dissociated polarons.[52] Thermal annealing of P3HT:PCBM blend films resulted in an almost 2-fold increase in the yield of dissociated P3HT polarons. The magnitude of this enhancement in charge photogeneration upon annealing, on a time scale relevant to device perfor-

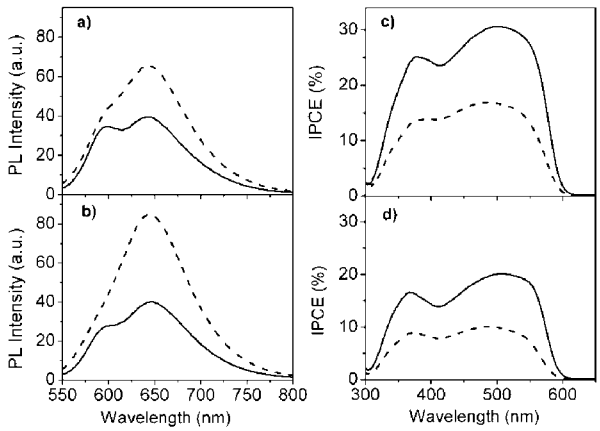

Figure 20. Photoluminescence spectra of (a) M3EH-PPV:CN-ether-PPV and (b) MEH-M3EH-PPV:CN-ether-PPV before (dashed line) and after (solid line) thermal annealing, with the corresponding IPCE spectra shown in c and d, respectively. Reprinted with permission from ref 26. Copyright 2007 American Institute of Physics.

mance,[74] was sufficient for it to be a significant contributor to the improvement in photocurrent. By discounting other possibilities for the origin of this enhanced charge photogeneration yield (such as increases in photon absorption and exciton dissociation efficiency), the authors attributed it to a reduction in geminate recombination losses, thereby increasing the yield of dissociated polarons. In addition, the authors suggested that the enhanced crystallinity of the P3HT phase, which increases the planarity of the polymer backbone and thus the delocalization of the polymer polaron, lowers the ionization potential of the P3HT and thus increases the free energy of charge separation ΔG_{CS}. Following the polaron yield dependence upon ΔG_{CS} reported by Ohkita et al.,[23] this increase in ΔG_{CS} was sufficient to explain the observed increase in polaron yield with annealing. Further studies looking at the effect of annealing as a function of PCBM composition also observed an increase in polaron yield with annealing, in agreement with increases in photocurrent densities.[184]

There are several other annealing studies that provide direct evidence of the role of geminate recombination of charge-transfer states in limiting charge photogeneration. For example, Savenije et al. performed time-resolved microwave conductivity measurements on both P3HT:PCBM[224] and MDMO-PPV:PCNEPV[174] blends; the higher photoconductivity observed after annealing was attributed to the greater phase segregation, allowing the charge carriers to more easily diffuse away from the interface, thus reducing geminate recombination. On the basis of ultrafast transient absorption measurements, Moses et al.[120] concluded that thermal annealing of P3HT:PCBM decreased the lifetime of the CT state by increasing its dissociation efficiency. Furthermore, an annealing study by Kietzke et al.[26] of PPV-derivative polymer:polymer blends indicated a negative correlation between PL efficiency of the CT state and device efficiency. Specifically, thermal annealing induced a reduction in the quantum yield of CT emission and an increase in EQE in both blends studied (Figure 20). This is consistent with enhanced dissociation of the CT state after annealing (with fewer CT states to recombine radiatively), as concluded by Moses et al. for P3HT:PCBM.[120] Similarly, the effect of thermal annealing on the CT state of MDMO-PPV:PCNEPV blends[22] has also been investigated, where it was observed that the CT-state photoluminescence quantum yield decreased while the yield of polymer polarons increased after annealing. Again, this implies a greater dissociation rate of the CT state after annealing, and this was correlated with an improvement in device efficiency.

Thermal annealing usually enhances the phase segregation and increases the crystallinity present in a blend film. There are now several studies that suggest that this can favor the dissociation of interfacial CT states, thereby reducing geminate recombination and enhancing the overall yield of charge photogeneration.

3.10. Other Factors Influencing Charge Photogeneration: Influence of Molecular/Interface Structure

The preceding sections have focused upon the role of electric fields, nanomorphology, and the overall reaction free energy (ΔG_{CS}) in driving charge photogeneration at organic donor/acceptor interfaces. However, theoretical considerations and analogies with other charge photogeneration interfaces all suggest that additional factors are also likely to be important in determining the efficiency of charge photogeneration. These include the magnitudes of the electronic coupling (both across the donor/acceptor interface and between neighboring donors/neighboring acceptors), the polarization (reorganization) energies of the states involved, the thermalization distance and time scale, the presence of interface dipoles, the polarizability of the materials and interface, the mobilities of the charge carriers, the potential presence of effective redox relays, and the energetic/structural inhomogeneities of the materials and interface. However, the importance of all these factors in influencing charge photogeneration remains to a large extent unresolved due to a lack of clear experimental data. Several of these factors are also likely to impact upon the lifetime of the charge-separated states and therefore upon charge collection efficiency in photovoltaic devices. For example, Nelson modeled the influence of electronic coupling upon the processes of charge separation and recombination and concluded that there is an optimum coupling for overall device efficiency.[115] In particular, there is a lack of reliable structural data (either experimental or theoretical) on interface structure on the molecular length scale (as opposed to nanomorphology studies of phase segregation). In this section, we review what limited studies there have been to date on these issues.

Some of the key theoretical challenges associated with modeling charge photogeneration in organic solar cells have been recently discussed by Brédas et al.[38] In particular, Kanai and Grossman[187] examined interfacial charge transfer in P3HT:C_{60} blends. Their density functional theory (DFT) results suggested that a highly efficient adiabatic electron transfer from the polymer to C_{60} is favorable. A 'bridging' electronic state was predicted (shown in Figure 21), resulting from wave function overlap across the interface between a P3HT π^* state and one of the triply degenerate unoccupied orbitals on the C_{60} (t_{1u} state). This suggests that electron transfer to the C_{60} may proceed adiabatically by occupying the bridging, lowest energy, state while the hole remains in the P3HT π state. This bridging state is analogous to a hot CT state. In addition to this, the bridging state overlaps energetically with other unoccupied fullerene-localized orbitals, with vibronic coupling between these states potentially facilitating efficient exciton dissociation to generate the CT state. If PCBM was used in the calculation rather than C_{60},

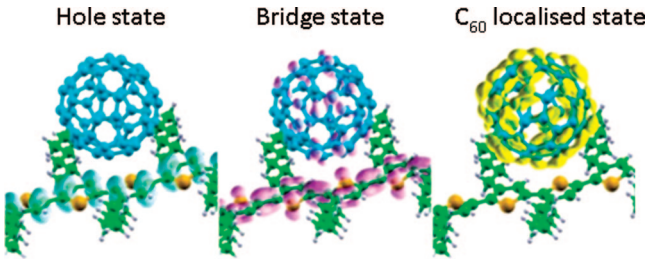

Figure 21. Isosurfaces of the hole state, bridging state (lowest excited state), and the near-degenerate C_{60}-localized states calculated for the P3HT:C_{60} interface. Reprinted with permission from ref 187. Copyright 2009 American Chemical Society.

the bridging electronic state was still present but the unoccupied fullerene orbitals had lost their degeneracy (due to the decrease in molecular symmetry). These results clearly indicate that the details of the donor/acceptor electronic interaction may play an important role in determining the kinetics and mechanism of charge photogeneration.

A recent theoretical quantum mechanical study provided insight into how the properties of CT states are likely to be sensitive to the detailed molecular structure of the interface.[228] Calculations were performed for PFB:F8BT and TFB:F8BT blends. These systems are interesting as they show evidence of thermally relaxed CT states that, being immobile at the interface and strongly bound by the Coulomb interaction, are unlikely to contribute to the photocurrent efficiency.[21] Similarly to what Kanai and Grossman observed for P3HT:PCBM,[187] the lowest excited states of the polymer:polymer blends were calculated to exhibit significant charge-transfer character (using ground-state geometries in a configuration that induces an 'attractive' interaction). The PFB:F8BT calculations predicted a nonradiative CT state with full ionic character (that is, full charge transfer between the two polymers has occurred), explaining the low electroluminescence efficiency observed for this system. Despite the structural homology between PFB and TFB (Figure 4), this fully ionic CT state was not observed for TFB:F8BT. Crucially, it was found that the character of the calculated CT state was dependent upon the relative positions and orientations of the two polymer chains. It was thus concluded that the details of molecular packing at the interface have a pronounced influence on the characteristics of the CT state.

Charge-transfer polymers, comprising donor and acceptor moieties within their monomer units, are currently attracting interest for lower band-gap organic photovoltaic devices, as the intramolecular charge-transfer transition between the donor and acceptor unit can result in a strong, lower energy absorption band. Initial studies[183] comparing the energetic requirements for charge photogeneration in PCBM blend films with such charge-transfer polymers suggests that this charge-transfer character can have a significant impact. In particular, it was observed that the low-band-gap polymer PCPDTBT (structure shown in Figure 2) was able to achieve efficient charge photogeneration with a significantly smaller ΔG_{CS} than that observed for polythiophene:PCBM blends (Figure 22). It was suggested that the charge-transfer character of PCPDTBT might favor charge photogeneration by reducing the Coulomb attraction of the CT state. This could be achieved if the donor component of the polymer was orientated away from the polymer:PCBM interface. In this context, optical excitation of the polymer could result in the formation of an intramolecular charge-transfer exciton, with the partial charge separation in this exciton subsequently

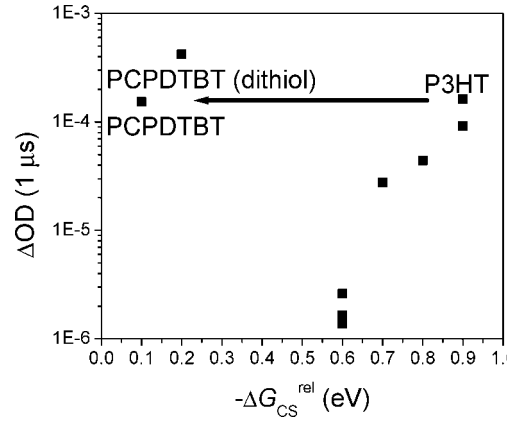

Figure 22. Comparison of charge photogeneration yields versus ΔG_{CS} for a series of polythiophene/PCBM blend films (■) with blend films employing the charge-transfer polymer PCPDTBT. Reprinted with permission from ref 183. Copyright 2009 Royal Society of Chemistry.

favoring dissociation of the CT state. A further possibility is that the charge-transfer character of the polymer might increase its polarizability, thereby also reducing the Coulomb attraction of the interfacial CT state. In either case, this observation suggests that introducing intramolecular charge-transfer character into the polymer may be an effective strategy to enhance charge photogeneration. This enhancement will clearly be dependent upon the orientation of the polymer with respect to the interface and will therefore not be generic to all charge-transfer polymers. We note that dye-sensitized solar cells typically employ charge-transfer dyes, with the intramolecular charge transfer orientated with respect to the charge-separation interfaces, to achieve high photovoltaic device efficiencies.[43,229] Furthermore, it is interesting to note that recent advances in the efficiency of organic polymer:fullerene solar cells have almost all been based upon the use of charge-transfer polymers.[2,3,230]

Onsager theory would suggest that charge dissociation may be favored by increasing the mobility of the charge carriers (eq 7). In this regard, it is surprising to note that Okhita et al.[23] did not observe a correlation between polymer hole mobility and charge photogeneration yields, despite the polymers studied varying in hole mobility by 4 orders of magnitude. However, in a more recent study, Shoaee et al.[186] observed enhanced charge photogeneration in polythiophene:perylene diimide blend films compared to polymer:PCBM films. This increased charge photogeneration may originate from an increase in acceptor domain size. However, it is interesting to note that the perylene diimide employed also exhibited an electron mobility 2 orders of magnitude higher than PCBM. Charge separation in such devices is based upon LUMO to LUMO electron transfer (rather than HOMO to HOMO hole transfer). As such, it is plausible that electron mobility may be a more important determinant of charge photogeneration efficiency than hole mobility, consistent with the observation by Shoaee et al.

Another example relating molecular structure to the CT states was provided by Dyer-Smith et al.,[124] where a series of polyfluorene−triarylamine copolymers in blends with silole derivatives was studied. It was observed that using fluorinated siloles as the acceptor resulted in a lower quantum yield of emissive CT states, higher polymer polaron yields, and higher EQEs compared to nonfluorinated siloles. These results therefore indicate that, in addition to radiative recombination of the CT state being a loss mechanism

detrimental to device performance, subtle changes in molecular structure can affect morphology and hence the CT-state properties.

There have been extensive studies comparing charge photogeneration and/or CT-state properties for different materials combinations,[18,19,21–23,25,26,28,31,32,124,130,137,159,173] all of which have been reviewed in the sections above. We already reviewed how these studies address the influence of nanomorphology, crystallinity (thermal annealing), electric field, and interfacial energetics upon charge photogeneration. However, it is already evident that these four factors are not the only ones that influence efficient charge photogeneration at organic donor/acceptor interfaces. Identifying the importance of other factors is a key challenge for our understanding and optimization of charge photogeneration in organic solar cells.

3.11. Summary of the Role of Charge-Transfer States in Influencing Charge Photogeneration

The preceding sections have reviewed the current state of knowledge of charge photogeneration in organic bulk heterojunction solar cells. A recurrent theme in the current literature is the role of interfacial charge-transfer states, with geminate recombination of these CT states being suggested in many studies to be a key loss mechanism limiting device performance. There is now clear evidence of the presence of CT states localized at the donor/acceptor interface. However, evidence for the functional importance of these states in limiting charge photogeneration remains rather indirect and is often based on correlations that are either qualitative or lack clear evidence of a causal relationship between CT-state function and photocurrent generation. Much of this uncertainty comes from the experimental difficulty in unambiguously observing these short-lived CT states. In this regard, the observation of exciplex-like emission from the states has proved particularly useful. Theoretical modeling, typically based upon Onsager theory, is consistent with these CT states playing a key role in charge photogeneration but is reliant upon parameter inputs which often have large experimental uncertainties. Furthermore, quantum mechanical studies indicate that the properties of these CT states are strongly dependent upon the molecular nature of the interface and therefore that their importance may vary significantly between different materials systems. Nevertheless, experimental and theoretical evidence is steadily accumulating that these charge-transfer states do indeed play a significant role in determining the efficiency of charge photogeneration in organic solar cells and that optimization of charge photogeneration is an important challenge for achieving further advances in photovoltaic device efficiencies.

4. Implications for Organic Photovoltaic Materials and Device Design

The development of predictive models relating materials' structures to photovoltaic device performance is crucial for the optimization of organic solar cells. Such models enable rational materials design to enhance device performance and, more realistically, provide a powerful tool to aid materials and device design.

Significant progress has been made in recent years in relating device voltage output to materials properties. In particular, it has been shown that the device open-circuit voltage is primarily determined by the energy difference between the donor's IP and acceptor's EA.[156] This model has proven successful in making reasonable predictions of device V_{OC} from material IP and EA values, with real device efficiencies, after processing optimization, typically being within 0.2 V of that predicted. Furthermore, it has been clearly shown that the energy of the CT state correlates directly with V_{OC}.[25,27,32] For example, a study of electroluminescence in polymer:PCBM solar cells observed a fully linear relationship between E_{CT} and V_{OC} with a y-axis offset of 0.4 eV,[28] suggesting that V_{OC} is determined by the energy of the CT state and not simply by $IP_D - EA_A$.

Progress in predicting device photocurrent generation on the basis of materials properties has, however, proved much more problematic. Much attention has focused upon enhancing light-harvesting efficiency by reducing the optical band gap of the photoactive layer, as discussed in a recent review.[36] Most models of device efficiency have typically assumed a unity yield for exciton dissociation into separated charges, requiring only that the donor/acceptor LUMO level offset is greater than 0.3 eV (corresponding to the assumed nominal exciton binding energy). In practice, these models have proved rather poor in predicting the photocurrent densities of real devices, even after processing optimization. While some materials (e.g., P3HT:PCBM) have indeed achieved photocurrent densities consistent with near unity internal quantum efficiencies for photocurrent generation, most new materials evaluated for their performance in organic photovoltaic devices have yielded much lower photocurrent densities and consequently poor device performance (we note that data for these 'unsuccessful' materials are often not published). In some cases, the low photocurrent densities can be attributed to poor charge collection due, for example, to low carrier mobilities resulting in increased bimolecular recombination and/or space charge effects. In other cases, the low photocurrent can be attributed to poor exciton quenching due to insufficient mixing of the donor and acceptor components. However, in many cases, it appears that the low photocurrents derive neither from poor exciton separation nor poor charge collection but rather from suboptimum dissociation efficiencies of the interfacial charge-transfer states with the photogenerated CT states undergoing geminate recombination. It appears likely that developing strategies to enhance charge photogeneration is an important issue for the future development of organic photovoltaic devices.

The studies we reviewed above suggest that several factors can favor dissociation of interfacial charge-transfer states, including a large overall free energy loss driving charge separation (ΔG_{CS}), large domain sizes, and strong macroscopic electric fields. However, in all these cases, modulating these parameters to enhance charge photogeneration may have a negative impact upon other aspects of device performance. For example, requiring a large ΔG_{CS} reduces the proportion of the exciton free energy that can be retained in the free energy of the separated charges and therefore the cell voltage. This is particularly an issue as the optical band gap is reduced, reducing the overall energy available in the exciton to drive charge photogeneration and device voltage. Similarly, increasing the domain size to favor CT-state dissociation can reduce the efficiency of exciton diffusion to the interface, while increasing the internal electric field by reducing the photoactive layer thickness would reduce light absorption. As a consequence, an important concern

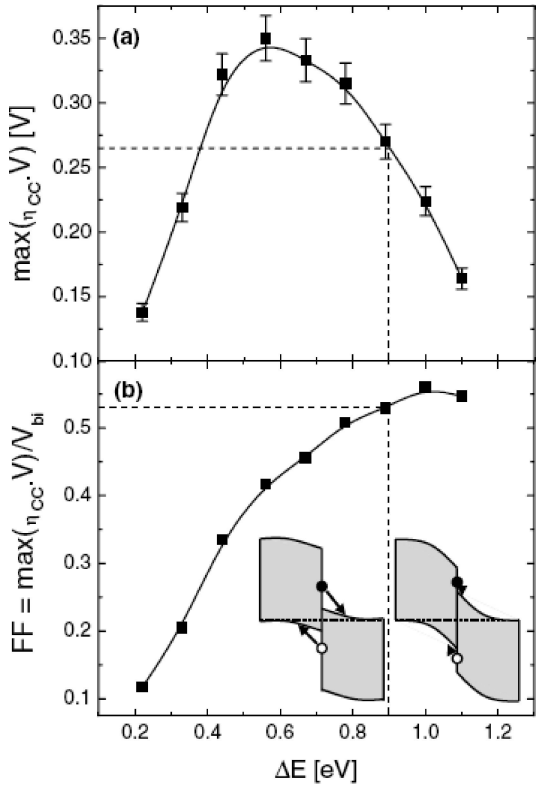

Figure 23. Maximum of the product $\eta_{CC}V$ (charge collection efficiency × voltage) as a function of the LUMO level offset, ΔE (a) and the value of $\eta_{CC}V/V_{bi}$ (where V_{bi} = built-in potential), approximately the fill factor (FF) of the cell, as a function of ΔE (b). The insets show the possible effect of the energy level offset on the thermalization length, *a*. Reprinted with permission from ref 24. Copyright 2004 Elsevier.

for optimizing OPV device efficiency is to identify strategies that enhance photogeneration efficiency but impact less negatively upon other aspects of device performance.

The balance between ΔG_{CS} and device performance has been modeled by Peumans and Forrest[24] for CuPc:C_{60} devices, employing Onsager-type Monte Carlo simulations of charge dissociation as a function of LUMO level offset (corresponding to changes in ΔG_{CS}). The simulations indicated that increasing the LUMO level offset increased charge photogeneration due to increased thermal energy of the initially generated CT state but decreased the free energy of the separated charges and therefore cell voltage. The maximum of the product $\eta_{CC}V$ (charge collection efficiency × voltage), which is proportional to the power conversion efficiency of a device, reached an optimum for a LUMO level offset of ~0.55 eV (Figure 23a). Furthermore, the value of $\eta_{CC}V/V_{bi}$ (where V_{bi} is the built-in potential), which can be approximated as the fill factor (FF) of the device, increased with increasing LUMO level offset and saturated at ~1 eV (Figure 23b).

In general, following Onsager theory, charge photogeneration should be favored by reducing the Coulomb binding energy of the CT states, E_B^{CT}. Several strategies can be envisaged to achieve this, including increasing the dielectric constant of the materials[231] and/or introduction of redox relays or insulator layers at the donor/acceptor interface. We note that introduction of insulator layers at the charge-separation interface and the use of redox relays have both been shown to enhance the performance of dye-sensitized solar cells.[43] However, the achievement of such structural control of the interface of organic donor/acceptor layers remains a significant challenge. In this regard, strategies to control interface morphology, such as the use of donor/acceptor block copolymers,[232,233] are of particular interest. The observation of efficient charge separation for polymer:PCBM blends employing a charge-transfer polymer[2,3,183] with only a small ΔG_{CS} is particularly promising, suggesting that the intramolecular charge transfer associated with optical excitation of the polymer may serve to facilitate charge photogeneration. A further strategy that may favor charge photogeneration would be to increase the thermalization length of the electron *a* after injection into the acceptor material. This might be achieved by either increasing the electron mobility or retarding the kinetics of thermalization. In both cases (reducing E_B^{CT} or increasing *a*), the CT dissociation efficiency might be expected to show an increased sensitivity to macroscopic electric fields, favoring efficient photocurrent generation.

We hope the reader has found some insights in this review over the current state of the art of charge photogeneration in organic solar cells. This current knowledge is far from complete. However, rapid progress is being made and will no doubt have been made between the time of writing this review and the time at which you are reading it. This progress holds out the potential both to understand the fundamentals of charge photogeneration at organic donor/acceptor interfaces and to apply this knowledge to the optimization of materials and device design for efficient photovoltaic solar cells.

5. Acknowledgments

We are very grateful for the many helpful discussions that guided the writing of this review and, in particular, acknowledge the input of Jenny Nelson, Safa Shoaee, Fiona Jamieson, Simon King, Chris Shuttle, and James Kirkpatrick. Funding from the EPSRC Nanotechnology Grand Challenge and Supergen programmes and BP Solar is gratefully acknowledged. Colleagues who have provided us with preprints of their publications are gratefully acknowledged.

6. References

(1) Kim, J. Y.; Lee, K.; Coates, N. E.; Moses, D.; Nguyen, T.-Q.; Dante, M.; Heeger, A. J. *Science* **2007**, *317*, 222.
(2) Park, S. H.; Roy, A.; Beaupre, S.; Cho, S.; Coates, N.; Moon, J. S.; Moses, D.; Leclerc, M.; Lee, K.; Heeger, A. J. *Nat. Photonics* **2009**, *3*, 297.
(3) Peet, J.; Kim, J. Y.; Coates, N. E.; Ma, W. L.; Moses, D.; Heeger, A. J.; Bazan, G. C. *Nat. Mater.* **2007**, *6*, 497.
(4) Brédas, J.-L.; Cornil, J.; Heeger, A. J. *Adv. Mater.* **1996**, *8*, 447.
(5) Antoniadis, H.; Hsieh, B. R.; Abkowitz, M. A.; Jenekhe, S. A.; Stolka, M. *Synth. Met.* **1994**, *62*, 265.
(6) Riess, W.; Karg, S.; Dyakonov, V.; Meier, M.; Schwoerer, M. *J. Lumin.* **1994**, *60−61*, 906.
(7) Hoppe, H.; Sariciftci, N. S. *J. Mater. Res.* **2004**, *19*, 1924.
(8) Tang, C. W. *Appl. Phys. Lett.* **1986**, *48*, 183.
(9) Forrest, S. R. *MRS Bull.* **2005**, *30*, 28.
(10) Peumans, P.; Bulovic, V.; Forrest, S. R. *Appl. Phys. Lett.* **2000**, *76*, 2650.
(11) Peumans, P.; Forrest, S. R. *Appl. Phys. Lett.* **2001**, *79*, 126.
(12) Kroeze, J. E.; Savenije, T. J.; Warman, J. M. *Adv. Mater.* **2002**, *14*, 1760.
(13) Sariciftci, N. S.; Smilowitz, L.; Heeger, A. J.; Wudl, F. *Science* **1992**, *258*, 1474.
(14) Kraabel, B.; Lee, C. H.; McBranch, D.; Moses, D.; Sariciftci, N. S.; Heeger, A. J. *Chem. Phys. Lett.* **1993**, *213*, 389.
(15) Yu, G.; Gao, J.; Hummelen, J. C.; Wudl, F.; Heeger, A. J. *Science* **1995**, *270*, 1789.
(16) Rumbles, G. *Chem. Rev.* Submitted for publication.
(17) Brabec, C. J.; Durrant, J. R. *MRS Bull.* **2008**, *33*, 670.

(18) Benson-Smith, J. J.; Goris, L.; Vandewal, K.; Haenen, K.; Manca, J. V.; Vanderzande, D.; Bradley, D. D. C.; Nelson, J. *Adv. Funct. Mater.* **2007**, *17*, 451.
(19) Loi, M. A.; Toffanin, S.; Muccini, M.; Forster, M.; Scherf, U.; Scharber, M. *Adv. Funct. Mater.* **2007**, *17*, 2111.
(20) McNeill, C. R.; Westenhoff, S.; Groves, C.; Friend, R. H.; Greenham, N. C. *J. Phys. Chem. C* **2007**, *111*, 19153.
(21) Morteani, A. C.; Sreearunothai, P.; Herz, L. M.; Friend, R. H.; Silva, C. *Phys. Rev. Lett.* **2004**, *92*, 247402.
(22) Offermans, T.; Hal, P. A. v.; Meskers, S. C. J.; Koetse, M. M.; Janssen, R. A. J. *Phys. Rev. B* **2005**, *72*, 045213.
(23) Ohkita, H.; Cook, S.; Astuti, Y.; Duffy, W.; Tierney, S.; Zhang, W.; Heeney, M.; McCulloch, I.; Nelson, J.; Bradley, D. D. C.; Durrant, J. R. *J. Am. Chem. Soc.* **2008**, *130*, 3030.
(24) Peumans, P.; Forrest, S. R. *Chem. Phys. Lett.* **2004**, *398*, 27.
(25) Veldman, D.; Opek, O.; Meskers, S. C. J.; Sweelssen, J.; Koetse, M. M.; Veenstra, S. C.; Kroon, J. M.; Bavel, S. S. v.; Loos, J.; Janssen, R. A. J. *J. Am. Chem. Soc.* **2008**, *130*, 7721.
(26) Yin, C.; Kietzke, T.; Neher, D.; Horhold, H.-H. *Appl. Phys. Lett.* **2007**, *90*, 092117.
(27) Veldman, D.; Meskers, S. C. J.; Janssen, R. A. J. *Adv. Funct. Mater.* **2009**, *19*, 1939.
(28) Tvingstedt, K.; Vandewal, K.; Gadisa, A.; Zhang, F.; Manca, J.; Inganaìs, O. *J. Am. Chem. Soc.* **2009**, *131*, 11819.
(29) Bruevich, V. V.; Makhmutov, T. S.; Elizarov, S. G.; Nechvolodova, E. M.; Paraschuk, D. Y. *J. Exp. Theor. Phys.* **2007**, *105*, 469.
(30) Goris, L.; Haenen, K.; Nesladek, M.; Wagner, P.; Vanderzande, D.; Schepper, L. D. *J. Mater. Sci.* **2005**, *40*, 1413.
(31) Panda, P.; Veldman, D.; Sweelssen, J.; Bastiaansen, J. J. A. M.; Langeveld-Voss, B. M. W.; Meskers, S. C. J. *J. Phys. Chem. B* **2007**, *111*, 5076.
(32) Vandewal, K.; Gadisa, A.; Oosterbaan, W. D.; Bertho, S.; Banishoeib, F.; Severen, I. V.; Lutsen, L.; Cleij, T. J.; Vanderzande, D.; Manca, J. V. *Adv. Funct. Mater.* **2008**, *18*, 2064.
(33) Pivrikas, A.; Sariciftci, N. S.; Juscaronka, G.; Österbacka, R. *Prog. Photovoltaics* **2007**, *15*, 677.
(34) Hoppe, H.; Sariciftci, N. S. *J. Mater. Chem.* **2006**, *16*, 45.
(35) Thompson, B. C.; Frechet, J. M. J. *Angew. Chem., Int. Ed.* **2008**, *47*, 58.
(36) Kroon, R.; Lenes, M.; Hummelen, J. C.; Blom, P. W. M.; De Boer, B. *Polym. Rev.* **2008**, *48*, 531.
(37) Brédas, J.-L.; Beljonne, D.; Coropceanu, V.; Cornil, J. *Chem. Rev.* **2004**, *104*, 4971.
(38) Brédas, J.-L.; Norton, J. E.; Cornil, J.; Coropceanu, V. *Acc. Chem. Res.* Accepted for publication.
(39) Dennler, G.; Scharber, M. C.; Brabec, C. J. *Adv. Mater.* **2009**, *21*, 1323.
(40) Riede, M.; Mueller, T.; Tress, W.; Schueppel, R.; Leo, K. *Nanotechnology* **2008**, *19*, 424001.
(41) Schueppel, R.; Schmidt, K.; Uhrich, C.; Schulze, K.; Wynands, D.; Bredas, J. L.; Brier, E.; Reinold, E.; Bu, H. B.; Baeuerle, P.; Maennig, B.; Pfeiffer, M.; Leo, K. *Phys. Rev. B* **2008**, *77*, 085311.
(42) Gledhill, S. E.; Scott, B.; Gregg, B. A. *J. Mater. Res.* **2005**, *20*, 3167.
(43) Durrant, J. R.; Haque, S. A.; Palomares, E. *Chem. Commun.* **2006**, 3279.
(44) Iwata, S.; Barber, J. *Curr. Opin. Struct. Biol.* **2004**, *14*, 447.
(45) Gust, D.; Moore, T. A.; Moore, A. L. *Acc. Chem. Res.* **2000**, *34*, 40.
(46) Harriman, A. *Angew. Chem., Int. Ed.* **2004**, *43*, 4985.
(47) Wasielewski, M. R. *Chem. Rev.* **1992**, *92*, 435.
(48) Wasielewski, M. R. *J. Org. Chem.* **2006**, *71*, 5051.
(49) Fukuzumi, S.; Kotani, H.; Ohkubo, K.; Ogo, S.; Tkachenko, N. V.; Lemmetyinen, H. *J. Am. Chem. Soc.* **2004**, *126*, 1600.
(50) Bittner, E. R.; Santos, R. J. G.; Karabunarliev, S. *J. Chem. Phys.* **2005**, *122*, 214719.
(51) Muntwiler, M.; Yang, Q.; Tisdale, W. A.; Zhu, X. Y. *Phys. Rev. Lett.* **2008**, *101*, 196403.
(52) Clarke, T. M.; Ballantyne, A. M.; Nelson, J.; Bradley, D. D. C.; Durrant, J. R. *Adv. Funct. Mater.* **2008**, *18*, 4029.
(53) Mandoc, M. M.; Veurman, W.; Sweelssen, J.; Koetse, M. M. *Appl. Phys. Lett.* **2007**, *91*, 073518.
(54) Mihailetchi, V. D.; Koster, L. J. A.; Blom, P. W. M.; Melzer, C.; de Boer, B.; van Duren, J. K. J.; Janssen, R. A. J. *Adv. Funct. Mater.* **2005**, *15*, 795.
(55) Scheblykin, I. G.; Yartsev, A.; Pullerits, T.; Gulbinas, V.; Sundstrom, V. *J. Phys. Chem. B* **2007**, *111*, 6303.
(56) Markov, D. E.; Amsterdam, E.; Blom, P. W. M.; Sieval, A. B.; Hummelen, J. C. *J. Phys. Chem. A* **2005**, *109*, 5266.
(57) McBranch, D. W.; Kraabel, B.; Xu, S.; Kohlman, R. S.; Klimov, V. I.; Bradley, D. D. C.; Hsieh, B. R.; Rubner, M. *Synth. Met.* **1999**, *101*, 291.
(58) Österbacka, R.; Wohlgenannt, M.; Shkunov, M.; Chinn, D.; Vardeny, Z. V. *J. Chem. Phys.* **2003**, *118*, 8905.
(59) Scully, S. R.; McGehee, M. D. *J. Appl. Phys.* **2006**, *100*, 034907.
(60) Stubinger, T.; Brutting, W. *J. Appl. Phys.* **2001**, *90*, 3632.
(61) Wang, Z.; Mazumdar, S.; Shukla, A. *Phys. Rev. B* **2008**, *78*, 235109.
(62) Janssen, R. A. J.; Smilowitz, L.; Sariciftci, N. S.; Moses, D. *J. Chem. Phys.* **1994**, *101*, 1787.
(63) Chosrovian, H.; Rentsch, S.; Grebner, D.; Dahm, D. U.; Birckner, E.; Naarmann, H. *Synth. Met.* **1993**, *60*, 23.
(64) Köhler, A.; dos Santos, D. A.; Beljonne, D.; Shuai, Z.; Bredas, J. L.; Holmes, A. B.; Kraus, A.; Mullen, K.; Friend, R. H. *Nature* **1998**, *392*, 903.
(65) Cuff, L.; Kertesz, M. *J. Chem. Phys.* **1997**, *106*, 5541.
(66) Gao, Y.; Liu, C.-G.; Jiang, Y.-S. *J. Phys. Chem. A* **2002**, *106*, 5380.
(67) Clarke, T. M.; Gordon, K. C.; Officer, D. L.; Grant, D. K. *J. Chem. Phys.* **2006**, *124*, 164501.
(68) Graham, S. C.; Bradley, D. D. C.; Friend, R. H.; Spangler, C. *Synth. Met.* **1991**, *41*, 1277.
(69) Chasteen, S. V.; Harter, J. O.; Rumbles, G.; Scott, J. C.; Nakazawa, Y.; Jones, M.; Horhold, H. H.; Tillman, H.; Carter, S. A. *J. Appl. Phys.* **2006**, *99*, 033709.
(70) Arkhipov, V. I.; Emelianova, E. V.; Bässler, H. *Phys. Rev. Lett.* **1999**, *82*, 1321.
(71) Arkhipov, V. I.; Emelianova, E. V.; Barth, S.; Bässler, H. *Phys. Rev. B* **2000**, *61*, 8207.
(72) Basko, D. M.; Conwell, E. M. *Phys. Rev. B* **2002**, *66*, 155210.
(73) Gulbinas, V.; Zaushitsyn, Y.; Sundström, V.; Hertel, D.; Bässler, H.; Yartsev, A. *Phys. Rev. Lett.* **2002**, *89*, 107401.
(74) Blom, P. W. M.; Mihailetchi, V. D.; Koster, L. J. A.; Markov, D. E. *Adv. Mater.* **2007**, *19*, 1551.
(75) Lüer, L.; Egelhaaf, H. J.; Oelkrug, D.; Cerullo, G.; Lanzani, G.; Huisman, B. H.; de Leeuw, D. *Org. Electron.* **2004**, *5*, 83.
(76) Kroeze, J. E.; Savenije, T. J.; Vermeulen, M. J. W.; Warman, J. M. *J. Phys. Chem. B* **2003**, *107*, 7696.
(77) Bakulin, A. A.; Martyanov, D. S.; Paraschuk, D. Y.; Pshenichnikov, M. S.; van Loosdrecht, P. H. M. *J. Phys. Chem. B* **2008**, *112*, 13730.
(78) Brabec, C. J.; Zerza, G.; Cerullo, G.; De Silvestri, S.; Luzzati, S.; Hummelen, J. C.; Sariciftci, S. *Chem. Phys. Lett.* **2001**, *340*, 232.
(79) Marcus, R. A. *J. Chem. Phys.* **1956**, *24*, 966.
(80) Verhoeven, J. W.; Ramesdonk, H. J. v.; Groeneveld, M. M.; Benniston, A. C.; Harriman, A. *ChemPhysChem* **2005**, *6*, 2251.
(81) Brédas, J. L.; Beljonne, D.; Cornil, J.; Calbert, J. P.; Shuai, Z.; Silbey, R. *Synth. Met.* **2001**, *125*, 107.
(82) Petrella, A.; Cremer, J.; De Cola, L.; Bauerle, P.; Williams, R. M. *J. Phys. Chem. A* **2005**, *109*, 11687.
(83) van Hal, P. A.; Meskers, S. C. J.; Janssen, R. A. J. *Appl. Phys. A: Mater.* **2004**, *79*, 41.
(84) Beljonne, D.; Ye, A.; Shuai, Z.; Brédas, J. L. *Adv. Funct. Mater.* **2004**, *14*, 684.
(85) Piotrowiak, P. *Chem. Soc. Rev.* **1999**, *28*, 143.
(86) Closs, G. L.; Calcaterra, L. T.; Green, N. J.; Penfield, K. W.; Miller, J. R. *J. Phys. Chem.* **1986**, *90*, 3673.
(87) Schmickler, W. *Interfacial Electrochemistry*; Oxford University Press; Oxford, 1996.
(88) Handa, S.; Giacalone, F.; Haque, S. A.; Palomares, E.; Martín, N.; Durrant, J. R. *Chem.—Eur. J.* **2005**, *11*, 7440.
(89) Shoaee, S.; Eng, M. P.; An, Z.; Zhang, X.; Barlow, S.; Marder, S. R.; Durrant, J. R. *Chem. Commun.* **2008**, 4915.
(90) Onsager, L. *Phys. Rev.* **1938**, *54*, 554.
(91) Gregg, B. A.; Chen, S.-G.; Cormier, R. A. *Chem. Mater.* **2004**, *16*, 4586.
(92) Tachiya, M. *J. Chem. Phys.* **1988**, *89*, 6929.
(93) Borsenberger, P. M.; Ateya, A. I. *J. Appl. Phys.* **1979**, *50*, 909.
(94) Hong, K. M.; Noolandi, J. *J. Chem. Phys.* **1978**, *69*, 5026.
(95) Singh, J.; Baessler, H. *Phys. Status Solidi b* **1974**, *63*, 425.
(96) Mihailetchi, V. D.; Koster, L. J. A.; Hummelen, J. C.; Blom, P. W. M. *Phys. Rev. Lett.* **2004**, *93*, 216601.
(97) Braun, C. L. *J. Chem. Phys.* **1984**, *80*, 4157.
(98) Onsager, L. *J. Chem. Phys.* **1934**, *2*, 599.
(99) Choi, H. T.; Sethi, D. S.; Braun, C. L. *J. Chem. Phys.* **1982**, *77*, 6027.
(100) Wojcik, M.; Tachiya, M. *Radiat. Phys. Chem.* **2005**, *74*, 132.
(101) Barth, S.; Bässler, H. *Phys. Rev. Lett.* **1997**, *79*, 4445.
(102) Pan, J.; Scherf, U.; Schreiber, A.; Haarer, D. *J. Chem. Phys.* **2000**, *112*, 4305.
(103) Barth, S.; Hertel, D.; Tak, Y. H.; Bässler, H.; Hörhold, H. H. *Chem. Phys. Lett.* **1997**, *274*, 165.
(104) Lenes, M.; Morana, M.; Brabec, C. J.; Blom, P. W. M. *Adv. Func. Mater.* **2009**, *19*, 1106.
(105) Mihailetchi, V. D.; Xie, H. X.; de Boer, B.; Koster, L. J. A.; Blom, P. W. M. *Adv. Funct. Mater.* **2006**, *16*, 699.
(106) Koster, L. J. A.; Smits, E. C. P.; Mihailetchi, V. D.; Blom, P. W. M. *Phys. Rev. B* **2005**, *72*, 085205.
(107) Arkhipov, V. I.; Heremans, P.; Bassler, H. *Appl. Phys. Lett.* **2003**, *82*, 4605.
(108) Offermans, T. T. *J. Chem. Phys.* **2003**, *119*, 10924.

(109) Athanasopoulos, S.; Kirkpatrick, J.; Martinez, D.; Frost, J. M.; Foden, C. M.; Walker, A. B.; Nelson, J. *Nano Lett.* **2007**, *7*, 1785.
(110) Kirkpatrick, J.; Nelson, J. *J. Chem. Phys.* **2005**, *123*, 084703.
(111) Yi, Y.; Coropceanu, V.; Brédas, J.-L. Manuscript in preparation, 2009.
(112) Koehler, M.; Santos, M. C.; Luz, M. G. E. d. *J. Appl. Phys.* **2006**, *99*, 053702.
(113) Hertel, D.; Soh, E. V.; Bässler, H.; Rothberg, L. J. *Chem. Phys. Lett.* **2002**, *361*, 99.
(114) Arkhipov, V. I.; Bässler, H.; Emelianova, E. V.; Hertel, H.; Gulbinas, V.; Rothberg, L. J. *Macromol. Symp.* **2004**, *212*, 13.
(115) Nelson, J.; Kirkpatrick, J.; Ravirajan, P. *Phys. Rev. B* **2004**, *69*, 035337.
(116) Gulbinas, V.; Hertel, D.; Yartsev, A.; Sundstrom, V. *Phys. Rev. B* **2007**, *76*, 235203.
(117) Müller, J. G.; Lupton, J. M.; Feldmann, J.; Lemmer, U.; Scharber, M. C.; Sariciftci, N. S.; Brabec, C. J.; Scherf, U. *Phys. Rev. B* **2005**, *72*, 195208.
(118) Westenhoff, S.; Howard, I. A.; Hodgkiss, J. M.; Kirov, K. R.; Bronstein, H. A.; Williams, C. K.; Greenham, N. C.; Friend, R. H. *J. Am. Chem. Soc.* **2008**, *130*, 13653.
(119) Nishihara, Y.; Fujii, A.; Ozaki, M.; Yoshino, K.; Frankevich, E. *Jpn. J. Appl. Phys.* **2003**, *42*, L538.
(120) Hwang, I. W.; Moses, D.; Heeger, A. J. *J. Phys. Chem. C* **2008**, *112*, 4350.
(121) Hwang, I.-W.; Cho, S.; Kim, J. Y.; Lee, K.; Coates, N. E.; Moses, D.; Heeger, A. J. *J. Appl. Phys.* **2008**, *104*, 033706.
(122) Hwang, I.-W.; Soci, C.; Moses, D.; Zhu, Z.; Waller, D.; Gaudiana, R.; Brabec, C. J.; Heeger, A. J. *Adv. Mater.* **2007**, *19*, 2307.
(123) Lane, P. A.; Wei, X.; Vardeny, Z. V. *Phys. Rev. B* **1997**, *56*, 4626.
(124) Dyer-Smith, C.; Benson-Smith, J. J.; Bradley, D. D. C.; Murata, H.; Mitchell, W. J.; Shaheen, S.; Haque, S. A.; Nelson, J. *J. Phys. Chem. A* Submitted for publication.
(125) Morteani, A. C.; Friend, R. H.; Silva, C. *Chem. Phys. Lett.* **2004**, *391*, 81.
(126) Samuel, I. D. W.; Rumbles, G.; Collison, C. J. *Phys. Rev. B* **1995**, *52*, R11573.
(127) Morteani, A. C.; Friend, R. H.; Silva, C. *J. Chem. Phys.* **2005**, *122*, 244906.
(128) Morteani, A. C.; Dhoot, A. S.; Kim, J. S.; Silva, C.; Greenham, N. C.; Murphy, C.; Moons, E.; Ciná, S.; Burroughes, J. H.; Friend, R. H. *Adv. Mater.* **2003**, *15*, 1708.
(129) Alam, M. M.; Jenekhe, S. A. *J. Phys. Chem. B* **2001**, *105*, 2479.
(130) Hallermann, M.; Haneder, S.; Como, E. D. *Appl. Phys. Lett.* **2008**, *93*, 053307.
(131) Hasharoni, K.; Keshavarz-K, M.; Sastre, A.; Gonzalez, R.; Bellavia-Lund, C.; Greenwald, Y.; Swager, T.; Wudl, F.; Heeger, A. J. *J. Chem. Phys.* **1997**, *107*, 2308.
(132) Zhou, Y.; Tvingstedt, K.; Zhang, F.; Du, C.; Ni, W.-X.; Andersson, M. R.; Inganas, O. *Adv. Funct. Mater.* Submitted for publication.
(133) Goris, L.; Poruba, A.; Hod'akova, L.; Vanecek, M.; Haenen, K.; Nesladek, M.; Wagner, P.; Vanderzande, D.; Schepper, L. D.; Manca, J. V. *Appl. Phys. Lett.* **2006**, *88*, 052113.
(134) Drori, T.; Sheng, C. X.; Ndobe, A.; Singh, S.; Holt, J.; Vardeny, Z. V. *Phys. Rev. Lett.* **2008**, *101*, 037401.
(135) Veldman, D.; Chopin, S. p. M. A.; Meskers, S. C. J.; Janssen, R. A. J. *J. Phys. Chem. A* **2008**, *112*, 8617.
(136) Barford, W. *Phys. Rev. B* **2004**, *70*, 205204.
(137) Benson-Smith, J. J.; Ohkita, H.; Cook, S.; Durrant, J. R.; Bradley, D. D. C.; Nelson, J. Submitted for publication.
(138) Cook, S.; Ohkita, H.; Durrant, J. R.; Kim, Y.; Benson-Smith, J. J.; Nelson, J.; Bradley, D. D. C. *Appl. Phys. Lett.* **2006**, *89*, 101128.
(139) Schueppel, R.; Uhrich, C.; Pfeiffer, M.; Leo, K.; Brier, E.; Reinold, E.; Baeuerle, P. *ChemPhysChem* **2007**, *8*, 1497.
(140) Ohkita, H.; Cook, S.; Astuti, Y.; Duffy, W.; Heeney, M.; Tierney, S.; McCulloch, I.; Bradley, D. D. C.; Durrant, J. R. *Chem. Commun.* **2006**, 3939.
(141) Ford, T. A.; Avilov, I.; Beljonne, D.; Greenham, N. C. *Phys. Rev. B* **2005**, *71*, 125212.
(142) Ford, T. A.; Ohkita, H.; Cook, S.; Durrant, J. R.; Greenham, N. C. *Chem. Phys. Lett.* **2008**, *454*, 237.
(143) Lee, C. H.; Yu, G.; Moses, D.; Heeger, A. J. *Phys. Rev. B* **1994**, *49*, 2396.
(144) Moses, D.; Wang, J.; Heeger, A. J.; Kirova, N.; Brazovski, S. *Proc. Natl. Acad. Sci. U.S.A.* **2001**, *98*, 13496.
(145) Yee, K. C.; Chance, R. R. *J. Polym. Sci., Polym. Polym. Phys.* **1978**, *16*, 431.
(146) Sebastian, L.; Weiser, G. *Phys. Rev. Lett.* **1981**, *46*, 1156.
(147) Hasegawa, T.; Ishikawa, K.; Koda, T.; Takeda, K.; Kobayashi, H.; Kubodera, K. *Synth. Met.* **1991**, *43*, 3151.
(148) Maniloff, E. S.; Klimov, V. I.; McBranch, D. W. *Phys. Rev. B* **1997**, *56*, 1876 LP.
(149) Hendry, E.; Schins, J. M.; Candeias, L. P.; Siebbeles, L. D. A.; Bonn, M. *Phys. Rev. Lett.* **2004**, *92*, 196601.
(150) Shuai, Z.; Brédas, J. L.; Su, W. P. *Chem. Phys. Lett.* **1994**, *228*, 301.
(151) Romanovskii, Y. V.; Gerhard, A.; Schweitzer, B.; Scherf, U.; Personov, R. I.; Bässler, H. *Phys. Rev. Lett.* **2000**, *84*, 1027.
(152) Beljonne, D.; Shuai, Z.; Pourtois, G.; Bredas, J. L. *J. Phys. Chem. A* **2001**, *105*, 3899.
(153) Deussen, M.; Haring Bolivar, P.; Wegmann, G.; Kurz, H.; Bässler, H. *Chem. Phys.* **1996**, *207*, 147.
(154) Deussen, M.; Scheidler, M.; Bässler, H. *Synth. Met.* **1995**, *73*, 123.
(155) Liess, M.; Jeglinski, S.; Vardeny, Z. V.; Ozaki, M.; Yoshino, K.; Ding, Y.; Barton, T. *Phys. Rev. B* **1997**, *56*, 15712.
(156) Scharber, M. C.; Mühlbacher, D.; Koppe, M.; Denk, P.; Waldauf, C.; Heeger, A. J.; Brabec, C. J. *Adv. Mater.* **2006**, *18*, 789.
(157) Halls, J. J. M.; Cornil, J.; dos Santos, D. A.; Silbey, R.; Hwang, D. H.; Holmes, A. B.; Brédas, J. L.; Friend, R. H. *Phys. Rev. B* **1999**, *60*, 5721.
(158) Rand, B. P.; Burk, D. P.; Forrest, S. R. *Phys. Rev. B* **2007**, *75*, 115327.
(159) Sensfuss, S.; Al-Ibrahim, M.; Konkin, A.; Nazmutdinova, G.; Zhokhavets, U.; Gobsch, G.; Egbe, D. A. M.; Klemm, E.; Roth, H.-K. *SPIE-Proc. Org. Photovoltaics IV* **2004**, 129.
(160) Miller, J. R.; Calcaterra, L. T.; Closs, G. L. *J. Am. Chem. Soc.* **2002**, *106*, 3047.
(161) Veldman, D.; Bastiaansen, J. J. A. M.; Langeveld-Voss, B. M. W.; Sweelssen, J.; Koetse, M. M.; Meskers, S. C. J.; Janssen, R. A. J. *Thin Solid Films* **2006**, *511−512*, 581.
(162) Hukka, T. I.; Toivonen, T.; Hennebicq, E.; Brédas, J. L.; Janssen, R. A. J.; Beljonne, D. *Adv. Mater.* **2006**, *18*, 1301.
(163) Bensasson, R. V.; Bienvenüe, E.; Fabredagger, C.; Janot, J.-M.; Land, E. J.; Leach, S.; Leboulaire, V.; Rassat, A.; Roux, S.; Seta, P. *Chem.—Eur. J.* **1998**, *4*, 270.
(164) van Hal, P. A.; Janssen, R. A. J.; Lanzani, G.; Cerullo, G.; Zavelani-Rossi, M.; De Silvestri, S. *Phys. Rev. B* **2001**, *64*, 075206.
(165) De, S. S. *J. Am. Chem. Soc.* **2007**, *129*, 8466.
(166) Meskers, S. C. J.; van Hal, P. A.; Spiering, A. J. H.; Hummelen, J. C.; van der Meer, A. F. G.; Janssen, R. A. J. *Phys. Rev. B* **2000**, *61*, 9917 LP.
(167) Shoaee, S.; Eng, M. P.; Espíldora, E.; Delgado, J. L.; Campo, B.; Martín, N.; Vanderzande, D.; Durrant, J. R. *Nano Lett.* Submitted for publication.
(168) Mandoc, M. M.; Kooistra, F. B.; Hummelen, J. C.; Boer, B. d.; Blom, P. W. M. *Appl. Phys. Lett.* **2007**, *91*, 263505.
(169) Montanari, I.; Nogueira, A. F.; Nelson, J.; Durrant, J. R.; Winder, C.; Loi, M. A.; Sariciftci, N. S.; Brabec, C. *Appl. Phys. Lett.* **2002**, *81*, 3001.
(170) Nelson, J. *Phys. Rev. B* **2003**, *67*, 155209.
(171) Nogueira, A. F.; Montanari, I.; Nelson, J.; Durrant, J. R.; Winder, C.; Sariciftci, N. S.; Brabec, C. *J. Phys. Chem. B* **2003**, *107*, 1567.
(172) Offermans, T.; Meskers, S. C. J.; Janssen, R. A. J. *Org. Electron.* **2006**, *7*, 213.
(173) Pensack, R. D.; Banyas, K. M.; Barbour, L. W.; Hegadorn, M.; Asbury, J. B. *Phys. Chem. Chem. Phys.* **2009**, *11*, 2575.
(174) Quist, P. A. P.; Savenije, T. J.; Koetse, M. M.; Veenstra, S. C.; Kroon, J. M.; Siebbeles, L. D. A. *Adv. Funct. Mater.* **2005**, *15*, 469.
(175) Zhang, F.; Jespersen, K. G.; Björström, C.; Svensson, M.; Andersson, M. R.; Sundström, V.; Magnusson, K.; Moons, E.; Yartsev, A.; Inganäs, O. *Adv. Funct. Mater.* **2006**, *16*, 667.
(176) Müller, J. G.; Lemmer, U.; Feldmann, J.; Scherf, U. *Phys. Rev. Lett.* **2002**, *88*, 147401.
(177) Ma, W. W.; Yang, C.; Gong, X.; Lee, K.; Heeger, A. J. *Adv. Funct. Mater.* **2005**, *15*, 1617.
(178) Reyes-Reyes, M.; Kim, K.; Carroll, D. L. *Appl. Phys. Lett.* **2005**, *87*, 083506.
(179) Kim, Y.; Choulis, S. A.; Nelson, J.; Bradley, D. D. C.; Cook, S.; Durrant, J. R. *Appl. Phys. Lett.* **2005**, *86*, 063502.
(180) Nguyen, L. H.; Hoppe, H.; Erb, T.; Günes, S.; Gobsch, G.; Sariciftci, N. S. *Adv. Funct. Mater.* **2007**, *17*, 1071.
(181) Österbacka, R.; An, C. P.; Jiang, X. M.; Vardeny, Z. V. *Science* **2000**, *287*, 839.
(182) Westerling, M.; Österbacka, R.; Stubb, H. *Phys. Rev. B* **2002**, *66*, 165220.
(183) Clarke, T.; Ballantyne, A.; Jamieson, F.; Brabec, C.; Nelson, J.; Durrant, J. *Chem. Commun.* **2009**, 89.
(184) Keivanidis, P. E.; Clarke, T. M.; Durrant, J. R.; Bradley, D. D. C.; Nelson, J. Manuscript in preparation.
(185) Clarke, T. M.; Ballantyne, A. M.; Tierney, S.; Heeney, M.; Duffy, W.; McCulloch, I.; Nelson, J.; Durrant, J. R. *J. Phys. Chem. C* Submitted for publication.
(186) Shoaee, S.; An, Z.; Zhang, X.; Barlow, S.; Marder, S. R.; Duffy, W.; Heeney, M.; McCulloch, I.; Durrant, J. R. *Chem. Commun.*, in press.
(187) Kanai, Y.; Grossman, J. C. *Nano Lett.* **2007**, *7*, 1967.
(188) Ruseckas, A.; Theander, M.; Andersson, M. R.; Svensson, M.; Prato, M.; Inganas, O.; Sundstrom, V. *Chem. Phys. Lett.* **2000**, *322*, 136.

(189) Shuttle, C. G.; Regan, B. O.; Ballantyne, A. M.; Nelson, J.; Bradley, D. D. C.; Durrant, J. R. *Phys. Rev. B* **2008**, *78*, 113201.
(190) Marsh, R. A.; Groves, C.; Greenham, N. C. *J. Appl. Phys.* **2007**, *101*, 083509.
(191) Barker, J. A.; Ramsdale, C. M.; Greenham, N. C. *Phys. Rev. B* **2003**, *67*, 075205.
(192) Groves, C.; Koster, L. J. A.; Greenham, N. C. *J. Appl. Phys.* **2009**, *105*, 094510.
(193) Wojcik, M.; Tachiya, M. *J. Chem. Phys.* **2009**, *130*, 104107.
(194) Kirchartz, T.; Pieters, B. E.; Taretto, K.; Rau, U. *J. Appl. Phys.* **2008**, *104*, 094513.
(195) Moulé, A. J.; Meerholz, K. *Appl. Phys. B: Laser Opt.* **2008**, *92*, 209.
(196) Yang, F.; Forrest, S. R. *ACS Nano* **2008**, *2*, 1022.
(197) Marsh, R. A.; McNeill, C. R.; Abrusci, A.; Campbell, A. R.; Friend, R. H. *Nano Lett.* **2008**, *8*, 1393.
(198) Liu, A.; Zhao, S.; Rim, S. B.; Wu, J.; Könemann, M.; Erk, P.; Peumans, P. *Adv. Mater.* **2008**, *20*, 1065.
(199) Chasteen, S. V.; Sholin, V.; Carter, S. A.; Rumbles, G. *Sol. Energy Mater. Sol. Cells* **2008**, *92*, 651.
(200) Ruseckas, A.; Shaw, P. E.; Samuel, I. D. W. *Dalton Trans.* Accepted for publication.
(201) Lindner, S. M.; Hüttner, S.; Chiche, A.; Thelakkat, M.; Krausch, G. *Angew. Chem., Int. Ed.* **2006**, *45*, 3364.
(202) Lindner, S. M.; Thelakkat, M. *Macromolecules* **2004**, *37*, 8832.
(203) Sommer, M.; Hüttner, S.; Wunder, S.; Thelakkat, M. *Adv. Mater.* **2008**, *20*, 2523.
(204) Roncali, J. *Chem. Soc. Rev.* **2005**, *34*, 483.
(205) Hoppe, H.; Glatzel, T.; Niggemann, M.; Schwinger, W.; Schaeffler, F.; Hinsch, A.; Lux-Steiner, M. C.; Sariciftci, N. S. *Thin Solid Films* **2006**, *511*−*512*, 587.
(206) Quist, P. A. C.; Martens, T.; Manca, J. V.; Savenije, T. J.; Siebbeles, L. D. A. *Sol. Energy Mater. Sol. Cells* **2006**, *90*, 362.
(207) Erb, T. T. *Thin Solid Films* **2006**, *511*, 483.
(208) Li, G.; Shrotriya, V.; Yao, Y.; Yang, Y. *J. Appl. Phys.* **2005**, *98*, 043704.
(209) Savenije, T. J.; Kroeze, J. E.; Yang, X.; Loos, J. *Thin Solid Films* **2006**, *511*, 2.
(210) Zhokhavets, U.; Erb, T.; Hoppe, H.; Gobsch, G.; Sariciftci, N. S. *Thin Solid Films* **2006**, *496*, 679.
(211) van Duren, J. K. J.; Yang, X.; Loos, J.; Bulle-Lieuwma, C. W. T.; Sieval, A. B.; Hummelen, J. C.; Janssen, R. A. J. *Adv. Funct. Mater.* **2004**, *14*, 425.
(212) Müller, C.; Ferenczi, T. A. M.; Campoy-Quiles, M.; Frost, J. M.; Bradley, D. D. C.; Smith, P.; Stingelin-Stutzmann, N.; Nelson, J. *Adv. Mater.* **2008**, *20*, 3510.
(213) De, S.; Kesti, T.; Maiti, M.; Zhang, F.; Inganäs, O.; Yartsev, A.; Pascher, T.; Sundström, V. *Chem. Phys.* **2008**, *350*, 14.
(214) Shaheen, S. E.; Brabec, C. J.; Sariciftci, N. S.; Padinger, F.; Fromherz, T.; Hummelen, J. C. *Appl. Phys. Lett.* **2001**, *78*, 841.
(215) Yang, X.; van Duren, J. K. J.; Janssen, R. A. J.; Michels, M. A. J.; Loos, J. *Macromolecules* **2004**, *37*, 2151.
(216) Martens, T.; D'Haen, J.; Munters, T.; Beelen, Z.; Goris, L.; Manca, J.; D'Olieslaeger, M.; Vanderzande, D.; De Schepper, L.; Andriessen, R. *Synth. Met.* **2003**, *138*, 243.
(217) Groves, C.; Marsh, R. A.; Greenham, N. C. *J. Chem. Phys.* **2008**, *129*, 114903.
(218) Arias, A. C.; MacKenzie, J. D.; Stevenson, R.; Halls, J. J. M.; Inbasekaran, M.; Woo, E. P.; Richards, D.; Friend, R. H. *Macromolecules* **2001**, *34*, 6005.
(219) McNeill, C. R.; Frohne, H.; Holdsworth, J. L.; Dastoor, P. C. *Nano Lett.* **2004**, *4*, 2503.
(220) Coffey, D. C.; Ginger, D. S. *Nat. Mater.* **2006**, *5*, 735.
(221) Mayer, A. C.; Michael, F. T.; Shawn, R. S.; Jonathan, R.; Christoph, J. B.; Marcus, S.; Marcus, K.; Martin, H.; Iain, M.; Michael, D. M. *Adv. Funct. Mater.* **2009**, *19*, 1173.
(222) Chirvase, D.; Parisi, J.; Hummelen, J. C.; Dyakonov, V. *Nanotechnology* **2004**, *15*, 1317.
(223) Campoy-Quiles, M.; Ferenczi, T.; Agostinelli, T.; Etchegoin, P. G.; Kim, Y.; Anthopoulos, T. D.; Stavrinou, P. N.; Bradley, D. D. C.; Nelson, J. *Nat. Mater.* **2008**, *7*, 158.
(224) Savenije, T. J.; Kroeze, J. E.; Yang, X.; Loos, J. *Adv. Funct. Mater.* **2005**, *15*, 1260.
(225) Yamanari, T.; Taima, T.; Hara, K.; Saito, K. *J. Photochem. Photobiol. A: Chem.* **2006**, *182*, 269.
(226) Erb, T.; Zhokhavets, U.; Gobsch, G.; Raleva, S.; Stühn, B.; Schilinsky, P.; Waldauf, C.; Brabec, C. J. *Adv. Funct. Mater.* **2005**, *15*, 1193.
(227) McNeill, C. R.; Halls, J. J. M.; Wilson, R.; Whiting, G. L.; Berkebile, S.; Ramsey, M. G.; Friend, R. H.; Greenham, N. C. *Adv. Funct. Mater.* **2008**, *18*, 2309.
(228) Huang, Y. S.; Westenhoff, S.; Avilov, I.; Sreearunothai, P.; Hodgkiss, J. M.; Deleener, C.; Friend, R. H.; Beljonne, D. *Nat. Mater.* **2008**, *7*, 483.
(229) Nazeeruddin, M. K.; Kay, A.; Rodicio, I.; Humphry-Baker, R.; Mueller, E.; Liska, P.; Vlachopoulos, N.; Graetzel, M. *J. Am. Chem. Soc.* **2002**, *115*, 6382.
(230) Lee, J. K.; Ma, W. L.; Brabec, C. J.; Yuen, J.; Moon, J. S.; Kim, J. Y.; Lee, K.; Bazan, G. C.; Heeger, A. J. *J. Am. Chem. Soc.* **2008**, *130*, 3619.
(231) Lenes, M.; Kooistra, F. B.; Hummelen, J. C.; Severen, I. V.; Lutsen, L.; Vanderzande, D.; Cleij, T. J.; Blom, P. W. M. *J. Appl. Phys.* **2008**, *104*, 114517.
(232) Leclere, P.; Surin, M.; Brocorens, P.; Cavallini, M.; Biscarini, F.; Lazzaroni, R. *Mater. Sci. Eng., R* **2006**, *55*, 1.
(233) Scherf, U.; Gutacker, A.; Koenen, N. *Acc. Chem. Res.* **2008**, *41*, 1086.

CR900271S